Hochschule für Angewandte Wissenschaften Hamburg
Hamburg University of Applied Sciences

Bachelorarbeit

Tushit Luchmun

Development of a Noise Power Transfer Prediction Model for VIP Aircraft Cabin

Fakultät Technik und Informatik
Department Fahrzeugtechnik und Flugzeugbau

Faculty of Engineering and Computer Science
Department of Automotive and Aeronautical Engineering

Tushit Luchmun

Development of a Noise Power Transfer Prediction Model for VIP Aircraft Cabin

Bachelor-/Masterarbeit eingereicht im Rahmen der Bachelor-/Masterprüfung

im Studiengang Fahrzeugbau
am Department Fahrzeugtechnik und Flugzeugbau
der Fakultät Technik und Informatik
der Hochschule für Angewandte Wissenschaften Hamburg

in Zusammenarbeit mit:
Lufthansa Technik AG
Abteilung T/OS 45 Interiors
Weg beim Jäger 193
22335 Hamburg

Erstprüfer/in: Prof. Dr.-Ing Benedikt Plaumann
Zweitprüfer/in: M.S.c Ashish Chodvadiya

Abgabedatum: 14.01.2025

Zusammenfassung

Tushit Luchmun

Thema der Bachelorthesis

Entwicklung eines Modells zur Vorhersage der Schallleistungsübertragung in VIP-Flugzeugkabinen

Stichworte

Schallleistung, Empirisches Modell, Schalldruckpegel, Akustik, VIP-Flugzeug, Turbulente Grenzschicht, Triebwerkslärm, Lärmminderungsmaßnahme, Mehrschichtübertragung, Übertragungsfunktion, Übertragungspfadanalyse, Luftschall, Körperschall

Kurzzusammenfassung

Diese Arbeit beschäftigt sich mit der Entwicklung eines Tools zur Vorhersage der Schallleistung in VIP-Flugzeugkabinen, wobei der Schwerpunkt auf der Vereinfachung der Schallanalyse unter Beibehaltung einer praktischen Genauigkeit liegt. Ziel ist es, die Schallleistung (W) vorherzusagen und dominante Schallpfade mithilfe von Übertragungsfunktionen und Bodentestdaten zu identifizieren.

Tushit Luchmun

Title of the paper

Development of a Noise Power Transfer Prediction Model for VIP Aircraft Cabin

Keywords

Sound power, Empirical model, Sound pressure level, Acoustic, VIP aircraft, Turbulent boundary layer, Engine noise, Noise control measure, Multi-layer transmission, Transfer function, Transfer path analysis, Airborne noise, Structure-borne noise

Abstract

This thesis aims to develop a tool to predict sound power in VIP aircraft cabins, focusing on simplifying noise analysis while maintaining practical accuracy. The goal is to predict sound power (W) and identify dominant sound paths using transfer functions and on-ground measurement data.

I. Table of content

II. List of figures

III. List of tables

IV. List of abbreviations

ABN	Airborne noise
BEM	Boundary Element Methode
CLF	Coupling Loss Factors
dB	Decibel
DBEM	Direct Boundary Element Method
DIN	German institute for standardization, deu. *Deutsches Institut für Normung*
DLF	Damping Loss Factors
DoF	Degree of Freedom
ECU	Engine Control Unit
EN	European Norm deu. *Europäische Norm*
ENTIRETY	Engineered Tailored Tranquility
FAA	Federal Aviation Administration
FE	Finite Element
FEA	Finite Element Analysis
FEM	Finite Element Method
FFT	Fourier Transform Functions
FL	Flight Level
FRF	Frequency Response Function
HAW	Hamburg University of Applied Sciences, deu. *Hochschule für Angewandte Wissenschaften*
HCAT	Hamburg Centre of Aviation Training
Hz	Hertz
IBEM	Indirect Boundary Element Method
ICAO	International Civil Aviation Organisation
ID	Identification
ISA	International Standard Atmosphere
ISO	International Organization for Standardization
K	Kelvin
LHT	Lufthansa Technik AG
m	Metre
MATLAB	Matrix Laboratory
MRO	Maintenance, Repair and Overhaul

N	Newton
OEM	Original Equipment Manufacturer
OPA	Operational Path Analysis
OTPA	Operational Transfer Path Analysis
Pa	Pascal
RMS	Root mean square
s	Second
SBN	Structure-borne noise
SEA	Statistical Energy Analysis
SPL	Sound Pressure Level
STL	Sound Transmission Loss
SVD	Singular Value Decomposition
TAS	True airspeed
TBL	Turbulent Boundary Layer
TF	Transfer Function
TL	Transmission Loss
TPA	Transfer Path Analysis
VDI	Nationale Richtlinien des Vereins Deutscher Ingenieure
VIP	Very Important Person
W	Watt
ZAL	Center of Applied Aeronautical Research, deu. *Zentrum für Angewandte Luftfahrtforschung GmbH*

V. List of symbols

α_i	Absorption coefficient
A	Area
$\bar{A}_{eq}$	Equivalent absorption surface rea of specimen
A_i	Incident area
$\bar{A}_i$	Equivalent absorption area
$\bar{A}_j$	Equivalent absorption area irregular objects
$\bar{A}_{total}$	Total equivalent absorption Area
c	Speed of sound
c_f	Coefficient of friction
C	Coupling factor
Δf	Bandwidth
f	Frequency
f_r	Ratio function
f_m	Middle frequency
f_u	Upper frequency
f_L	Lower frequency
$F(\omega)$	Engine force
H	Transfer function
$H(j\omega)$	Transfer function matrix
$H_1(\omega)$	Transfer function for region 1
I	Intensity
I_0	Reference intensity
I_ϵ	Incident sound intensity
I_τ	Transmitted sound intensity
II_2	Radiated sound power
k	Wave number
K_0	Correction factor
L_W	Sound power level
L_P	Sound pressure level

m	Mass per unit area or number of irregular objects
n	Number of regular surfaces
ρ	Air density
p	Sound pressure of source
p_0	Reference pressure
p_{rms}	Mean pressure
q	Dynamic pressure
r	Radius
r_H	Reverberation radius
R	Specific gas constant
R_i	Reduction index
S	Surface area
S_0	Reference area
S_i	Total surface area
t	Time
τ	Transmission coefficient
τ_w	Shear stress
T	Reverberation time, or Temperature
u	Speed of aircraft
${v^2}_{rms,St\Delta}$	Mean square surface velocity over frequency band
v	Particle velocity
v_{rms}	Root mean square value of velocity
V	Volume, or resonance factor
ω	Frequency in radians per second
ω_0	Natural frequency
W	Source power
W_0	Reference sound power
W_S	Total sound power
$W_{\Delta S}$	Radiated sound power
$x(\omega)$	Periodic signal
$x(j\omega)$	Reference vector of system
X	Matrix of the signal, or input power page

γ	Adiabatic constant of air
$y(\omega)$	Response signal
$y(j\omega)$	Response vector
Y	Response matrix, or radiated power output page
Z	Acoustic impedance
$\emptyset$	Phase difference
δ	Thickness of the boundary layer
σ	Coefficient of radiation
σ_f	Uncertainty
$\sigma_{\Delta S}$	Efficiency of radiation
φ_y	Phase response
$€/dB$	Cost per noise reduction

1. Introduction

1.1 Motivation

The demand for VIP aircraft has surged in recent years, driven by the growing need for privacy, security, and luxury among high-profile individuals such as government officials, business executives, and celebrities. These aircraft offer exclusive cabin designs, spacious seating and personalised services, transforming air travel into a more exclusive experience. With the global business jet market expected to reach $36 billion by 2028, a $5 billion increase in just three years, the VIP aviation sector continues to expand rapidly, especially in the corporate industry, where time is money and comfort is precious. On the other hand, the Covid-19 pandemic further accelerated this trend, as private VIP flights provide an alternative to safer, faster and less restricted travel. The growing demand for private jets does not only include aircraft rentals but also an increase in the number of deliveries in the coming years [1]. For Lufthansa Technik AG, perhaps, the most attractive clients are governmental VIP jets. These types of aircraft share slightly different requirements compared to traditional private VIP jets, with a focus on productivity and constrained by the price, operating costs and accommodating more passengers - they are rather considered as a productivity tool, reducing business travel from a whole day to a few hours. The Lufthansa Technik AG in Hamburg (LHT) is a leader in the Maintenance, Repair, and Overhaul (MRO) sector and provides tailored solutions for VIP aircraft cabin configurations. Figure 1 shows a prediction for the business jet market size in billion US dollars. It remains, however, unclear whether the forecast include the contribution of governmental VIP market. [1]

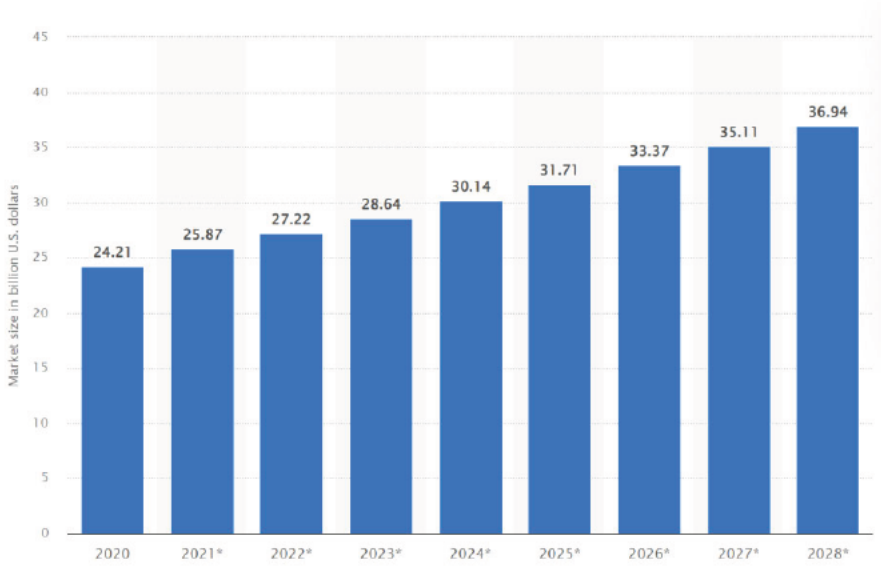

Figure 1: Graph showing expected market size of the business jet market worldwide from 2020 to 2028 in USD [1]

Unlike commercial airlines, where cost, weight, and efficiency are the primary considerations, VIP aircrafts also prioritise cabin comfort. Comfort refers to a state of physical and emotional well-being, characterised by the absence of discomfort or stress. Determining comfort is complex since it is inherently individual; different people have varying preferences and perceptions [2]. In the context of air travel, cabin comfort refers to the overall satisfaction and experience of passengers and crew. Passenger comfort during air travel is mostly influenced by ergonomic and anthropometric considerations such as available seat space, legroom, headroom, airline services for luggage storage, catering, cleanliness and hygiene in the cabin, and the aircraft itself. Although assessing cabin comfort is subjective, it can still be objectively analysed through specific criteria and standards that evaluate the different factors, such as air quality, visual comfort, thermal comfort, but also acoustic comfort [3]. In the cabin, passenger discomfort occurs if the noise levels exceed a certain “unacceptable” threshold (further discussed in chapter 2.2). Aircraft are

significant noise sources, radiating sound through the atmosphere to the ground and transmitting a huge portion into the cabin through the fuselage structure. Long exposure to noise can adversely affect both the physiological and psychological health and comfort of cabin crews and frequent travellers, such as VIP passengers [4]. Hence, keeping noise levels low is required to ensure a pleasant sound quality with no annoyance. This is even more crucial in VIP aircrafts where business meetings, private conversations and uninterrupted resting are common. Although VIP aircrafts are less constrained by weight and cost limitations compared to commercial aircraft, achieving acoustic comfort is not always easy. One reason is that each aircraft is customised, and every cabin design is a unique noise problem in itself. Additionally, modifying OEM (original equipment manufacturer) cabins, requires creative solutions as they were not initially designed for its new purpose [5]. Most importantly, adding mass to achieve customer requirements cannot be blindly done as noise control measures often come with the trade-off: increasing the weight negatively impacts the operational efficiency of the aircraft. Hence, acoustic engineers are constantly faced with an ongoing challenge of finding the appropriate balance between effective noise reduction and fuel efficiency, while at the same time, sustainability and the requirements of customers remain a key focus.

In this context, the project, ENTIRETY (Engineered Tailored Tranquility), which is a collaboration among the Lufthansa Technik AG (LHT), ZAL Center of Applied Aeronautical Research (ZAL), and the University of Applied Sciences of Hamburg (HAW), aims to address this issue, by investigating and developing a fast and practical noise prediction tool for VIP aircraft cabins. Early identification of critical noise paths during the cabin design process is essential to prevent cost overruns and project delays. Although there already exists various sound prediction tools and models, these are often costly and necessitates high computational power and skills. Unlike these traditional tools, this model focuses on simplicity and speed, producing results within just a few hours. This is particularly attractive for smaller VIP completions cabin design companies, where time and resources are limited, and complex simulation-based tools may not be feasible. The purpose of the tool is not to replace existing noise prediction tools but instead provide an alternative for quick insights into most dominant transmission paths and noise mitigation in the cabin. This will allow cabin manufacturers to implement targeted solutions, without the need of costly flight tests or simulation tools.

Hence, an empirical model which will be developed using acoustic measurements using the VIP Aircraft Cabin Demonstrator, at the Hamburg Centre of Aviation (HCAT). The tool should be able to estimate sound power contributions for various aircraft configurations using “Transfer Functions”. Additionally, the tool will account for serial and parallel transmission paths to represent sound transmission through the cabin.

1.2 Task

Using the knowledge acquired from Tom Ziegner, (2023) [5] and Bennett Bögle (2024) [6], a noise prediction model will be developed to determine the sound power inside the aircraft cabin. The model should be valid for a range of aircraft types and configurations and should identify the most dominant paths through which noise enters the cabin. The model will incorporate both serial and parallel transmission paths to represent sound propagation and/or attenuation within the cabin. Additionally, the limitations of model and their impact on the noise prediction should be discussed.

1.3 Goal

The ENTIRETY project ultimately aims to create a cost-effective and user-friendly prediction model that provides fairly accurate results within a short timeframe, while at the same time maintaining the overall weight of the VIP cabin. By bridging the gap between fundamental acoustic theory, practical and achievable experiments, the tool will simplify noise management analysis in VIP aircraft. This makes it a valuable resource for stakeholders including the LHT VIP Completion Centre, ensuring high fuel efficiency, low noise annoyance and high comfort in VIP aircraft cabins.

1.4 Approach and structure of this thesis

The development of the noise prediction tool follows a structured process close to the VDI 2221, combining theoretical knowledge and practical measurements. This paper starts with a literature review to explore existing models and transfer path methods, and potential gaps that the tool may address. This ensures the model builds on proven acoustic principles. In chapter 2, the relevant fundamentals principle of acoustics including sound power and acoustic behaviour sound waves will be introduced to provide a physical basis for the model. Chapter 3 aims to provide an understanding of the main sources of noise and their transmission paths through which they enter the cabin as well as the different parameters which influence cabin noise during flight. Chapter 4 explains how cabin noise measurements were conducted, what parameters were measured, and how this data can be integrated into the tool. Based on this, the approach of using transfer functions for predicting sound power will be further discussed. Chapter 5 defines the requirements of the tool ensuring it remains simple and functional. The framework focuses on how to make the tool practical, and easy to use while aligning itself with industry standards and best practices as well as strict aviation regulations. The development and the implementation of the necessary formulae to calculate power output will be described in chapter 6. Validation follows in chapter 7, comparing predictions against existing measurements to ensure accuracy. Chapter 8 outlines the assumptions and limitations of the tool, from which the errors primarily occur, and some potential improvement will be suggested. Finally, chapter 9 is the concluding chapter. Figure 2 summarises the approach and structure of this paper. Index IX serves as a user manual, where using real measurements, it will be demonstrated how to use the tool.

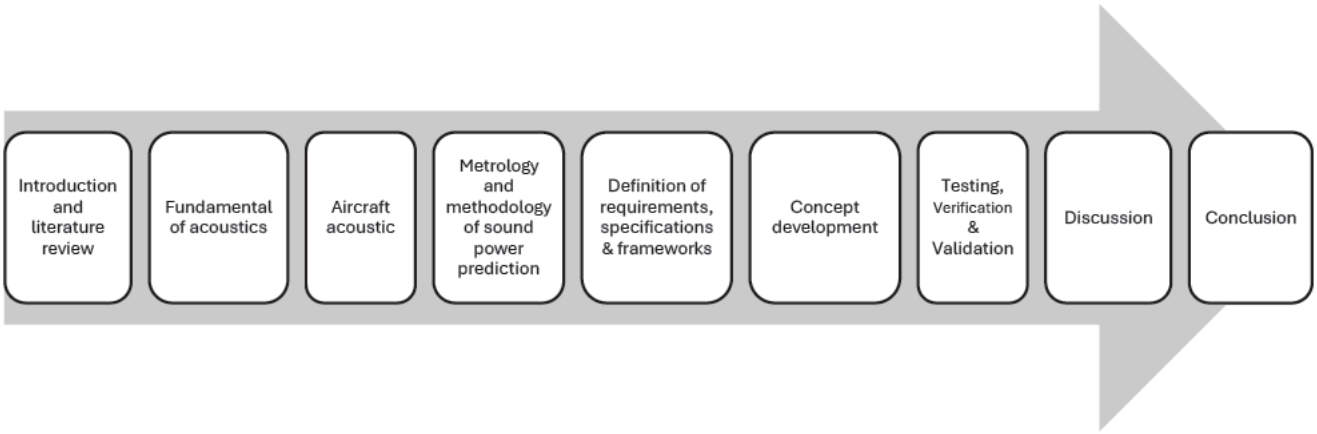

Figure 2: Approach and structure of this work

1.5 Literature review

The aviation market demands for increased flight comfort, including lower cabin noise levels. At the same time, the production cycle is required to be as short as possible, while both the production and operational costs of the aircraft need to be kept low. An aircraft cabin is an enclosed system surrounded by the skin of the fuselage. The cabin moves in a fluid medium. The noise inside the cabin is an interior noise problem and the main sources of noise are typically found beyond the surrounded boundary. These include mechanical vibration (structure-borne) of various components of the aircraft and the pressure fluctuations caused by the turbulent boundary layer (TBL) on the fuselage [7]. The main mechanism through which sound travels to the cabin is the structure-borne pathway and airborne transmission. When sound energy hits a material (fuselage), not all of the energy is transmitted. Some will be reflected; a fraction will be absorbed by the material and the rest is transmitted [8]. The path through which the energy travels from the source to the receiver is known as the transmission path or transfer path. The relationship between the input power (from the source, just before hitting the fuselage) to the output power (at the receiving point) is known as the transfer path function or transfer function, TF [9]. Research and interviews with stakeholders have shown that noise prediction is determined for each aircraft configuration in the pre-design and design stage. Since real flight testing is costly and difficult to carry out, several tools and software are employed in the practice to determine the overall noise inside the cabin. This chapter summarises the key findings and approach employed to determine cabin noise. It is worth highlighting that the conducted research could not find any sound power prediction tool for VIP cabin based on the software (MS) Microsoft Excel.

1.6 FE and SEA sound models

It is difficult to analytically predict physical response of real structures [10]. For a defined enclosed system, this is typically done using theoretical and computational (FE and SEA) models. Although there exists no model which can be universally applied, understanding the fundamental and physics behind these models can be helpful. At low frequencies, Boundary Element Analysis (BEM), Finite Element Analysis (FEA) and modal coupling analysis using MATLAB are more appropriate for noise analysis, while at higher frequencies, Statistical Energy Analysis (SEA) provide more reliable results [11]. These models differ significantly in their underlying assumptions, mathematical formulations, and parameter dependencies. The purpose of this section is not to discuss on the details of FE models or reiterate what have already been covered in the work from Ziegner (2023) and Bögle (2024), but rather learn about the parameters, boundary conditions, variables and assumptions employed by each model. The details of the derivation from FE models can be read in [5], [6], [11]. Based on the findings, the requirements and structure of the model will be defined in chapter 5.

1.6.1 Low frequency models

In a region of low-frequency frequency, the Finite Element Method (FEM) is most effective to calculate the response of the structure when a mechanical force or an acoustic field is applied to a closed room or on structures having complex geometries. Softwares for numerical analysis are very popular because they are quick straight-forward to use and easily accessible. In this method, the geometry of the surface (for example the panel of the fuselage) is divided into a discrete number of small elements. For acoustic prediction, FEM uses the Helmholtz equation at the frequency domain to calculate the pressure at each node of the defined element. In vibro-acoustic problems (interaction of structural vibrations with acoustics waves in a fluid medium), the fluid and structural models are

coupled together. This process requires much computational power, memory and time. As the number of nodes increases (more than 50 nodes), the required element size becomes small. This demand for even more computational power and the accuracy of the model decreases. Often, it is more efficient to calculate the structural response using FEM and subsequently determine the radiated sound power using the Rayleigh Integral. The actual distribution of sound pressure distribution within the room can be calculated using the modal coupling analysis (e.g. using MATLAB). [11]

The Boundary Element Method (BEM) is another numerical approach which solves partial equations defining the boundary rather than the entire volume of the element. Unlike FEM, BEM uses the “Green identities” to convert the equation of volume double integral into a sum of integrals over the area. This reduces computational and memory requirements making it more suitable for scenarios involving complex geometry such as the cabin of an aircraft. The physical variables which need to be defined using (direct) BEM are pressure and velocity. Although, solving the equations using the BEM requires less computational capacity compared to FEM, they usually take longer to be solved. Common use of BEM includes prediction of noise inside an enclosed volume, determining noise radiation from a vibrating structure, and analysis of the acoustic field. Figure 3 shows the difference in the mesh and definition of the nodes for the BEM and FEA models. [11]

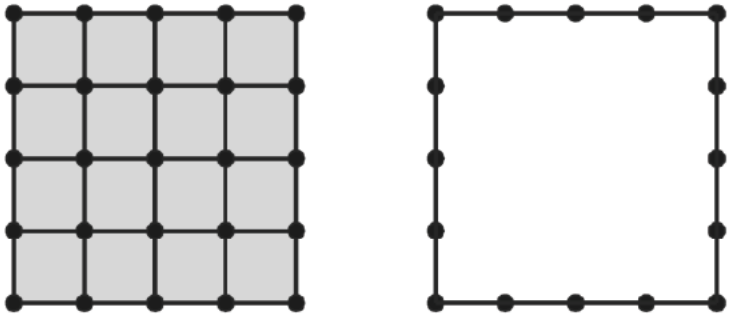

Figure 3: Location of nodes in FEM (left) and BEM (right) [11]

1.6.2 High frequency regions model – Statistical Energy Analysis

In high-frequency regions, the Statistical Energy Analysis (SEA) is used to calculate the vibration and acoustic energy of the system. The total sound power radiated by the structure is the sum of each individual panels or parts making up the structure. The energy distribution among modes in SEA models are given in frequency bands. For a structure of area A, the radiated sound power $W_{\Delta S}$ is given as:

$$W_{\Delta S} = A \cdot \rho \cdot c \cdot \sigma_{\Delta S} \cdot {v^2}_{rms,St\Delta} \qquad 2.1$$

Here ρ is the air density, c is the speed of sound, $\sigma_{\Delta S}$ is the efficiency of radiation for the surface A, ${v^2}_{rms,St\Delta}$ is the mean square surface velocity over the frequency band Δ, A is the surface area and t is the time. The SEA equation for radiated sound power is fundamentally similar to the structure-borne noise power calculation. Both approaches rely on the velocity of the panel and radiation efficiency to estimate the sound power radiated into the cabin. The main difference is that SEA assumes energy is statistically distributed across multiple vibrational modes, while structure-borne noise calculations typically focus on specific paths. SEA works by balancing the energy input, energy storage, and energy loss (through damping) in vibrational modes. It assumes that energy is spread equally across all modes in a subsystem. The method uses Coupling Loss Factors (CLFs) to describe energy transfer between connected parts and Damping Loss Factors (DLFs) to represent internal energy losses. Accurate CLFs and DLFs are essential for reliable SEA

predictions, as they determine how energy flows between panels. However, SEA is mainly effective above 500 Hz and is less reliable at lower frequencies. Below 200 Hz, deterministic methods like FEM are better suited. There is a gap between 200 Hz and 500 Hz where neither method works perfectly, which is why hybrid approaches are sometimes used to improve accuracy. Hence, using only one type of method for every aircraft cabin noise problem is not possible, as the frequency range of the noise sources are very broad. The table below summaries the key features of the different methods:

Table 1: Key features of the FE and SEA models

Method	Frequency range	Parameters	Pros	Cons
FEA	Low to Mid	Mesh density, material properties, ω	Accurate for complex shapes, coupled problems	High computational cost at higher frequencies
BEM	Low to mid	Boundary geometry, fluid properties, ω	Only surface discretisation, good for infinite domains	Time consuming
SEA	High	CLFs, DLFs	Efficient for large, complex systems at high frequencies	Statistical assumptions, less local detail, costly

1.6.3 Existing sound prediction models based of TF

Further research has further shown that each noise problem is unique in its way and depends on factors such as the environmental conditions of the sound field, the physical and acoustical characteristic of the medium, and the material properties through which sound travels[8], [11], [12], [13].The influence of each factor will be thoroughly discussed in chapter 2. During real flight, noise is stochastic, that is random over time and its behaviour cannot be precisely predicted. However, since the positions of the cabin monuments (lavatories, galleys, and seats) and the transmission properties of the skin of fuselage remain relatively stable with frequency of the excitation, predicting cabin noise using TFs is particularly suitable if information on the noise coming from outside is known. In other words, the idea is to perform on ground experiment in acoustic laboratories using random noise to simulate the excitation on the skin of the fuselage. If the input acoustic quantity (pressure, power, intensity, etc) incident on fuselage of the cabin and the transmitted quantity from the receiving surface of the cabin are known or can be determined, the TF is given as follows: [9]

$$x(j\omega) = H(j\omega) \cdot y(j\omega) \tag{2.2}$$

Equation 2.2 shows the linear relationship between the excitation and the response where $x(j\omega)$ is reference vector of the system, $y(j\omega)$ is the response vector and $H(j\omega)$ is the transfer function matrix. [9] Figure 4 illustrates the systematic approach of tackling noise problems using TF.

Figure 4: systematic approach of the transfer function approach to predict cabin noise

To assess the feasibility of this approach, the literature review further explored whether this method has been adopted in any previous work with similar noise issue.

I. Operational transfer path analysis for identifying most dominant paths in vehicle interior

A study based on Operational Transfer Path Analysis (OTPA) was carried out by Putner, (2012) [9] to predict and rank the contributions of various sound sources and transfer paths to interior vehicle noise. Unlike traditional TPA which requires controlled experiment set-ups, the OTPA is based on real operating conditions. The real noise sources were simulated by running a 3-L diesel engine car on an acoustic roller dynamometer. Piezoelectric accelerometers were used to measure the acceleration of structure-borne noise and microphones captured airborne sound (sensors were placed on engine, gearbox, tires, among others). The TFs were then derived using multichannel measurements during various engine operating condition by varying the throttle level. The TFs relate the linear relationship between input excitations and output responses:

$$X \cdot H = Y \tag{2.3}$$

X is the matrix of the reference signal (input degrees of freedom, DoFs), Y is the response matrix and H the transfer function matrix. Since the system was overdetermined, that is the number of measure data point were more than the unknows, the Singular Value Decomposition (SVD) method was applied to solve the matrix by finding the “best possible” solution to minimise the overall error. The engine excitation was varied through different throttle level using an engine control unit, ECU. The results showed good agreement between the measured and synthesised sound pressure levels (SPLs), validating the approach and confirming that OTPA is effective in identifying dominant noise sources and paths under real operating conditions.

II. Study to determine how varying cabin configuration impacts TF

Cho and Chang (2019) further investigated how and if varying the number of passengers in the vehicle influenced the measured TFs [14]. The measurements were conducted inside an SUV placed in a semi-anechoic chamber for different test layouts. The experimental setup can be read in [14]. The results showed a change of $\pm 2\ dB$ in the response of the signal between the different passenger configurations used, confirming a change in the cabin configuration changes its mass distribution and absorption characteristics. While this study did not explicitly investigate how the absorption properties of the cabin changed, the change in dB is due to the fact, that increasing the number of passengers in an enclosed space typically increases the overall absorption surface area (human bodies and clothing). The sound level of the cabin as well as the reverberation time decreases, and less sound is reflected back into the space. The effect of absorption and reflection will be further discussed in Section 2.6. Although this conclusion does not directly apply to aircraft cabins, it is to be highlighted , hat the number of passengers and the cabin layout (mass distribution) should also be taken into consideration when determining the TFs for a specific cabin configuration. The experiment further validated that the linear relationship between the response and the excitation can be used to predict cabin interior noise, as long as the TFs remain constant. This makes the approach of using TFs typically suitable for VIP aircrafts, as the number of passengers travelling will most likely be constant or can changes by no significant deviation. Furthermore, the overall cabin layout remains unchanged throughout its lifespan, ensuring that the derived TFs stay consistent over time. Figure 5 shows the results of the experiment carried out by [9]. Each

signal colour represents a different cabin setup, with the left figure corresponding to the left ear (microphone) and the right figure to the right ear (microphone).

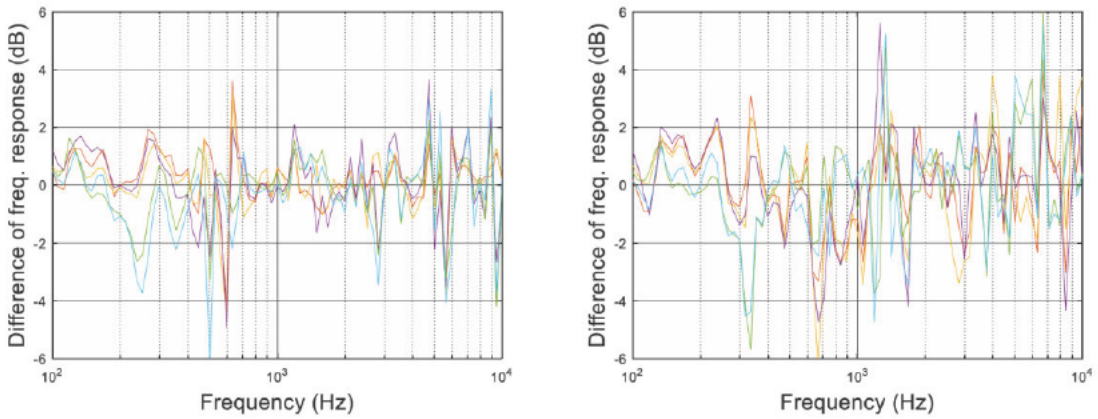

Figure 5: Difference of the response signal [dB] for different configuration. [left: left ear; right: right ear] [9]

III. Simcenter Testlab Transfer path analysis

The Simcenter Testlab is a commercial tool noise and vibration diagnostic tool from Siemens based on the TPA. The tool is also able to identify the dominant transmission paths from noise sources to target locations in complex structures. As the approach is similar to the previous tool, description the method will be omitted. This can be read in [15]. The highlighting part from this paper was how the model breaks down noise problems into: the source, transfer, and target components by creating virtual “cuts” or “splits” between the source and structure. This approach allows users to separate structure-borne and airborne paths and define transmission paths based on the nature of the force transmission. Airborne paths involve acoustic forces that travel directly through the air from the source to the receiver, while structure-borne paths involve mechanical forces transmitted through structural elements such as mounts, frames, or panels [15]. Figure 6 shows how the tool breaks down the source and receiver parts into sections.

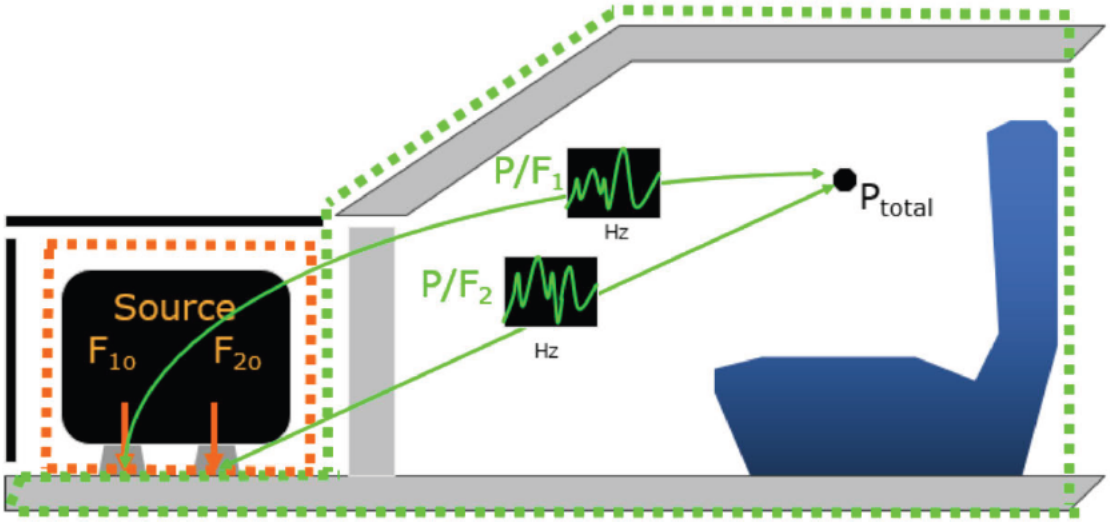

Figure 6: "Cutting" method to separate source and receiver [15]

2 Fundamentals of acoustic

This chapter provides an overview of the fundamentals of acoustics and the mathematical formulas that will be later implemented in the tool to predict sound power. Understanding how noise is created and the mechanisms through which it travels in the air until it is perceived by human ears is essential for the successful implementation of the prediction tool. The chapter also covers key definitions and metrics used to quantify sound.

If a stone is thrown into water, water waves (ripples) spread away from the point where the stone hit the water. Similarly, when an object vibrates, the surrounding air particles oscillate back and forth from their original position. This creates alternating regions of compression and rarefaction, such that the pressure fluctuates, as shown in Figure 7. The sound pressure p depends on the distance from the source and the surrounding environment. For a region, pressure is often given as its root mean square value p_{rms}. The human ears can perceive these sound waves if their frequency lies within the audible range, between 20 Hz and 20,000 Hz. Frequencies outside this range are inaudible to most humans but may still be measured by specialised sensors. [2]

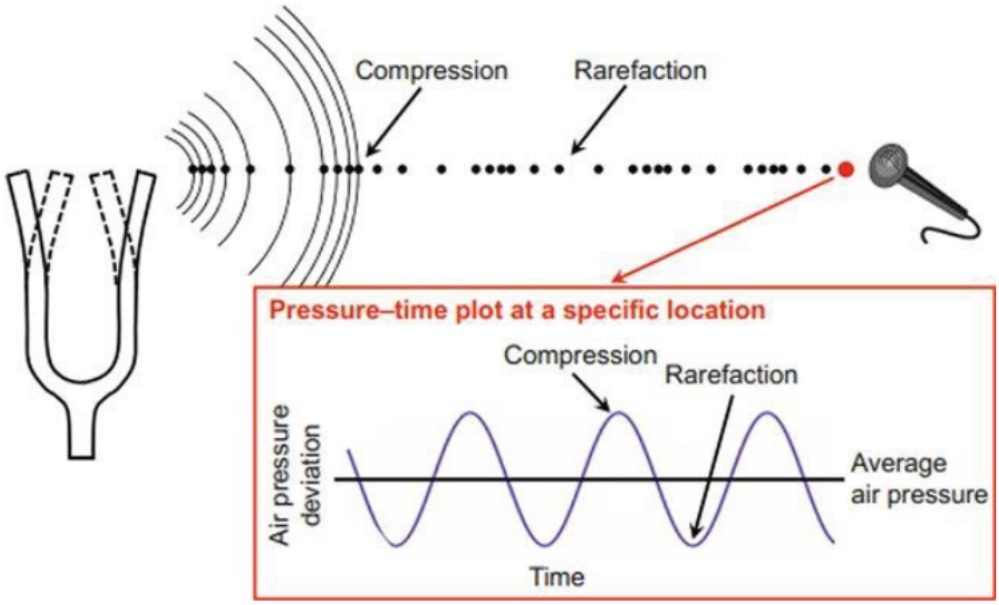

Figure 7: Sound wave with regions of compression and rarefaction [16]

2.1 Sound power

Sound power W is defined as the total acoustic energy emitted by a sound source per unit time in all directions. Power is a natural property of the source of sound and does not depend on environmental factors such density, pressure, temperature within the path of propagation, making it a fundamental measure for noise analysis. On the other hand, sound pressure level (SPL) varies with environmental conditions and distance and the effects of reflection, absorption, diffraction. SPL decreases with the square of the distance from the source. However, sound power cannot be directly measured but instead involves using alternative measurable acoustic quantities such as sound pressure, velocity or intensity. [8]

The total sound power W_S across a finite surface can be derived by integrating the intensity I across the area A: [7]

$$W_S = \int_A I \cdot cos\emptyset \, dA \tag{2.1}$$

Depending on the purpose of the measurement campaigns, there exists different experimental methods, which are standardised through DIN-ISO norms. This will be further discussed in chapter 4. In practice, sound power of a source is commonly expressed in the logarithmic scale as sound power level L_W: [8]

$$L_W = 10 \log\left(\frac{W}{W_0}\right) dB \tag{2.2}$$

W is the power of a source, $W_0 = 10^{-12} W$ is the reference sound power corresponding to the human threshold of hearing. Acoustic measurements data from experiments are very large and not practical to be plotted linearly. Instead, the decibel (dB) is preferred, which compresses the large range of measurements into a more practical scale, making comparisons easier. Similarly, the logarithmic scale for sound pressure level (SPL) L_P in dB is given by: [8]

$$L_P = 20 \log\left(\frac{p}{p_0}\right) = 10 \log\left(\frac{p^2}{{p_0}^2}\right) dB \tag{2.3}$$

Where p is the sound pressure of the source, p_0 is the reference pressure ($p_0 = 20\ \mu Pa = 2 \times 10^{-5}\ N/m^2$ for air) which also corresponds to the average human threshold of hearing. Doubling of the sound pressure, results in an increase of 6 dB in SPL, intensity and sound power.

Sound intensity is the amount of sound power W, transmitted per unit area A, perpendicular to the direction sound travel: [8]

$$I = \frac{W}{A} \quad \left[\frac{W}{m^2}\right] \tag{2.4}$$

Intensity is a vector quantity and can also be given as the product of sound pressure p and the particle velocity v: [8]

$$I = p \cdot v \tag{2.5}$$

The intensity level is used to express sound intensity on the logarithmic scale, relative to the reference intensity, $I_0 = 10^{-12} W$: [8]

$$L_I = 10 \log\left(\frac{I}{I_0}\right) dB \tag{2.6}$$

2.2 Human hearing and psychoacoustics

The study of noise involves consideration of the physical properties of sound and how the human ear perceives it. Figure 8 shows the auditory field of an average young and healthy human being. The lower curve corresponds to the quietest sound that can be heard, while noise beyond the upper curve, causes discomfort and pain in the ears. The sensitivity of

the human ear depends on both sound frequency, which is from 20 Hz to 20 kHz (also 16 Hz to 16 kHz in other references), and also the SPL. At the threshold of hearing, SPL is 0 dB. The upper frequency limit decreases with age and physical condition. Speech occurs mainly between 250 Hz to 6000 Hz or at sound pressure levels between almost 30 to 80 dB. Above 140 dB, discomfort and pain occur [2].

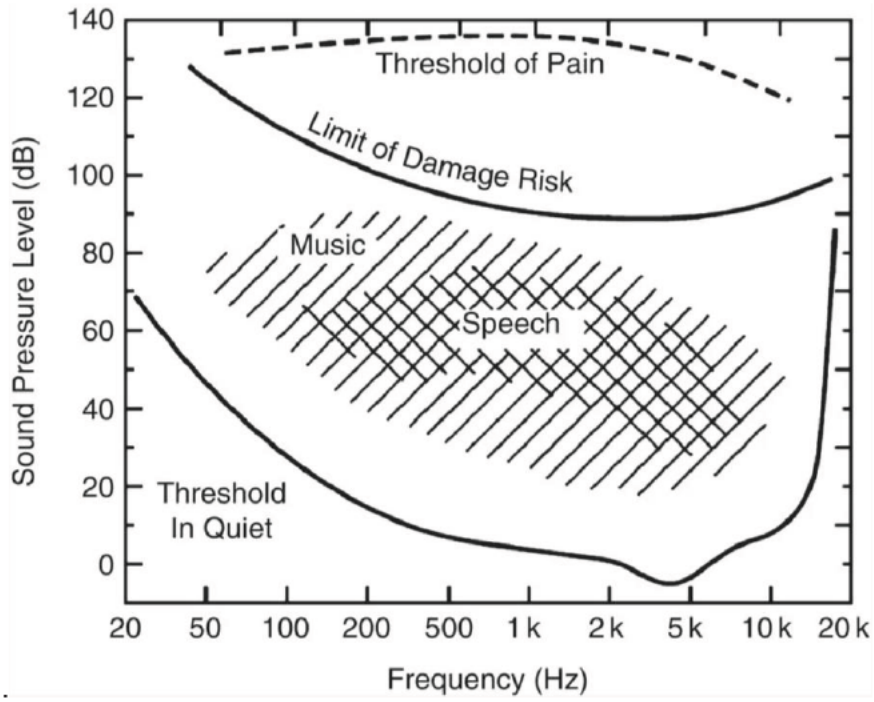

Figure 8: Range of human hearing [2]

Loudness refers to the subjective perception of sound intensity. It is expressed in “phons” and corresponds to the SPL of a 1000 Hz tone. The human ear is more sensitive to mid-range frequencies than to very high and low frequencies [2]. Experience and experiments have shown that doubling the power of a noise source results in an increase of 3 dB in SPL. This is barely noticeable to the human ear. Table 2 illustrates the subjective human perception of noise in response to changes in sound level. [8]

Table 2: Subjective perception of noise to changes in the sound level. Modified from [8]

Change in sound level (dB)	Change in power		Human perception of the change
3	1/2	2	Barely noticeable
5	1/3	3	Clearly noticeable
10	1/10	10	Half or twice as loud
20	1/100	100	Much quieter or louder

2.3 Types of noise and vibration waves

Noise and vibration signals can be divided into stationary and non-stationary. Stationary waves are further divided into deterministic or random noise. Deterministic waves can be mathematically described as a combination of sinusoidal waves with discrete amplitude, for example, vibrations from rotating aircraft engines at constant speeds. Random noises are stochastic such that they cannot be fully described by mathematical functions. Common examples of random noise in aircraft are TBL noise or ventilation noise in aircraft cabins. White noise with constant spectral content is often used in ground acoustic

experiments to simulate random noises. Non-stationary noises are categorised into transient and continuous types. Transient waves are short lasting signals such as noise caused by the overhead compartment closures or abrupt seat adjustments in an aircraft. A non-stationary continuous wave is a wave whose amplitude, frequency, or phase varies with time, such that it is difficult to predict its characteristic in time. [2]

2.4 Sound transmission mechanisms

Sound wave motion involves the transport of mechanical energy with no net movement of mass [2]. The velocity at which air particles oscillate is denoted by v and differ from the speed of wave propagation c. At room temperature, it can be assumed that sound waves travel at a constant speed ($c \approx 340 \frac{m}{s} at\ room\ temp.$) and sound energy travel through air from the source to the receiver. These pathways are known as the airborne transmission paths. Depending on the medium through which sound waves travels, it can be categorised into airborne transmission, fluid-borne sound or structure-borne sound [8]. Fluid-borne pathways are very rare in the cabin and will be omitted. Figure 9 shows how sound from outside (TBL and aero-acoustic noise) enter the cabin through the structure of the fuselage.

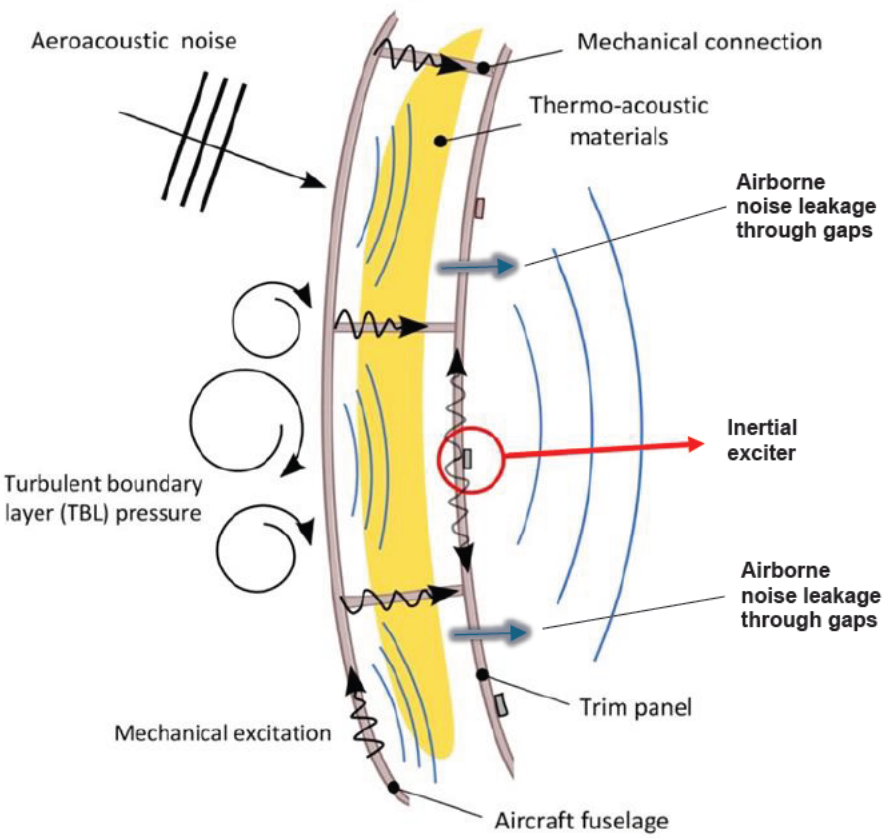

Figure 9: Sound transmission through the fuselage structure [modified] [17]

As the name suggests, airborne sound travels in the air as pressure waves. When an object vibrates, the surrounding air molecules are forced to vibrate too [8]. When airborne sound waves hit solid structures, the sound energy is propagated in the solid structure through the structure-borne sound transmission. This causes the structure to vibrate, and the mechanical vibrations radiate additional noise into the cabin [8]. Together, both the

airborne and structure-borne sound contribute to the overall SPL inside the aircraft cabin. The total sound power emission of a system, for instance the cabin, is therefore the sum of the airborne (ABN) and structure-borne (SBN) components: [8]

$$W_{total} = \sum_i W_{ABN,i} + \sum_i W_{SBN,i} \tag{2.7}$$

While the total noise can only be perceived as airborne noise by the receiver, distinguishing between the type of transmission is necessary for implementing the most appropriate noise reduction measure. This means, the sources and paths of the airborne and structure-borne noises must be separately analysed to identify the "weak points" of the whole system. Figure 10 shows a schematic representation of the transmission paths through which noise enters the cabin.

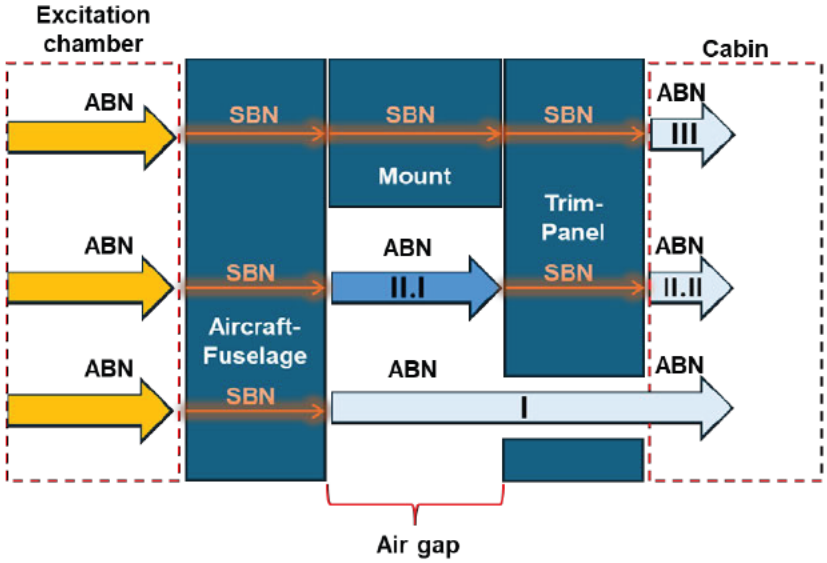

Figure 10: Schematic representation of the sound pathways through the fuselage structure

I. Direct Airborne Path:

Airborne noise (ABN) from outside excites the outer skin of the fuselage to vibrate (SBN). These vibrations radiate as airborne noise (ABN) in the air gap between the layer of fuselage and through the opening in the trim panel. The sound energy then travels as ABN into the cabin to the receiver. Hence, ABN → SBN → ABN.

II. Airborne-Induced Structural Transmission:

Airborne noise (ABN) from outside excites the outer skin of the fuselage to vibrate (SBN). Compared to path I, the radiated airborne noise (ABN) travels into the air gap between the layers and hits the inner side of the trim panel. The sound energy travel as SBN and is finally radiated into the cabin as ABN. Hence, ABN → SBN → ABN → SBN → ABN.

III. Structure-Borne Transmission:

Vibrations (ABN) from external noise sources are transmitted as structure-borne noise (SBN) through the fuselage and mounts. Sound cannot travel through the air gap but instead directly through the mounts to the trim panel, where they "re-converted" into airborne noise as they travel in the cabin to the receiver (ABN). Hence, ABN → SBN → SBN → SBN → ABN.

2.5 Sound fields and sound field quantities

When sound travels in an enclosed space like the cabin, a sound field is created, where the pressure and particle velocities vary. Sound waves interact with the surrounding environment such that the sound propagation will also be influenced by the characteristics of environment and the resistance of the medium. This is known as the acoustic impedance Z of the medium and is given as a relationship between the sound pressure p and particle velocity v in a medium: [8]

$$Z = \frac{p}{v} \tag{2.8}$$

At room temperature, Z is approximately 420 $\frac{Ns}{m^3}$. A fluid with high acoustic impedance has a greater resistance to sound field creation, if the excitations are due to sound pressure. In contrast, when particle velocity excites the fluid, a medium with higher impedance can produce greater sound pressure due to its resistance to particle movement [8]. At cruising altitude (approximately 8000 feet), aircraft cabins are pressurised to ensure passenger comfort [11]. The air density in the cabin decreases to approximately 0,909 $\frac{kg}{m^3}$ [18] resulting in lower SPL (for the same sound power as on-ground measurements). Hence, Z should also be taken into consideration when extrapolating on-ground measurements to real-flight scenarios. Figure 11 illustrates the relationship of sound level with the distance r from the source.

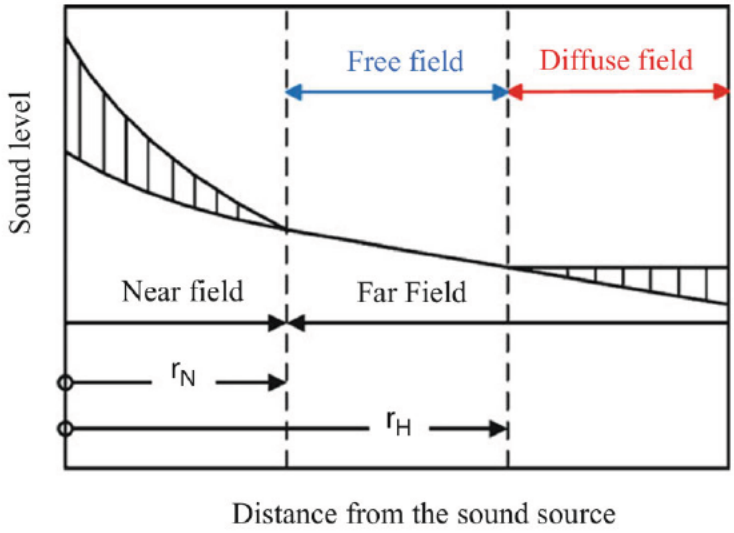

Figure 11: Relationship between SPL and a real sound field[19]

The sound field close to the source of sound is known as the near field. In this region, sound pressure and particle velocity are nearly out of phase. Beyond the near field and up to the reverberation radius r_H, the sound field almost behaves as a free field, in which sound can travel spherically without being reflected by any barriers [2]. The sound coming from the point source will be directly perceived at the receiver and can described using the following equation:

$$p^2 = \rho \cdot c \cdot I(r) = \frac{\rho \cdot c \cdot W_S}{4\pi r^2} \left[\frac{W}{m^2}\right] \tag{2.9}$$

where $p(r)$ is the sound pressure at a distance r (in metres) from a source of power W_S. $Z = \rho c$ is the acoustic impedance of the medium (ρ is the air density and c is the speed of sound). [8]

True free-field conditions are typically rare as the ground will usually reflect sound. In acoustic experiments, the characteristic of a free field is realised in an anechoic chamber where the effect from reflection can be neglected. In contrast, reflection occurs when the sound is interrupted at the boundary surfaces of the room. If the reflection component is large enough, a diffuse field is created such that sound pressure is the same across the room. This occurs beyond the reverberation r_H and depends on sound power of the source and the total equivalent absorption area $\bar{A}_{total}$. In a diffuse field $(r > r_H,)$, the sound intensity at any point is almost the same. At the transition point, that is $r = r_H$, both intensities are equal and can be calculated using as follows:[8]

$$I(r_H) = I_H = \frac{4 \cdot W_S}{\bar{A}_{total}} = \frac{W_S}{4\pi {r_H}^2} \quad \frac{W}{m^2} \tag{2.10}$$

The reverberation radius r_H as well as $\bar{A}_{total}$ are frequency dependant. In practice, a reverberation room is used to create a diffuse field using broadband noises. Higher frequencies sound (shorter wavelength) are absorbed more effectively, increasing $\bar{A}_{total}$ and reducing r_H. [8]

2.6 Sound reflection, absorption and transmission in a closed room

When a sound wave is incident on a surface, the incident sound energy is divided into 3 different components: reflected energy, absorbed energy and transmitted energy, as shown in Figure 12.

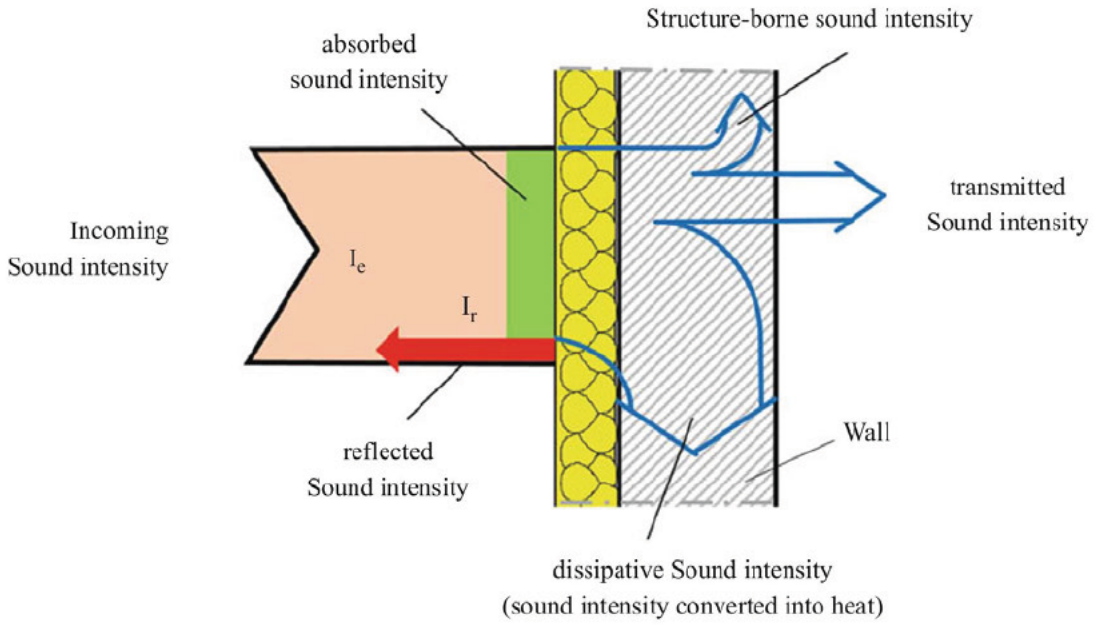

Figure 12: Mechanism of sound intensity transmission through a barrier[19]

The absorbed energy will be ultimately dissipated as heat in the wall. Transmitted energy passes through the wall and is radiated as airborne sound. Structure-borne sound energy excites the wall itself, causing vibration. A portion of the incident energy is reflected back into the air in front of the wall. The absorption capacity of the wall depends on its absorption coefficient α_i and the total surface area S_i. As mentioned earlier, the absorption capacity the passengers must also be taken into consideration. The equivalent absorption area for monuments with regular shapes can be calculated using equation 2.11. However, this might be difficult to determine if the room consists of objects with irregular geometry. In

this case, $\bar{A}_i = \alpha_i \cdot S_i$ is estimated based on experience. For instance, a seated passenger has an equivalent absorption area, $\bar{A}_{passenger}$, of 0,3 m^2 at a frequency of 250 Hz [8]. Hence the total equivalent absorption area $\bar{A}_{total}$ of an enclosed room with objects and persons is:

$$\bar{A}_{total} = \sum_{i}^{n} \alpha_i \cdot S_i + \sum_{i}^{m} \bar{A}_j \ [m^2] \qquad 2.11$$

Where n is the number of regular surfaces and m the number of irregular objects. In a VIP aircraft, $\bar{A}_{total}$ can be determined by measuring the reverberation time, T and solved using the Sabine's equation 2.12 [8]. This is a more reliable approach as estimating values for $\bar{A}_j$, α_i and the absorption of passengers is challenging, where , $T = T_S$ is the reverberation time, V is the volume of the room in m^3, and the constant value 0.163 $\frac{s}{m}$ applies if the air.

$$T = T_S = 0.163 \ \frac{s}{m} \cdot \frac{V}{\bar{A}_{total}} \cdot S \qquad 2.12$$

2.7 Transmission through multi-layer and transmission loss

According to the mass law, increasing the mass of a panel, results in an increase of the value of sound transmission loss (TL): As a rule of thumb, TL of a panel increases by 6 dB if its mass is doubled [3]. However, this cannot be blindly done due to the weight and space constraints in aircraft. Subsequently, there exists alternative panel designs which consists of double or triple layers. This is a cost-effective approach for achieving high TL values with relatively less weight in the aircrafts. The values of the TL can be further enhanced using acoustic absorptive materials, to reduce reflection and transmission of sound waves, in the air gaps between the layers. However, one problem which may arises with such a design is the so-called mass-air-mass resonance phenomenon. This occurs at the resonance frequency when the air gap between the panels behaves like a spring. At this frequency, both panel layers will be dynamically coupled and move out of phase. Subsequently more noise will be transmitted into the cabin [3]. The ratio of the transmitted sound intensity I_τ to incident sound intensity I_ϵ is known as the transmission coefficient τ, which is a measure of the reduction in sound energy as it travels through a barrier [8].

$$\tau = \frac{I_{transmitted}}{I_{incident}} = \frac{P_{transmitted}}{P_{incident}} \qquad 2.13$$

It is worth highlighting, that the transmission coefficient τ is analogous to the TF as seen in section 1.6.3, as both relate how effectively sound energy is transmitted through a barrier. This will be further discussed. In practice, this is often given in dB, known as the transmission loss index, TL (or sound reduction index, R_i in some literatures). For a single-layer panel isotropic (same material properties in all directions) with a uniform cross-sectional area, the mass law is used to determine the transmission loss, TL: [8]

$$TL = 10 \ \log_{10}\left(\frac{1}{\tau}\right) = 20 \cdot \log_{10}\left(\frac{\omega \cdot m}{2 \cdot p_0 \cdot c}\right) \qquad 2.14$$

Herein $p_0 \cdot c$ is the impedance Z, ω is the frequency of the wave for ($\omega \gg \omega_0$), and m is the mass per unit area of the partition. The incident sound waves are assumed to be normal to the surface of the panel. At low frequencies, double-panel partitions behave like a single panel of an equivalent total mass. However, as the frequency increases, the coupling effect in the air gaps also increases [3]. To compensate the increase in TL, equation *2.14* is modified by including the resonance amplification factor V (second term

in equation 2.15). For a double layer partition, the TL can be determined as follows if the natural frequency of the system is known, the TL can be calculated using equation 2.15:

$$TL = 20 \cdot \log_{10}\left(\frac{(m_1 + m_2) \cdot \omega}{2 \cdot \rho \cdot c}\right) + 40 \cdot \log_{10}\left(\frac{\omega}{\omega_0}\right) \quad 2.15$$

However, predicting the TL solely using equation 2.15 can be challenging. This is due to the complexity aircraft cabin, which consists of several monuments (seats, insulation panels) and passengers. As a result, the predicted TL will be inaccurate. The equation assumes ideal conditions, such as fully decoupled walls, isotropic materials and uniform size of the air gaps, which do not always apply in the reality. The natural frequency ω_0 is crucial when determining the resonance effects. While ω_0 itself depends on the material properties, dimensions and the coupling effect, this makes it difficult to measure or predict. Moreover, the air gap between the panels acts like a "spring", whose stiffness largely depends on the size of the gap [3]. The position of the cabin monuments might introduce additional sound transmission pathways, diffraction and absorption which are not taken into consideration by the equation. Finally, installation methods and boundary conditions, such as clamped or free edges as well as structural reinforcements or mounts in the panels also influence the TL and cannot be neglected. Although using equation 2.15 value is a useful theoretical approach, it should be noted for future reference that a more practical method of deriving TL is through experimental measurements. As established, the TF is also linked to the transmission coefficient, τ. This means that these findings are likely to be equally applicable to TFs (further discussed in section 4.1)

2.8 FFT, octave and third octave-filters

The Fourier Transform is an essential tool in acoustic and vibration analysis, which enables the transformation of time domain signals into the frequency domain. For noise and vibration analysis, knowing only the overall SPL or power level is not enough. In real-world situations, sound waves are not pure sinusoidal waves but complex waveforms consisting of multiple simple harmonic or random noise which are complex to be mathematically described. The Fourier Transform decomposes complex signals into their fundamental frequency components, making it easier to be analysed. The computation and interpretation of finite Fourier transform functions (FFT) are carried out using digital computers, which is able to break down a signal into a series of discrete frequency components knows as the FFT lines. These lines represent individual frequencies within the spectrum and are crucial for precise acoustic measurements [2].Figure 13 shows how a sinusoidal sound wave is transformed into its frequency domain signal.

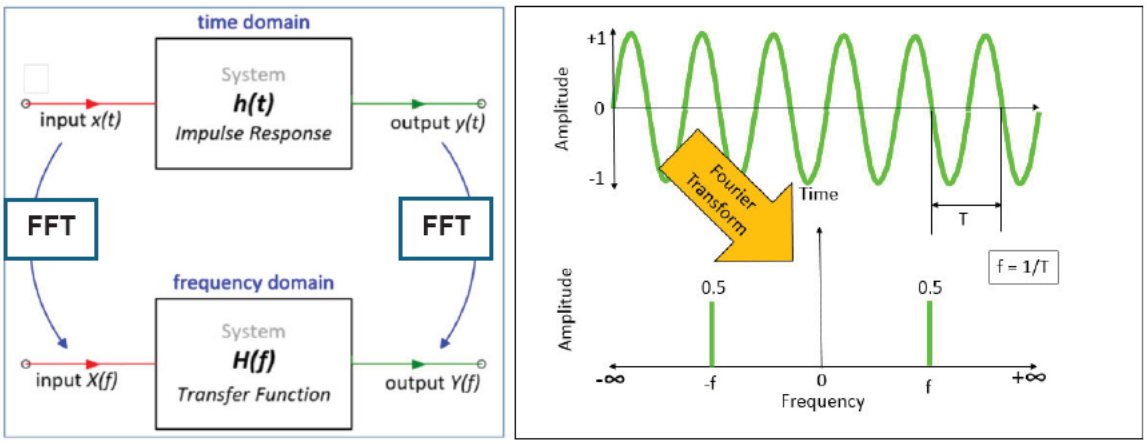

Figure 13: Schematic diagram showing transformation of time domain signal into frequency domain signal [20] [21]

A better and more practical method to analyse noise is to divide the frequency range into broader intervals using constant frequency band filters. If fine frequency is not required, high-resolution measurements like FFT are unnecessary as it provides no meaningful information. Measurements in broader bands are more reproducible [8]. Moreover, since white noise is used cabin interior noise experiment, spectral details are irrelevant and not practical. Hence, the audible frequency range is logarithmically divided into larger intervals using filters with a constant relative bandwidth. The most common filters used in cabin tests are the octave filter and the third-octave filters. The bandwidth Δf is difference between the upper frequency f_u boundary and the lower frequency f_L.boundary. Δf is therefore proportional to the middle frequency f_m, and can be determined as follows: [8]

$$f_m = \sqrt{f_u \cdot f_L}$$

2.16

The octave scale consists of 10 steps, with each step doubling the frequency as shown in Figure 14 (left), whereas a third-octave band divides an octave into three equal logarithmic parts. [19]

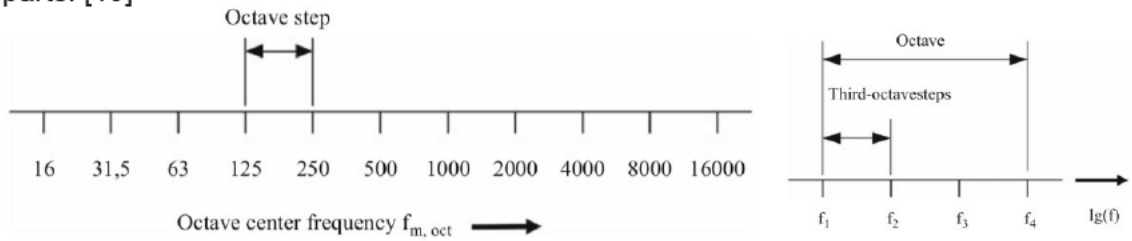

Figure 14: Octave scale (left), illustration of third-octave steps (right) [19]

When converting FFT spectra into third-octave or octave bands, spectral lines are aggregated using quadratic summation rather than simple arithmetic averaging. This approach ensures an accurate representation of the energy content within each band. Quadratic summation treats each FFT line as an independent contribution and calculates the total pressure by summing the squares of individual values and taking the square root of the result. Mathematically, this is expressed as: [22]

$$p_{octave} = \sqrt{\sum_{f_u}^{f_o} {p^2}_i(f)}$$

2.17

Herein, p_{octave} is the total sound pressure with the octave band in $[pa]$, ${p^2}_i$ is the SPL of each FFT line within the band and f_o, f_u are the upper and lower boundary limit respectively.

2.9 Fourier Transformation and Frequency Response Function

For acoustic and vibro-acoustic systems in the frequency domain, the Frequency Response Function (FRF) or Transfer functions (TFs) are used determine to analyse how a system respond to an input force or sound pressure. For of a linear and time-invariant system this relationship can be expressed as the ratio of the output to the input. In general, the system is excited by a periodic and complex signal, $x(\omega)$. The response $y(\omega)$ will of

the same frequency but consists of an amplitude response and phase response $(\varphi_y - \varphi_y)$. The FRF or TF, $H(\omega)$ shows the relationship between the output and input signal:

$$H(\omega) = \frac{y(\omega)}{x(\omega)} e^{i(\varphi_y - \varphi_y)} \quad 2.18$$

In noise path analysis within aircraft cabins, FRF or TFs are common and practical methods for identifying dominant transmission paths by characterising how sound energy propagates from outside into the cabin. The peaks of the FRFs correspond to the resonant frequencies of the structure, and the width of these peaks describe the damping characteristics of the system. [23]

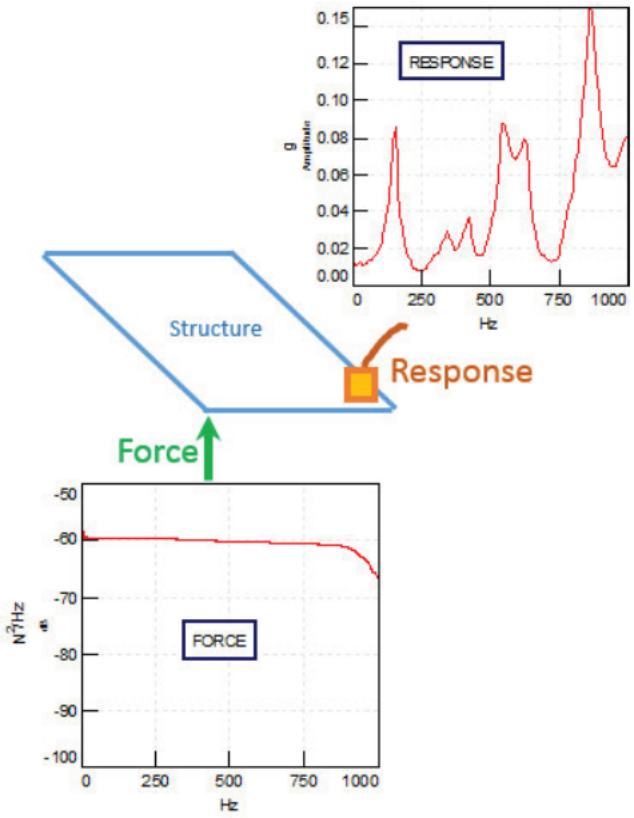

Figure 15: A force FRF to determine response and resonant frequencies of a structure [23]

Complex TFs can be calculated using computer and FFT to convert time-domain signals Depending on the measured quantities, there exists different types of TFs. While an amplification function (Verstärkungsfunktion) can only relate identical quantities (displacement or pressure), the FRF can also relate different physical quantities such as force and displacement or sound pressure and velocity. In more complex systems, Multiple Input Multiple Output (MIMO) transfer functions consist of matrices of individual FRFs, describing the effects of multiple input points on multiple output points. Specific types of transfer functions include compliance (displacement to force), mobility (velocity to force), and inertance (acceleration to force). [24]

In acoustic engineering, power-to-power TFs are employed to quantify how input sound energy is transmitted through barriers. This gives a clear and direct depiction of energy transfer in terms of power, enabling engineers to understand acoustic respond of materials and structures across a broad frequency range. For instance, by comparing TFs before and after the addition of mass layers, insights can be gained into how effective the noise control measure is.

3 Aircraft acoustic

Cabin noise is a natural by-product of flight which is generated from various sources, found both inside and outside the cabin. Analysing noise in a complex environment such as an aircraft, requires the consideration of multiple interconnected factors, rather than treating them in isolation. These factors include the type of aircraft, the operational conditions, the duration of the flight and the phase of flight. While noise during take-off and landing may exceed cruise levels (jet engine can reach up to 120 dB), it is acceptable due to the short duration. Long-duration commercial flights (12–16 hours) require stricter noise control due to prolonged exposure to noise [25]. This section deals with the current state of technological advancements in acoustic within the aeronautical and aircraft industries and aim to provide a deeper understanding of the sources of sound in aircraft cabins, their propagation pathways, and the state-of-the-art sound insulation measures employed in modern VIP aircraft.

3.1 Sources of noise in the cabin

As mentioned, aircraft noise can be categorised as internal and external noise sources. External noise includes engine noise and external aerodynamic flow, most precisely, the turbulent boundary layer noise (TBL). Additionally, onboard equipment inside the cabin further contributes to overall interior noise levels

3.1.1 Engine noise

Engine noise is generated by the fan, turbine, compressor, combustor, exhaust jet, and the pressure fluctuations during the mixing of the exhaust jet with the bypass airflow and is particularly critical during taxi and climb. Depending on the aircraft layout, flight characteristics, and engine type, cabin noise levels can vary considerably. For the purpose of this work, only aircraft propelled by turbofan engines will be considered.

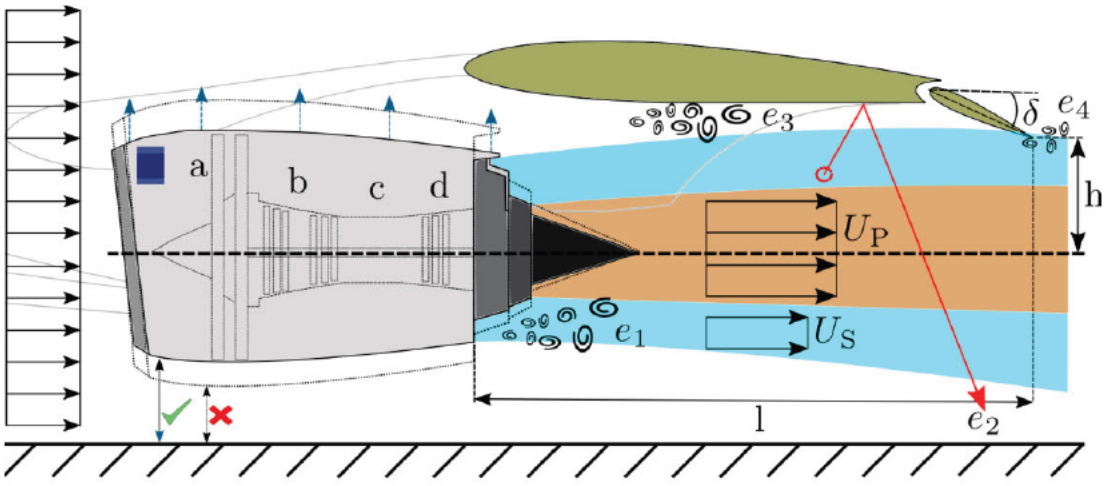

Figure 16: Schematic showing the principal engine noise sources of a turbojet engine[26]

a is the fan noise, b compressor noise, c combustion noise, and d turbine noise. The noise sources created by the exhausted jet are e_1 jet mixing noise, e_2 jet surface reflection noise, e_3 jet scrubbing noise and e_4 jet surface interaction noise

Turbofan engine noise consists of turbomachinery noise and jet noise. Turbomachinery noises occur inside the engine, from the fan, compressor, turbine, and combustion processes, whereas jet noise is produced outside the engine due to shear stresses caused

when the hot core mixes with cold bypass and ambient air. This mixing noise occurs when the jet operates at subsonic speeds (Mach number less than one) [26]. This noise is broadband and is generally more significant during take-offs and climb, whereas fan noise is discrete. At high cruise speeds, fan noise inside the cabin is usually negligible and only critical at low speed. The engine vibrations forces are transmitted through the engine mounts into the fuselage, which radiate as sound into the cabin. [13]

3.1.2 Turbulent boundary layer noise

The turbulent boundary layer noise (TBL) arises from pressure fluctuations caused by airflow interacting with the aircraft fuselage, landing gear, wings, high-lift devices, and stabilisers. At cruising conditions, TBL pressure fluctuations acting on the fuselage surface are the most dominant source of interior noise. These fluctuations exert forces on the fuselage, causing the skin to vibrate and radiate noise into the cabin. The fuselage acts as a “transducer”, converting external vibrations into acoustic energy [12]. which are transmitted into the cabin via airborne or structure-borne pathways. TBL noise are random noise, that is they are independent of time and space. A continuous spectrum with a near-normal amplitude distribution is observed near the fuselage wall. The surface roughness also influences pressure fluctuations, explaining why modern aircrafts consist of smooth fuselage skin. [26]

3.1.3 On-board equipment noise

Cabin noise can also originate from internal systems within the cabin itself. An aircraft cabin consists of the air conditioning, hydraulic, and electrical systems which emit noise. Noise from the air conditioning system comes from the exhaust valves, turbo-coolers, fans and the ejectors. Moreover, aircraft cabins are mandatorily designed with openings to maintain and regulate cabin pressure during changes in altitude [26]. This is a game changer in the overall cabin acoustic if noise from outside enters the cabin. This noise is particularly loud as it is often unattenuated as energy is not lost through absorption reflection. Therefore, the layout and positioning of the on-board equipment should be mutually designed in relation to the passenger area in order to achieve the best possible acoustic comfort in the cabin. Figure 17 shows the contribution of the different sources of noise during take-off and approach.

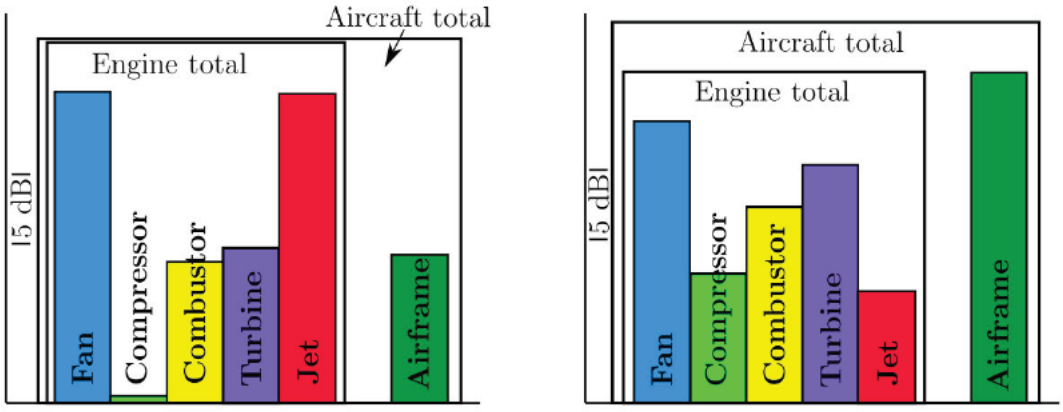

Figure 17: Noise component breakdown during take-off (left) and approach (right) of a commercial aircraft, fitted with a Rolls Royce Turbofan engine[26]

Table 3 shows the acoustic characteristics of the different source of noise in the cabin. Modified from [13]. Here the transmission mechanism of each source of noise is particularly of interest.

Table 3: Acoustic characteristics of the different source of noise in the cabin.

Noise source	Frequency characteristics	Main transmission path
A. Propulsion System		
Jet exhaust	Broadband	Airborne: Fuselage-sidewall
Fan	Discrete	Airborne: Fuselage-sidewall
Engine vibration	Discrete	Structure-borne: Engine mounts
Wing vibration	Discrete	Wing structure
B. External aerodynamic flow		
Turbulent boundary layer (TBL)	Broadband	Airborne: Fuselage sidewall
Separated flow	Broadband	Airborne: Fuselage sidewall
Air-mixing	Broadband	Airborne: Fuselage sidewall
C. On-board equipment		
Hydraulic system	Discrete	Structure-borne: Floor
Electrical system	Discrete	Structure-borne: Floor Airborne: Cabin
Air-conditioning	Broadband/ Discrete	Airborne: Duct
Auxiliary Power Unit	Discrete	Structure-borne: Mounts

3.2 Parameters influencing the sound pressure level during flight

As previously discussed, the overall sound level in the cabin is influenced by different sources of noise. This is the “excitation” which causes structural vibrations and radiate as sound waves into the cabin. The broadband exterior pressure field caused by the TBL depend on various parameters which vary over time and the flight phase, and the aerodynamic parameters (dynamic pressure q and the shear stress τ_w), true airspeed (TAS), flight level (FL) and thickness of the boundary layer δ. TAS is the actual speed of the aircraft relative to the air through which it is moving [27]. The relationship between exterior pressure fluctuations and interior sound levels depends on the ability of fuselage structure to transmit vibrations. This is influenced by the material impedance of the fuselage (mass, stiffness, and damping of the fuselage) and its joint acceptance, which is the resistance of the structure to external pressure fluctuations [13]. Moreover, cabin pressurisation and change in temperature causes strains in the panel which influences transmission paths and the velocity at which the panel vibrates. If the external pressure matches the natural frequency of the structure, aerodynamic coincidence occurs. Subsequently, the joint acceptance increases such that coupling occurs causing the interior noise levels to increase.

3.3 Approaches to Noise Control

Effective noise control in aircraft requires a comprehensive understanding of noise sources and their propagation mechanisms. The goal is to mitigate unwanted sound energy before it reaches the receiver. Noise control strategies can be classified into two categories: noise control at the source and noise control along the transmission path. Noise control

measures at the source reduce the creation of noise [13]. On the other hand, noise control along the transmission path focusses on isolating or absorbing sound energy from entering the cabin. This involves structural modifications, such as optimising the mass, stiffness, damping properties and impedance of the fuselage and the panels. Furthermore, engine and structural vibrations can be isolated using acoustic absorption materials, vibration isolators and dynamic absorbers [13]. In order to achieve the lowest possible SPL in the cabin, a combination of noise control strategies at both the source and transmission path is required. However, modifying noise control at the source can be challenging, especially for VIP aircraft configurations as the number of aircraft with a specific configuration is very low. Interviews with stakeholders revealed that implementing transmission path noise control measures on existing aircraft platforms with OEM engines and structural fuselage properties are the most cost-effective and practical approaches. This is achieved through two primary approaches namely active and passive noise control measures.

Active control measures use sensors and actuators to reduce noise or vibrations by generating counteracting sound waves or forces in real time. This approach relies on destructive interference, where the primary noise field is cancelled by an inverse secondary field [2]. Since this thesis rather focuses on passive noise control, the specifics of active noise measure details will not be addressed. On the other hand, passive noise control targets the airborne and structure-borne path transmission of the sound energy, using light weight damping materials, sidewall treatment and using passive dampers between joints. The aircraft structures and surfaces are excited into vibration by mechanical forces from the noise source. To reduce this, damping and porous materials are used, converting mechanical energy into heat. One method of noise tackling noise along the transmission path is the so called “sidewall treatment”, where damping materials are strategically placed on the structure of the fuselage to reduce noise transmission. Common materials include honeycomb panels, glass fibre batts, impervious septa, and cabin trim panels [2]. Figure 18 shows one way of how damping materials can be placed on the fuselage structure. This method is also known as a “stacked” damper system, which is placed between the stringers and frames [2]. Since material properties are temperature-dependent, it is crucial that the damping characteristics of viscoelastic materials remain stable at low temperatures. Any significant change in material properties will affect the derived TF, making it unreliable for predicting noise transmission accurately.

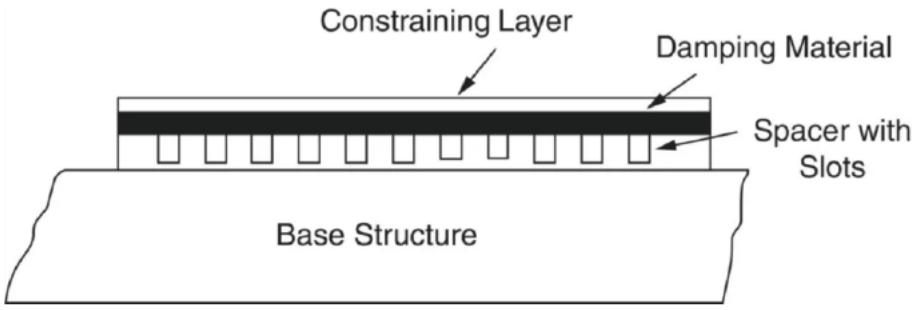

Figure 18: Stacked constrained layer damper system [2]

Figure 19 shows a simple cross section of a double-wall structure with an air gap between two panels. The air gaps may be partially or fully filled with porous material [13]. The thickness of the fiberglass batts (porous material) depends on the space available between the circumferential frames of the fuselage while the weight of the trim panel (interior covering of sidewall) is kept as low as possible. In order to improve sound transmission loss at low frequency, heavy materials such as lead-impregnated vinyl are often used [13]. However, this impacts the fuel efficiency of the aircraft. In aircraft cabins, the sound pressure level is influenced by the absorption properties of galleys, sidewall panels, seats,

carpets, partitions as well as the passengers. Lightweight materials such as viscoelastic layers, foam, and fiberglass, have good absorption characteristics and ability to dissipate vibrational energy. Porous materials like fiberglass are widely used in aircraft due to their ability to absorb sound across a range of frequencies. The advantage of absorption is that the absorptive material can be placed at various locations, near noise sources, along transmission paths, or close to the receiver. [2]

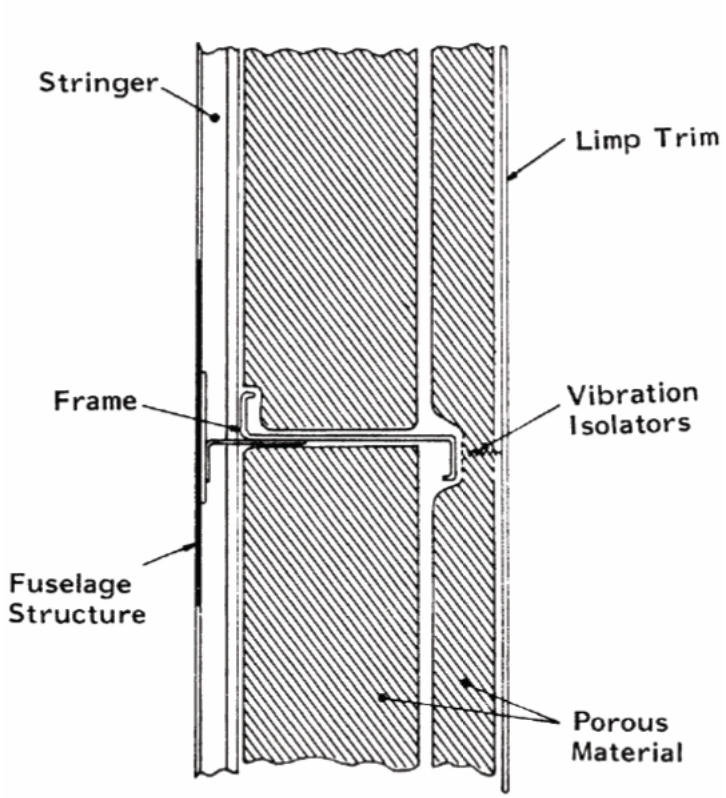

Figure 19: Cross-section through a typical sidewall treatment [13]

3.4 Aircraft layout

The development of VIP aircraft cabins represents a fusion of luxurious individuality and highly specialised technical requirements. These cabins, designed exclusively for private individuals or business professionals, differ significantly from the standardised interiors of commercial aircraft. While regular airplane cabins focus on being efficient, lightweight, and easy to maintain for airline needs, VIP cabins focus on custom designs, great comfort, and unique style. A defining characteristic of VIP cabin design is the use of premium materials and the ability to personalise interiors according to the preferences of the client. These cabins often have workspaces, lounge areas with fancy furniture, private bedrooms, meeting rooms, and even spaces for dining or exercise. Materials such as leather, fine fabrics, and specialised glass wool are selected to deliver a sense of visual sophistication. Adding these features needs both creative design and careful following of strict aviation rules. For example, all materials must meet rigorous certification standards for fire resistance and durability under significant stress and acceleration. These regulatory constraints demand innovative solutions to meet the custom needs of clients. Acoustic optimisation is another defining feature of VIP cabins, significantly enhancing their comfort and exclusivity. Unlike standard cabins, where practicality and weight considerations prevail, VIP cabins also prioritise the acoustic environment. This is achieved through the strategic use of materials and structural designs that absorb sound and reduce noise levels. Commonly used materials include thicker glass wool and additional mass layers

integrated into cabin walls, effectively reducing the transmission of engine and aerodynamic noise. Furthermore, insulating mats, specialised carpets, and sound-absorbing panels enhance acoustic quality while maintaining the luxurious appearance of the cabin. Another technical feature in VIP cabins is the dado panel, designed to enable rapid pressure equalisation during cabin depressurisation. While this feature is purely functional in standard cabins, VIP configurations often elevate it with sound-absorbing materials to improve both its visual appeal and functional efficiency. This illustrates how even safety-critical components in VIP cabins can be integrated seamlessly with elegance, without compromising their primary purpose. A comparison between the standard cabin and the VIP cabin is shown in the following figure. [3] [5] [28]

Figure 20: Standard cabin layout [29]

Figure 21: VIP cabin layout [28]

4 Metrology and methodology in the determination of sound power

This section describes how sound can be measured and an approach to include the measurements in a tool for determining sound energy transmission from the source to the cabin. The A-weighted sound power level is a critical acoustic metric in acoustic design which involves analysing how much power is emitted from the source and how much is transmitted into the cabin. Sound power level is derived from the sound pressure level or sound intensity level measurement according to the DIN EN ISO 9614-2 [8]. These measurements are typically carried out using acoustical and vibration sensors, which convert physical phenomena (e.g. pressure fluctuations or vibration) into electrical signals. The signals can then be processed and filtered [2]. Outside the cabin, SPL is typically measured as a function of sound pressure $[Pa]$, to quantify the sound excitation acting on the fuselage panels. This represents the input energy and is measured using condenser microphones which capture the pressure fluctuations in the acoustic chamber. Inside the cabin, sound intensity I is measured to assess the actual radiated sound power from panels, capturing directional energy flow and identifying dominant paths more effectively than pressure measurements. The sound intensity I is measured using a sound intensity probe, which consists of two condenser microphones placed a very small distance apart. The sound intensity measurement is based on measuring the pressure difference between the two microphones, the mean pressure, and the distance between the two microphones [8]. Would structure-borne vibration be of concern, this can be measured using piezoelectric accelerometers which measure the accelerations of the vibrations [8]. Therefore, the main parameters which are typically measured during noise analysis measurements in real-world scenarios, such as in an aircraft cabin, are sound pressure $[Pa]$, sound intensity I $[\frac{W}{m^2}]$, acceleration $[\frac{m}{s^2}]$, or velocity $[\frac{m}{s}]$. The next section describes the measurement campaigns which were carried out at the HCAT.

4.1 Intensity measurement campaign (M002) at the HCAT

This section summaries the measurement campaign (M002) which was conducted in the cabin demonstrator at HCAT. The experiment was carried out by Ziegner (2023) and further details can be read in [5]. The main purpose of the experiment is to identify the most dominant sound transmission paths from the source to the cabin. Analysing the results of this experiment is important, as the measurements will (i) later be stored in the database of the tool (ii) to predict sound power in the cabin and (iii) validate the ability of the tool to predict sound power. Moreover, for the development of the tool and the database, it is important to know what was measured, the raw data collected, and the range of parameters involved. The experiment was closely aligned to the DIN EN ISO 9614-2 with a few deviations to ensure that real flight measurements were simulated. As summarised in Table 3, TBL and engine noise acting on the skin of the fuselage are broad-spectrum random noise. As per the DIN ISO 3741 white noise are used in sound power experiments to simulate random noise, as they naturally distribute energy evenly in all spatial directions [30]. In the set-up (Figure 22), this was achieved using multiple $800W$ dodecahedron loudspeakers to create a diffuse acoustic field. The speakers were strategically positioned in the room, at varying heights, on both side of the fuselage allowing the sound fields to be overlapped. After some time, the sound waves were sufficiently mixed through multiple reflection from the walls of the room and the skin of the fuselage, such that it could be assumed that the pressure across the room was the same in all directions. Assuming a diffuse field was then validated by measuring the sound

pressure levels close to the outer skin of the fuselage (at about 10 cm). Figure 22 shows the experiment set-up of the excitation field in the acoustic chamber.

Figure 22: Experimental set-up with 4 dodecahedron speakers, 2 IQ12 speakers and 2 speakers [31]

For a diffuse field, the incident sound intensity on the skin of the fuselage panel can be calculated from the sound pressure and the characteristic impedance Z of the medium. For this specific experiment, the sound pressure in $[Pa]$ can be derived from the SPL measurement using equation 2.3. ${p_{rms}}^2$ is the space average mean square of sound pressure, ρ is the air density and c is the speed of sound: [2]

$$I_{incident} = \frac{{p_{rms}}^2}{\rho \cdot c} \qquad 4.1$$

Inside the cabin, the cross section of the fuselage was divided into 13 sections as shown in Figure 23. The sound intensity for each section was measured using an intensity probe with two phase-matched microphones, placed 10 cm away from the panel surfaces. This was repeated horizontally or vertically across each panel so that the complete area of the panel is covered. In this case, it was ensured that measurement inaccuracies due to tilting of the probe were within $\pm 0.6\ dB$. Using this approach, the dominant sound transmission paths could be identified. To prevent the effect of excessive background noise and neighbouring transmission paths from other panels, a foam-lined box (intensity box) was used to shield the probe in experiment M002. Unlike the sound field of the excitation chamber, the acoustic field of the cabin is reverberant and characterised by a combination of acoustic phenomenon including reflection and absorption. The SPL of the room (cabin) can be determined as follows: [8]

$$L_{P,\ cabin} = L_W - 10 \cdot \log_{10} \frac{\bar{A}_{eq}}{S_0} + 6 - K_0\ \ dB \qquad 4.2$$

Where, $L_{P,cabin}$ is the SPL of the cabin, L_W is the transmitted sound power, $\bar{A}_{eq}$ $[m^2]$ is the equivalent absorption surface area of the room and S_0 is the reference area typically 1 m^2, K_0 is the correction factor for the characteristic impedance and the 6 dB is a correction factor for SPL. [8]

Segment/Panel	Größe [m²]
1. Floor Panel Inboard	0,53
2. Floor Panel Middle	0,53
3. Floor Panel Outboard	0,47
4. Dado Gap	0,06
5. Dado Panel	0,42
6. Lower Sidewall Panel	0,55
7. Window (-Panel)	0,20
8. Upper Sidewall Panel	0,55
9. ECS Gap	0,03
10. Closure Panel	0,42
11. Service Area Panel	0,41
12. Ceiling ECS Gap	0,05
13. Ceiling	0,53

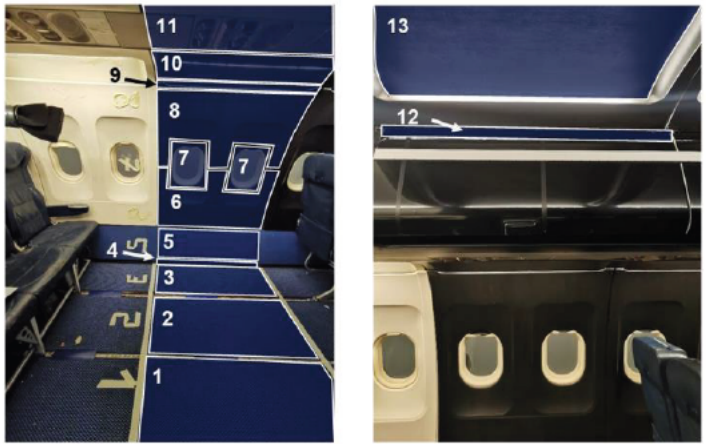

Figure 23: Segmentation of the fuselage [5]

Until now, STL experiments have been limited to considering only a single transmission path, from the source to the receiver. In Ziegner's model, the partition, panel, or fuselage layer is treated as a "black box," and the STL is calculated applying the mass law. However, this approach does not account for internal transmission paths within the multi layers panels and does not fully consider the frequency-dependent behaviour of the material properties. While this approach is mostly suitable in the mid frequencies, it becomes less accurate at very low and higher frequencies due to mass-resonance effects, coincidence frequencies, and the superposition of reflected sound waves. By breaking down the single transmission path into its respective "sub" airborne transmission paths, it will be investigated if the accuracy of the noise analysis can be improved. To address this, the experiment will be modified to incorporate the additional "subs" airborne transmission paths. This will be explained in the next chapter. Figure 24 demonstrates the schematic approach of determining the STL factor based on the Ziegner's Model [5].

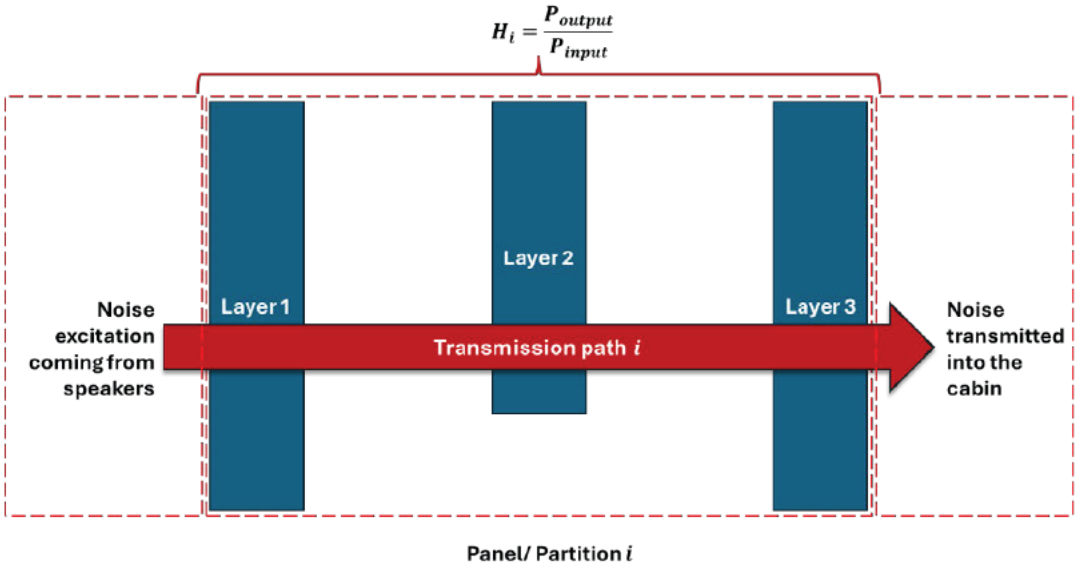

Figure 24: Transmission path approach based on Ziegner's Model

4.2 Methodology and approach to consider sub transmission paths

Using the knowledge gained until now and building on the insights from experiments carried out by Ziegner, this section discusses on the methodical approach that will be adopted for modelling and developing of the sound power prediction tool. The main objective is to create a sound power prediction model which is also capable of identifying the most dominant transmission paths in a section of an aircraft cabin. Moreover, the tool should also be able to capture the interaction between multi-transmission paths through which sound travel. However, determining whether the noise should be considered as airborne or structure-borne is not straightforward and often relies on the experience and judgement of the acoustic engineer [23]. Structure-borne noise is subsequently converted into airborne noise as it travels to the receiver. At this stage, it is assumed that the structure-borne contribution of the noise source is already included in the airborne transmission.

4.2.1 Approach and methodology for the development of the tool

As established in section 1.4, the design and development process of the tool will be guided as per the VDI 2221 [32], as far as possible. The process begins with defining the specifications, requirements, and parameters crucial for the proper functioning of the tool. However, the VDI 2221 cannot be fully adhered to, as the purpose of this paper is to investigate and develop a model using TFs, while the VDI process suggests evaluating different approaches. Instead, proposed solutions on the how the interface of the tool could look like, will be brainstormed and discussed with stakeholders before being structured. Additionally, frameworks will be created to ensure that the model is aligned with industrial practices and established guidelines and norms. During the design phase, the processes and stages of subsequently determining the output power will be illustrated using flowcharts. This approach ensures that all workflows are systematically structured. Sub-flowcharts will be introduced to refine specific decision stages, particularly, if they are “blocked” in the loop. After the development process, the tool will be tested and validated using the available measurements. Figure 25 summarises the next steps involved to developing the model.

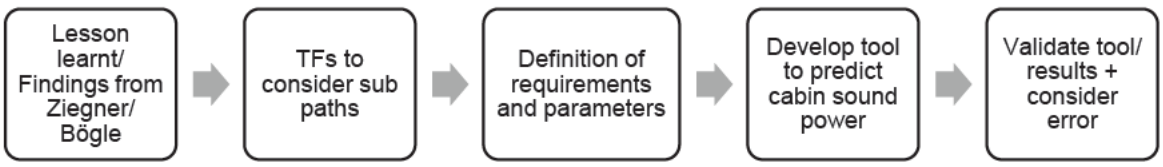

Figure 25: Flowchart illustrating the methodology to consider sub-transmission paths

The work from Tom Ziegner [5] and Bennett Bögle [6] serve as a foundation for defining the requirements of the tool. Moreover, key methodologies and calculation of the cabin SPL, can be adopted from Ziegner’s work. This approach also allows for a fair comparison of outcomes and the methods of predicting sound power. This also imply that the assumptions in both models remain aligned. While efforts will be made to maintain consistency, adjustments and modification will be inevitable to meet the specific goals of this study. The same segmentation of the demonstrator (refer to Figure 23) will be adopted for practical and easy comparison of the results. Instead of only considering incident sound power and the transmitted power at the outer surface of the layer, the interaction in the air gap between the multi-layers should also be considered. Although it is theoretically possible to measure through individual layers in OEM panels, this is not always an easy task in the practice – being difficult to access due to the geometry constraints of the fuselage structure. Additionally, each layer is firmly coupled together such that blindly separating the layers increases potential errors as the acoustic properties of the structure

might be altered. Theoretically, if the air gap in the fuselage is accessible, the transmission path can be analysed using sound intensity probes (airborne) or piezoelectric accelerometers to measure vibrations. If the impact of adding a supplementary insulation layer is to be investigated, sound attenuation can be quantified by comparing measurements before and after the addition of the layer. For instance, intensity measurements of sound radiation can be conducted near the vibrating surface interface to assess airborne sound transmission. Likewise, the impact of adding more layers can be investigated until the desired sound attenuation is achieved. The approach of determining the transmission paths will be further discussed in section 4.2.2.

4.2.2 Use of TFs to describe sound transmission and determine dominant paths

As discussed in the literature review, the Transfer Path Analysis can effectively analyse noise propagation in aircraft cabins. TPA identifies dominant transmission paths by decomposing the source-transfer-receiver system into smaller, measurable subsystems [23]. The objective is to break down a single transmission path (refer to Figure 24) into smaller manageable sub-paths, with the sound energy flow through each subsystem described by their respective TFs. Experience has shown that a transmission path through a cabin panel may involve up to three serial airborne paths. To accurately model these, the system is decoupled at boundaries where TFs can be determined, thereby creating individual subsystems. The approach is similar to the "splitting" method from the Simcenter Testlab paper from Siemens [15] (refer to section 1.6.3, III). However, a sub-system can only be established if both input and output power measurements are achievable at their boundaries. For example, in Figure 26, to determine the TF (H_1), transmission path 1 is divided into two subsystems: the active side, representing the sound source, and the passive side, representing the receiver. The TF (H_1) thus relates the flow of sound power between these two subsystems. Although measuring between the double layers in path 2 is technically challenging, path 2 can theoretically be represented by two TFs: $H_{2.1}$ for path 2.1 and $H_{2.2}$ for path 2.2. In transmission path 3, noise from outside is incident on the outer surface of layer 1, and travels as SBN until it is radiated as ABN into the cabin. Since the current model will not be considering SBN contribution, path 3 is represented by a single TF (H_3). If no complex acoustic phenomenon is happening, the value of this TF (H_3) will typically be lower than H_1, as noise transmission through this path will be attenuated by the structural mass. However, SBN can be more dominant than ABN if vibrations propagate through the structure, as insulation is only effective for ABN.

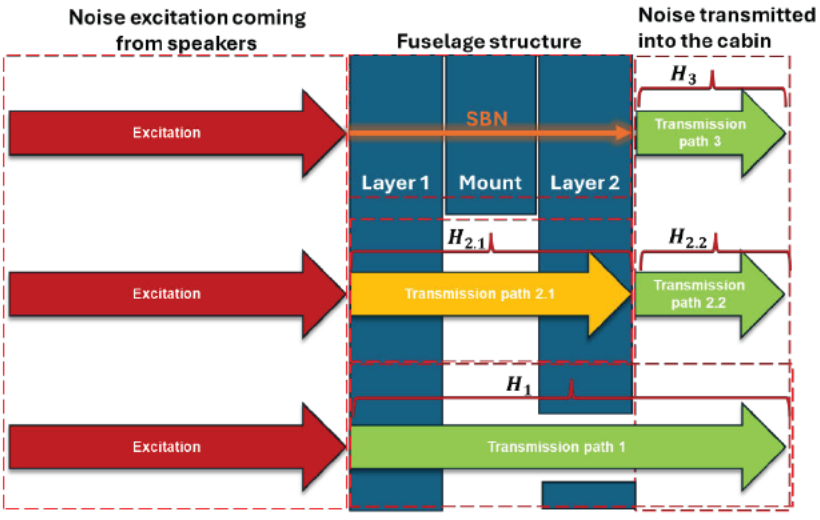

Figure 26: Splitting of a single transmission path into smaller sub paths

In simpler words, it can be imagined that the single black box path from Ziegner's approach (refer to Figure 24) will be further decomposed/ "split" into smaller sub-systems. Measurement of TFs is standardised under DIN ISO 13472-2 [36], in which sound pressures are measured both at the source and in the receiving room, and an amplifier and a two-channel FFT analyser are used to process the signals. For the purpose of this thesis, the focus is on measuring power-to-power TFs through sound pressure or sound intensity measurements. The TF H_i can therefore be expressed as follows:

$$H_i(\omega) = \frac{Power_{output}(\omega)}{Power_{\ input}(\omega)} = \frac{W_{Cabin}(\omega)}{W_{\ Excitation}(\omega)} \tag{4.3}$$

However, as mentioned, directly measuring acoustic power is not possible. The TF will be derived from pressure (SPL) or intensity measurements. This will be further explained in Chapter 7.3.

The advantage of TFs is their reciprocity: if one of the 3 variables is missing (input power, output power, or TF), the missing parameter can be easily determined. This makes TFs particularly suitable for predicting cabin noise under different conditions, as they allow for quick recalculations if the input conditions are varied. Additionally, using TFs for predicting cabin sound power, is suitable, as the cabin layout and material properties remain relatively constant throughout the life of the aircraft. Since materials exhibit frequency-dependent behaviour, this stability means that once the TFs are, they can represent sound transmission under various conditions. While the excitation of the source may vary, the TF, is unlikely to change. Therefore, the TF-based approach provides a practical balance between accuracy and usability without requiring repeated complex measurements for every new excitation scenario. When investigating noise in the cabin, the whole range of human hearing frequencies is of particular interest. For easy interpretation, the results can be presented in standard frequency bands, such as octave or one-third-octave bands. Although the process seems fairly straightforward, numerous parameters and variables must be accounted for to ensure highly accurate predictions. The next chapter aims to discuss into these parameters, define the specifications and requirements of the tool, and introduce the frameworks involved in its development.

5 Requirement, parameters and frameworks of the model

This chapter outlines the requirements and objectives of the tool, emphasising on what it should be able to do beyond predicting sound power in the cabin. In collaboration with stakeholders from the LHT, the HAW and building on the previous works from Bögle [6], a requirement list was compiled (annex VII and VIII). This list has been revised and modified, to address the specificities of this thesis. The main objective and requirement of the tool is to predict sound power in the cabin. The details and the requirements will therefore be outlined to assess whether and how these requirements can be achieved. For reliable noise prediction, the model should be able to consider and include these varying parameters that occur during real flight. However, unlike traditional FEM and sound prediction tools, it should remain as “simple as possible and accurate as needed”. To ensure that the tool is intuitive and easy to work with, it is important to define the framework and core structure of the tool. This can be done according to established engineering best practices and norms. Finally, it will be investigated whether the sound prediction tool shall comply with any aviation regulation from the industry.

5.1 Requirements of the sound power model

The below diagram shows the core requirements and the respective sub-requirements of the power model.

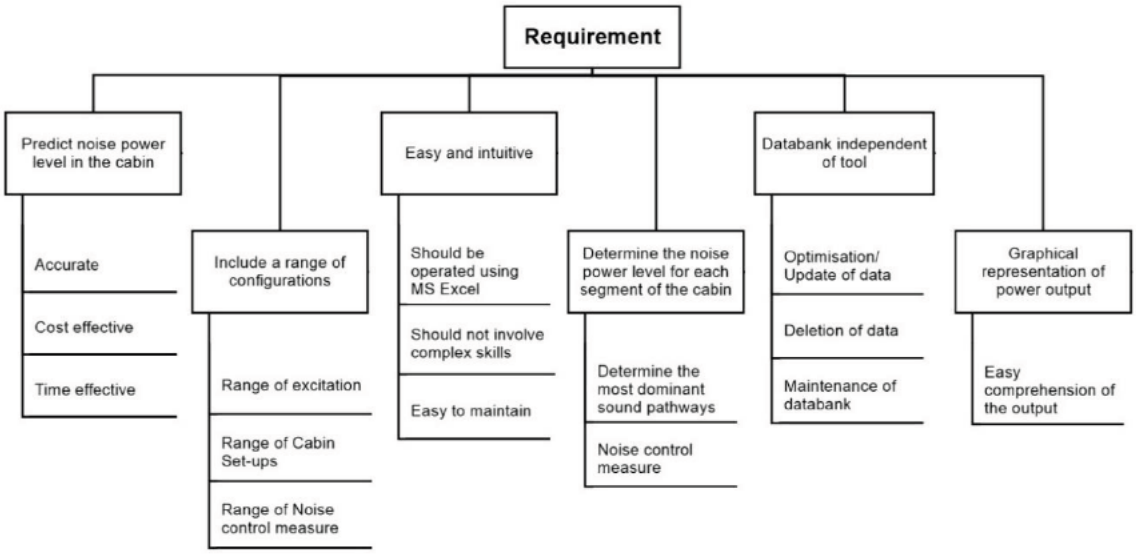

Figure 27: Tree-diagram of the requirements and sub requirements

The main objective of the sound power model is to predict sound power inside the cabin of a VIP aircraft. This should be possible for various configurations of an aircraft. Cabin configurations refer to the specific setup or design choices of the VIP cabin. For instance, for the cabin shown in Figure 23 (HCAT demonstrator), one configuration might involve the use of Carpet A for the floor panel, while another configuration for the same aircraft could involve Carpet B instead of A. The configuration of a VIP cabin is typically tailor-made according to the wish and preferences of the client. The reasons for different configurations may include better comfort, better design, geometric constraints or weight reduction. Moreover, the excitation varies across the frequency range due to the varying operational factors such as TBL and engine noise. Since the material and acoustic

properties of the structure are frequency-dependent, the TF will also change, reflecting the varying response of the system to sound excitations.

The second main requirement is to identify the most dominant sound paths. Although the same type of aircraft may share a similar fuselage structure, different configurations can result in varying transmission paths when noise enters the cabin. As a result, the TFs of these transmission paths will differ. The tool should be able to consider multiple transfer paths, whether they occur in series or parallel. As mentioned, this thesis focuses on airborne sound pathways, and structure-borne transmission will be excluded at this stage. However, it would be beneficial if the tool is designed in such a way, that it allows easy modifications to incorporate structure-borne noise contributions, should they become available in the future. For cabin sound power levels, it is not relevant whether the sound is direct airborne or structure-borne radiated as airborne sound. The measured intensity in the cabin already includes the structure borne contribution of the noise.

A common and practical approach to identify the most dominant paths is to divide the fuselage cross-section into segments. For consistency and ease of comparison, the same segmentation as described in Bögle (2024) [6] will be used. The tool should be able to predict the sound power of each segment and then sum these values to determine the overall cabin sound power in W. This approach will provide a clear indication of the areas where noise reduction measures can potentially be implemented. Without this analysis, there is a risk of applying measures to sound paths that do not significantly contribute to the overall cabin noise level. This results in unnecessary and inefficient use of resources. While the implementation of noise control measures and the comparison of results fall outside the scope of this work, the tool must be designed to allow future optimisation features without much change to its core structure. For instance, the tool should be prepared to account for the weights of each configuration or the noise control measures. This aspect is critical when implementing noise control measures as this directly impacts the fuel efficiency of the aircraft.

VIP cabin layouts are often “one-off” productions or made in relatively smaller numbers compared to traditional commercial aircrafts. The challenge, therefore, lies in achieving accurate sound power predictions with limited measurement data. As of now, the design process for the passive noise control measures at LHT depends on estimating sound pressure levels from empirical data, such as sound intensities, transmission loss of panels, and absorption coefficients, gathered from previous projects [5] [6]. Conducting experiments across the entire frequency band is not feasible due to time constraints, increasing the risk of missing measurements. While interpolating missing TF values might seem like a solution, it can introduce significant errors in the calculated sound power due to the quadratic averaging process involved when converting FFT data to octave bands. Interpolation is only feasible between linear FFT data points, provided the frequency resolution is sufficiently high. However, storing large FFT datasets would increase the complexity of the tool and database capacity requirements, particularly if the resolution is fine. Given these considerations, incorporating interpolation functionality directly into the tool or database might add unnecessary complexity. Instead, this pre-processing step is omitted and converted externally using already available FFT-to-octave conversion tool provided by LHT or the FFT lines convertor from the project Entirety.

The tool being developed is a (semi)-empirical model that combines theoretical principles of acoustics and physics with empirical measurements [33]. Another key requirement is that the tool should consist of a database to securely store data and measurements. The database must be able to store large amounts of data, including excitations, TFs, frequency ranges, measurement dates, weights, and configurations for various aircraft types. Unlike the “delta approach” to determine cabin noise level, the input excitation (due to TBL or engine noise) is also required in the transfer path method. Talks and interviews with stakeholders, has revealed that, the both the excitation and the TFs are typically

stored in the same database. Therefore, the tool should be able to differentiate between excitation and TF when retrieving data. At the same time, it should also be easy to maintain and allow the tool to efficiently retrieve specific information. Each measurement must have a unique ID to enable the tool to identify and use the correct data. By functioning independently from the tool, the database ensures flexibility, allowing multiple users to work with it or the tool without interference. It also enables data to be modified, optimised, or deleted as needed without affecting the functionality of the tool.

Since power is typically be derived from other acoustic quantities such as pressure, particle velocity, and for structure-borne noise using acceleration and force, to prevent conversion error when determining the TFs, it is crucial to maintain consistency in the units used. Hence, the database must include a pre-processing tool to convert measurements, such as decibel [dB], pressure [Pa], velocity [m/s], acceleration [m/s^2] or force [N], into power [W]. Consistency in the frequency scale is equally important. The measurement scale depends on the tools and equipment used during the measurement campaigns. Discussions with stakeholders have revealed that cabin sound measurements are typically conducted in third-octave bands (*de*. Terzband). Therefore, the tool and database will use the third-octave bands as the standard frequency scale. If measurements are only available in octave bands, individual third-octave levels cannot be directly reconstructed. One option is to assign identical values to the three corresponding third-octave bands. However, this approach is not accurate, since it ignores the natural variability of energy distribution across the narrower frequency band. A better solution is to manually input third-octave values as a temporary measure until a reliable formula for conversion can be developed.

The final requirement is cross-linked requirement to the previously discussed requirements. The complexity of the tool must be limited to ensure economic viability and should not require from users. For it to be easily accessible and user-friendly, both the tool and the associated database will be developed using Microsoft Excel. This approach also eliminates the need for extra cost on software license. While input parameters should be able to be extended, modified or deleted, the number of parameters involved in the calculation should be kept to a reasonable number to prevent unnecessary computational effort. Moreover, since VIP cabin layouts largely depend on individual customer requirements, the databank should be designed to allow the addition of new data. For each new measurement, a new row can be added in the database and the new measurement will be assigned a unique and distinct identification number allowing users and excel to quickly select and retrieve them. The generation of the IDs will be automatically made by Excel, preventing duplicates that could lead to calculation errors. Nevertheless, the tool should also provide the option for the user to manually enter an ID or save measurements under a custom ID name. The output results must be also easy and clear to interpret. This can be achieved using graphs and charts to provide intuitive visual representation of the results. The design follows engineering best practices, incorporating a legend and key for clarity. Details on how this will be achieved will be discussed in section 6.5.

Unlike traditional FE and SE models, this tool aims at providing a cost-effective solution for small production volume like the VIP cabin design industry. The main issue available commercial tools are that they are often not used to their maximum potential, due to a lack of skilled personnel or because many of their features are relevant only for specific projects, leading to wasted resources. Hence, this model should focus on specific features which are most relevant for VIP aircraft especially the LHT. This shall reduce the number of interventions required in the iteration loops, aligning the model closely to the operational, cost and personnel realities.

5.2 Parameters of the model

During real flight scenarios, operating conditions, environmental influences, and the acoustic and material properties of both noise control measures and the fuselage structure vary continuously. Additionally, noise from different sources also changes with time and frequency, contributing differently to the overall sound level in the cabin. The parameters refer to those variables which cannot be assumed to be constant across the frequency range when determining the noise level in the cabin. These parameters will be defined by the user according to the configuration of the cabin and operating conditions of the aircraft. While fan noises are more dominant at lower frequencies, TBL noise becomes more critical during cruising, typically at mid frequencies [34]. The noise coming from different sources are therefore more dominant within specific frequency ranges, contributing to the overall noise spectrum, as illustrated in the Figure 28.

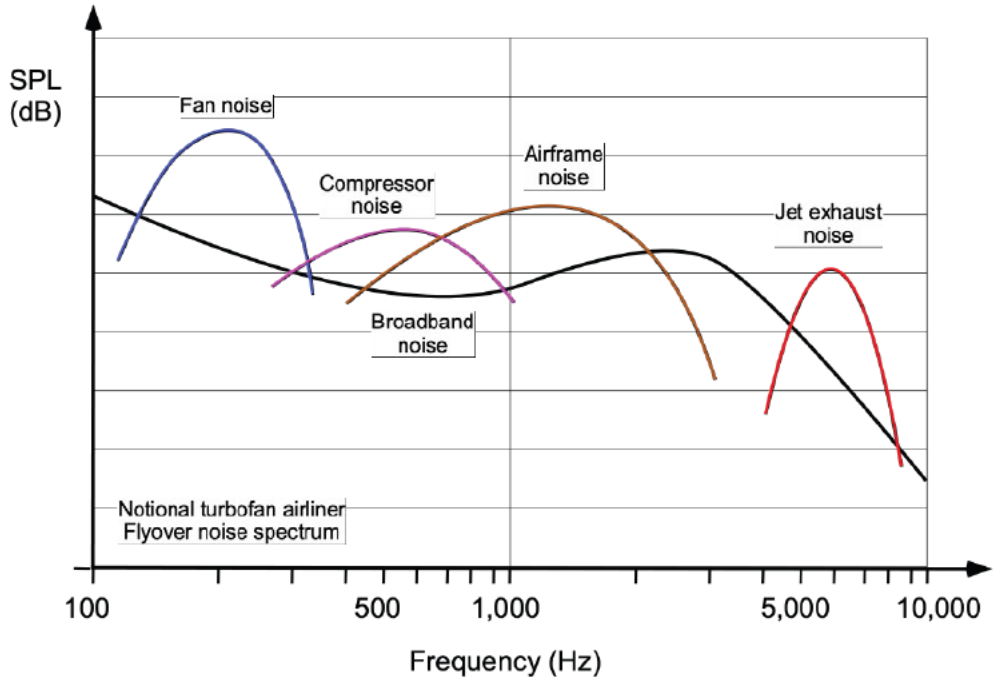

Figure 28: Contribution of the different sources of noise over the frequency range. [34]

To account for varying conditions, the user should be able to define parameters according to the cabin configuration and operating conditions of the aircraft. Therefore, the tool should be designed to allow parameter input, and by assigning different parameters to all 13 panels, the user should be able to analyse the cabin configuration, covering the entire fuselage section. These are the input parameters and include the excitation and the TFs of each 13 panel. When an ID is assigned to a segment, the tool should be able to automatically retrieve the required data from the database. On the other hand, if panel 1 (Floor Panel Inboard) and panel 2 (Floor Panel Middle) have the same configuration, such as Carpet A, the TF for sound transmission through the carpet will typically be the same. The tool should allow the same configuration to be assigned to multiple segments. Similarly, if the same excitation acts on a segment from a measurement campaign, it is be stored only once in the database and can be assigned to all relevant segments. This saves space and improves efficiency. Dividing the fuselage into distinct segments, group together areas having the same structural, material, and acoustic properties. For instance, segment 1 is the floor panel which is more like a structural barrier with predictable sound transmission characteristics. In contrast, the dado gap (Segment 4) is a semi-open “hole” that allows sound to travel more easily. This segmentation provides a clear overview of dominant noise paths and helps identify suitable noise control measures. Additionally, the

pre-defined segmentation is flexible and can be extended if future findings are gained or for future iteration of the tool to include SBN.

As defined in the requirements, the tool focuses on ease of use and user-friendliness. Although including more parameters could improve accuracy, this is not always practical due to time and cost constraints and the complexity involved in carrying out experimental measurements. To address this, the cabin power can be determined by defining only the excitation and TFs of the panel. If the user intends to analyse the impact of different flight conditions, the tool will be designed to allow seamless switching between excitation sets for efficient comparison. Each configuration will be assigned an automatically generated ID to minimise human error. Users can easily compare results by changing the ID in the input section, for instance, from the previous example of comparing carpet A against carpet B. Furthermore, common panel configurations can be compiled together under a unique name. For instance, if an aircraft A320.x frequently uses the same combination of floor carpets, absorber materials, and mass layers in Segment 1, this setup can be saved with a unique name, with the overall calculated transfer function of this setup.

Similar to the configuration ID and TF, each excitation power value will be assigned an ID number and stored in the databank. By defining this ID in the parameter input section, the tool retrieves the corresponding data from the databank and integrates them into the model. However, the tool should be able to differentiate between TF data and excitation. Since the measurement campaign will typically be conducted in a diffuse chamber, where pressure can be assumed to be uniform across the room, the input power per unit area would be the same for each segment. Nevertheless, assigning an excitation parameter to each segment is beneficial, for instance, if in future a secondary source of noise, is placed close to a segment. Finally, it should be distinguished whether the noise paths are in parallel or series. Their mathematical relationship will be discussed in the following chapter Process 6.3.

5.3 Frameworks and structure of the tool

The framework defines the boundaries, methodologies, and guidelines that will be followed during the development process described in section 6. In the aviation industry, strict adherence to regulatory compliance is mandatory. Any deviation or not respecting the norms and regulations can cause delays in the certification, impacting the whole design process. The frameworks ensure that the results produced are within the legal and technical boundaries. Although there are no specific regulations or laws that set mandatory noise limits levels in the cabin of commercial aircrafts, manufacturers and airlines usually follow industry standards and guidelines to ensure passenger comfort. For instance, the ISO-5129 standard describes the guidelines for measuring and evaluating noise levels in aircraft cabins [35]. The ICAO and the FAA do not directly regulate the cabin noise level. Annex 16 of the ICAO states that the main purpose of noise certification is to ensure that the aircraft is equipped with the latest available noise control measure [36]. While these are not legally binding, they help manufacturers design quieter cabins to enhance passenger comfort.

On the other hand, the structure, establishes the foundation for the reliability and user-friendliness of the tool. The interface and layout of the tool must be methodically designed according to engineering best practices and standards, for instance aligning to VDI-2221 guidelines, as far as possible. This provides a systematic methodology for technical product and systems development [32]. Moreover, continuous assessments throughout the whole development process of the tool will be conducted to ensure the requirements defined in section 5.1 are fulfilled. This ensures the effectiveness of the tool whilst being straightforward. The operational sequence of the model is illustrated using the flowchart below, in line with the DIN 66001 [37]. The tool shall be subsequently tested and validated

according to the ARP 4754A. This provides guidelines for the development of civil aircraft and systems. This involves defining requirements, validating them to identify potential safety-critical issues, and ensuring the that the tool aligns with safety standards [38]. Noise, being harmful to humans above 85 dB, necessitates clear hazard indication if levels exceed this threshold [8]. If this threshold is reached, it should visually highlight hazards, for example, by displaying results in red when noise levels exceed acceptable limits. The user interface of tool design will be designed according to the DIN-ISO 9241-210, which outlines processes for creating systems that prioritise user needs, ensuring ease of use, accessibility, and an improved overall user experience [39]. Talks and interviews with stakeholders have shown measurements and data are typically recorded in rows instead of columns. Colour schemes can be adapted according to corporate colours while maintaining readability and clarity. For the purpose of this job, a neutral blue colour chart close to the “HAW” blue will be chosen. Dark text on light backgrounds is used to create a high contrast. This reduces eyes fatigue and prevent human errors. The tool should also consist of a clear key and legend to ensure accurate interpretation. Finally, the output results shall be easy to interpret using coloured charts and graph.

Figure 29 illustrates a basic and simplified approach of how the tool can be made to estimate output power. This process involves a common computational methodology, where known parameters/ variables (input) together with mathematical and physical equations are used to determine the unknown power output. In the next chapter, the feasibility of these methods will be evaluated.

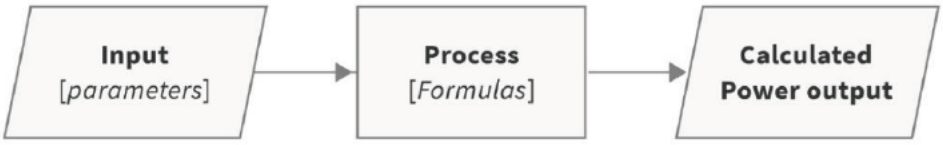

Figure 29: Simplified methodology for estimating output power

6 Development and modelling of the power model

This section outlines the development processes of the tool to predict sound power in an aircraft cabin with a VIP set-up. Since the tool is an empirical model, the prediction made fundamentally relies on experimental data which are stored separately in a database. The simplified approach from Figure 29 must therefore be adapted to include a pre-processing step to supply relevant data to the tool, as shown in Figure 30.

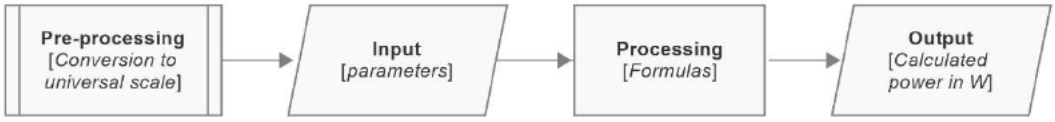

Figure 30: Modified flowchart of the main process in determining the sound power

6.1 Pre-processing

The pre-processing steps is carried out at the end of a measuring campaign or when storing new data in the database. This step ensures that the raw data are stored using the standardised scale as defined in the requirement list. The experimental campaigns are carried out in acoustic laboratories as discussed in 4.1 and 4.2. The pre-processing tool converts the data to the coherent unit (W) across the third octave scale. Figure 31 illustrates the steps involved in this loop.

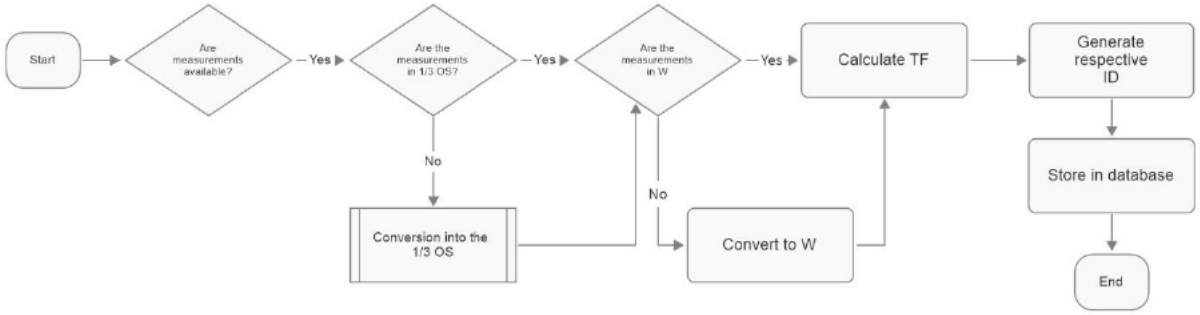

Figure 31: Flowchart involving the steps to store data in the database (pre-processing)

Ideally, the values are recorded using the one-third octave scale. If this is not the case, the raw FFT values for SPL should be converted to the one-third octave scale, using the FFT-to-one-third octave converter. This processes and filters the data into broader bands, making them easier to interpret. Once the raw data are converted into the one-third octave scale, it is to be checked whether the excitations as well as the recorded cabin output measurements are both in the unit Watts. A decision step involves converting quantities and units of the available measurement to sound power. This can be achieved using a so called “power-converter”, found in the first sheet of the database. The power-converter is a pre-processing tool, able to automatically convert SPL $[dB]$, sound intensity $[dB]$ and pressure $[Pa]$ into Watts $[W]$. The conversion step is critical to ensure that the coherency of the units as they will be later used to determine power for other configurations.

Figure 32 shows an extract of the pressure-to-power convertor.

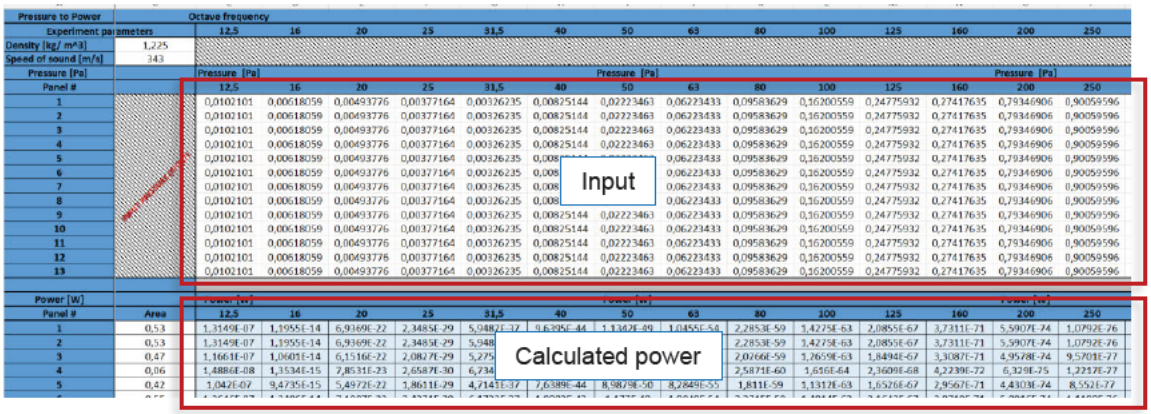

Figure 32: Pressure to power converter

If measurements of the excitation are available as a function of pressure (p_{rms}) in [Pa], the respective measurements can be manually given into the white input field, and the tool automatically converts them to power. Inside the excitation chamber the mean square pressure is assumed to be the same across the room. Close to the vibrating fuselage, the velocity of the air particles is given as their root mean square v_{rms}. The density of air is assumed to be 1,225 $\frac{kg}{m^3}$ (DIN ISO 2533) [18]. Using the equation of acoustic impedance 2.8 and the equation 4.1, the input power W of the excitation is calculated using the equation:

$$W = p_{rms} \cdot v_{rms} \cdot A_i = \frac{{p_{rms}}^2}{\rho \cdot c} \cdot A_i \quad [W] \tag{6.1}$$

Similarly, if SPL measurement, L_p, are available in [dB], they can be directly converted to W using the SPL-to-power section in the pre-processing tool (as shown in Figure 33), bypassing the need to calculate pressure first:

$$W = \left(p_0 \cdot 10^{\frac{L_p}{20}}\right)^2 \cdot \frac{{p_{rms}}^2}{\rho \cdot c} \cdot A_i \quad [W] \tag{6.2}$$

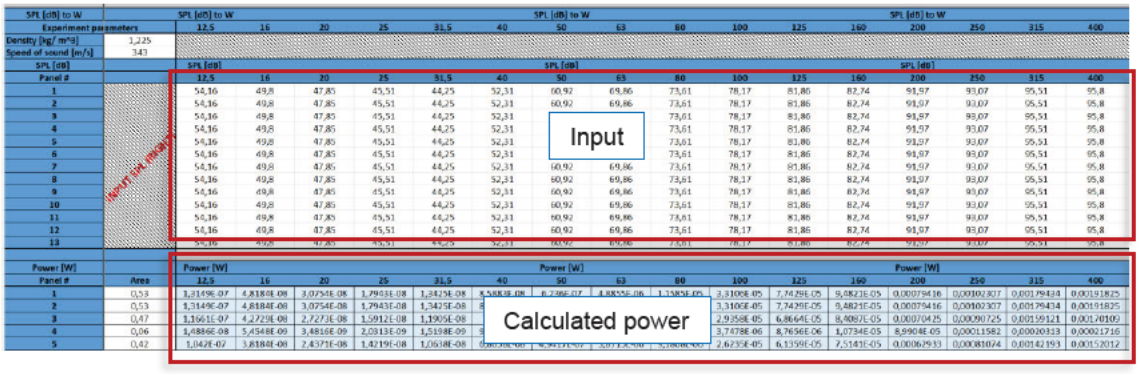

Figure 33: SPL to power converter

Inside the cabin, the cabin noise level is typically measured in intensity L_i level [dB]. Using the area, A_i, of each segment, the tool converts the cabin measurements to W, using the formula below:

$$W_i = I_0 \cdot 10^{\frac{L_i}{10}} \cdot A_i \quad [W] \tag{6.3}$$

Once both quantities for power input and power output have been converted to W, the TF can be calculated as the ratio of power output to input. The TF is unitless as the unit of power $[W]$ cancel out. If only the final value of the TF is to be recorded, this can be directly determined using the TF-calculator without individually converting the input and output quantities. Figure 57 , in Index section IX, shows an extract of the TF calculator which is found in the second sheet of the database. The TF can be calculated from power, pressure or the velocity of the particle. As mentioned, air density, speed of sound and the incident and radiated surface area of the panels are respectively the same in both the source room and the receiver room. However, their mean square pressure and velocity will not be the same. Using equation 6.1, the TF for power can be given as follows:

$$H_i = \frac{{p^2}_{rms,output}}{{p^2}_{rms,input}} = \frac{{v^2}_{rms,output}}{{v^2}_{rms,input}} \qquad 6.4$$

After successfully calculating the TF, an identification ID for each new set of data to be stored must be created, using the ID generation tool shown in Figure 34. First, the segment from which the measurement has been taken can be chosen from the dropdown list, containing the 13 panels. Secondly, the user defines the sub-path from which the measurement comes from. Afterwards, the ID will be automatically generated by the tool and shown in the column “Generated ID”.

Check ID	Segment	Sub-path	Configuration	Generated ID	Proposed ID	Status
Proposed ID #1	1	1		1-1-2		Available
Proposed ID #2				--1	121	Occupied
Proposed ID #3	1	2	A	1-2-A1		Available
Proposed ID #E	2			E21	E22	Available

Figure 34: ID generation tool (left)

In the adjacent cells, the ID-generator verifies whether the entered ID already exists within the database and display its status, with green indicating availability and red indicating that the ID is already in use, as illustrated in Figure 35 (blue box). This ensures that duplicate entries are avoided. If an ID is already taken, the right section of the ID-generator shows key details of the existing measurement, including a brief description and the recording date, allowing the user to quickly have an idea of the relevant information (red box).

Proposed ID	Status		Transfer ID	Segment	Serial path number	Description	Date
	Available						
	Available						
11A	Occupied		11A	1	1	A320-Auftrag 4848	4.8.2024
E22	Available						

Figure 35: ID generation tool (right)

An example of a combination of 3 paths in series in a standard sidewall panel. Path 1 is the transmission through the exterior skin of the fuselage (layer 1), path 2 through the OEM insulation layer (layer 2) and path 3 through the panel trim (layer 3). The ID generation logic follows a structured format, where the first digit (1-x-x) represents the segment number (ranging from 1 to 13), the second digit indicates the serial path number (1, 2, or 3), and the third digit ensures that the ID is unique within the database. Excel verifies the existing IDs and assigns the third digit as the next available number in a chronological sequence. For instance, for a measurement carried out on segment 1, involving only 1 transmission path, the generated ID in the Figure 34 is 1-1-2 (segment 1, path 1). The third digit of the ID (highlighted in the red box in Figure 34) is 2 since the ID

1-1-1 already exists in the database. As a result, the next available ID is 1-1-2. Alternatively, users can manually assign an ID or name to a measurement by entering their preferred ID in the "Proposed ID" cell. Figure 36 shows the systematic approach of labelling sub-serial paths.

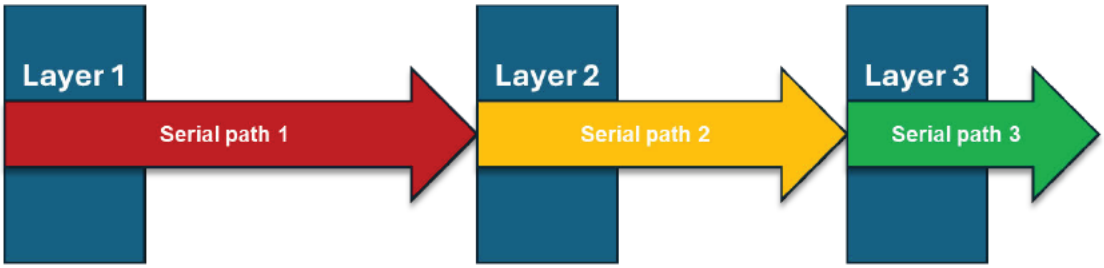

Figure 36: Illustration of 3 paths in series

The same principle applies for the generation of the excitation ID. The ID is automatically generated upon entering the segment number on which the input excitation acts (yellow box). As specified in the requirement list, all measurements will be stored in a single centralised database. To distinguish the excitations from the TFs, the excitation receives the prefix “E” in front of the ID number, for instance E22.

If the user intends to analyse the effect of adding a supplement insulation layer, the ID of the TF of the configuration is given in the input section instead of layer 3. Since the tool considers only airborne sound transmission, the TF of the configuration represents the radiated sound energy after passing through both layer 3 and the additional layer (red). Hence the TF is based on the new configuration path and the previously established Path 2. Likewise, the impact of the supplementary insulation layer can be systematically analysed. Figure 37 illustrates the configuration path, when a new layer is added to layer 3.

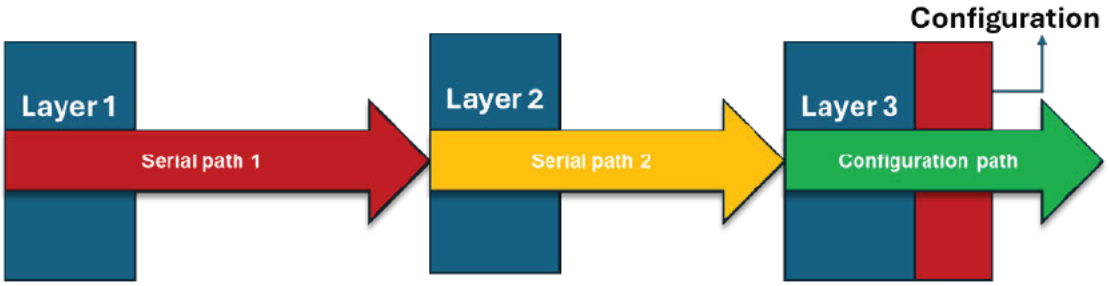

Figure 37: Illustration of serial transmission paths with a new configuration

Once each measurement is assigned an ID number, it can be recorded in the database, along with additional information such as the description and date of recording. Additionally, configurations include details such as weight, cost, panel surface area, and reverberation time, which can be useful for calculating the transmission properties of the configuration. Hence, the pre-processing stage ensures that the data are standardised and on a common scale, thereby reducing the risk of errors in the coming steps.

6.2 Input

In the input area, the user defines all the parameters by entering their ID number, including the number of transmission paths involved in the calculation and the respective excitation for each segment. When defining the transfer paths, it is important to distinguish between serial and parallel paths. The tool allows the calculation of up to 4 serial paths as well as one parallel path. The ID of the respective path is manually entered input field (highlighted in red in Figure 38).

On the right-hand side of the input field (yellow box), the tool verifies whether the entered ID are not stored in the database, preventing input errors of invalid or duplicate Ids.

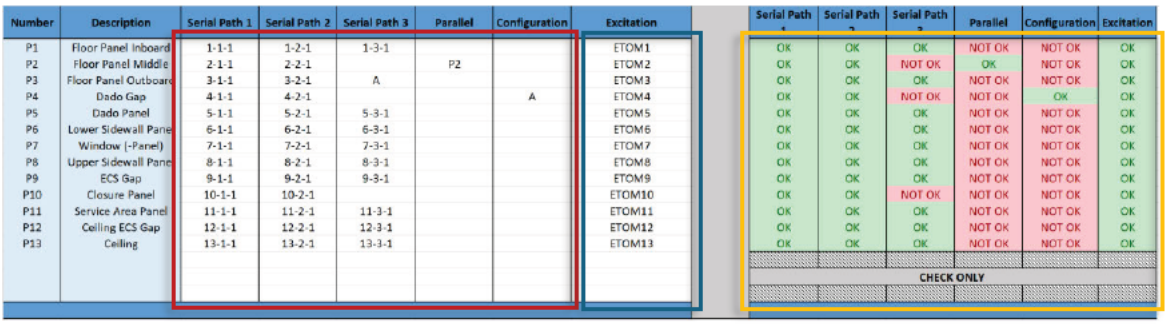

Number	Description	Serial Path 1	Serial Path 2	Serial Path 3	Parallel	Configuration	Excitation	Serial Path 1	Serial Path 2	Serial Path 3	Parallel	Configuration	Excitation
P1	Floor Panel Inboard	1-1-1	1-2-1	1-3-1			ETOM1	OK	OK	OK	NOT OK	NOT OK	OK
P2	Floor Panel Middle	2-1-1	2-2-1		P2		ETOM2	OK	OK	NOT OK	OK	NOT OK	OK
P3	Floor Panel Outboard	3-1-1	3-2-1	A			ETOM3	OK	OK	OK	NOT OK	NOT OK	OK
P4	Dado Gap	4-1-1	4-2-1			A	ETOM4	OK	OK	NOT OK	NOT OK	OK	OK
P5	Dado Panel	5-1-1	5-2-1	5-3-1			ETOM5	OK	OK	OK	NOT OK	NOT OK	OK
P6	Lower Sidewall Panel	6-1-1	6-2-1	6-3-1			ETOM6	OK	OK	OK	NOT OK	NOT OK	OK
P7	Window (-Panel)	7-1-1	7-2-1	7-3-1			ETOM7	OK	OK	OK	NOT OK	NOT OK	OK
P8	Upper Sidewall Panel	8-1-1	8-2-1	8-3-1			ETOM8	OK	OK	OK	NOT OK	NOT OK	OK
P9	ECS Gap	9-1-1	9-2-1	9-3-1			ETOM9	OK	OK	OK	NOT OK	NOT OK	OK
P10	Closure Panel	10-1-1	10-2-1				ETOM10	OK	OK	NOT OK	NOT OK	NOT OK	OK
P11	Service Area Panel	11-1-1	11-2-1	11-3-1			ETOM11	OK	OK	OK	NOT OK	NOT OK	OK
P12	Ceiling ECS Gap	12-1-1	12-2-1	12-3-1			ETOM12	OK	OK	OK	NOT OK	NOT OK	OK
P13	Ceiling	13-1-1	13-2-1	13-3-1			ETOM13	OK	OK	OK	NOT OK	NOT OK	OK
										CHECK ONLY			

Figure 38: Input field in the tool

6.3 Process

The processing stage is the main operation of the tool, involving the computation of data to determine the power. Figure 39 outlines the steps in this loop. These steps are pre-defined and automatically executed by the program. The tool consists of 8 sheets: an input sheet for defining parameters, a sheet for displaying retrieved data for the TFs and excitations, a sheet for performing the calculation using the appropriate formulas, and a sheet for displaying the final calculated power. Additionally, the results are graphically displayed on two sheets. The last sheet in the tool serves as a user manual and key for abbreviations used in the tool.

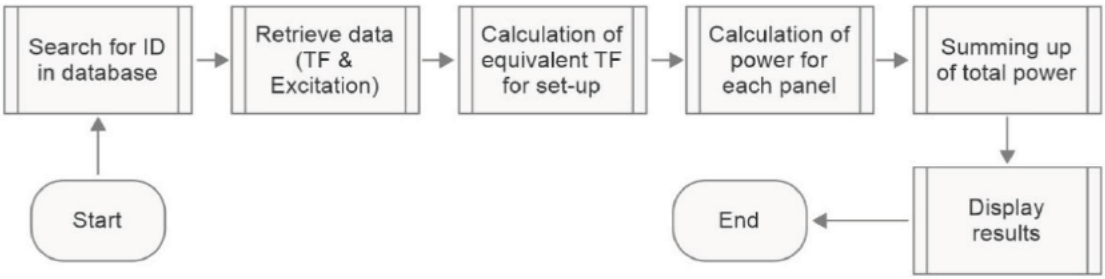

Figure 39: Flowchart showing the stages involved in processing the output results

After defining the parameter in the input section of the tool, the program automatically searches for the identical information in the database. If the user-defined ID matches the ID in the database, the corresponding measurements across the frequency range are retrieved and displayed in their respective sheet (TFs or excitation). The excitation sheet is the third sheet in the tool, as shown in Figure 40. This is listed systematically starting from the first to the last segment.

Segment	Excitation ID	Description	12,5	16	20	25	31,5	40
1	E1	Excitation with 3 Speakers (800W each)	3,49E-08	2,61E-08	1,67E-07	3,49E-08	2,61E-08	1,67E-07
2	E2	Test #88	3,49E-08	2,61E-08	1,67E-07	3,49E-08	2,61E-08	1,67E-07
3	E3	Test #89	3,49E-08	2,61E-08	1,67E-07	3,49E-08	2,61E-08	1,67E-07
4	E4	Test #90	3,49E-08	2,61E-08	1,67E-07	3,49E-08	2,61E-08	1,67E-07

Figure 40: Extract of the sheet for the excitation in the tool

Similarly, the measurements for the TFs are systematically listed in the second sheet of the tool (starting from the first 3 serial paths, the in-series configuration path followed by the parallel path). Once they are listed, the TF for each transmission is calculated, as shown in Figure 41. In cases where the configuration or parallel transmission paths are not defined by the user in the input section, the corresponding rows remain empty. It is essential to ensure that these cells remain empty rather than containing values such as "0" or "1", as this would lead to incorrect calculations. Specifically, multiplying in-series TFs by 0 results in 0, while TF values greater than 1 indicate that the sound power has increased, which is physically incorrect for most transmission paths through the fuselage.

Segment	TF ID	Description	12,5	16	20	25	31,5	40	50	63	80	100
1.1	1-1-1		1	1	1	1	1	1	1	1	1	1
1.2	1-2-1		1	1	1	1	1	1	1	1	1	1
1.3	1-3-1		1	1	1	1	1	1	1	1	1	1
Confi.	A		1	1	1	1	1	1	1	1	1	1
Parallel	P1		1	1	1	1	1	1	1	1	1	1
Total			2	2	2	2	2	2	2	2	2	2

Figure 41: Extract of the sheet for the TFs in the tool

With the excitation and the TFs, the output power for each transmission path and frequency band can be calculated. Reformulating equation 4.3 gives:

$$Power_{\ output}(\omega) = H_i(\omega) \cdot Power_{\ input}(\omega)$$

$$Power_{\ segment,\ i}(\omega) = TF_i(\omega) \cdot Excitation_{\ i}(\omega) \qquad 6.5$$

This part of the process is helpful for identifying the dominant sub-path within a segment, enabling the user to implement targeted noise control measures more effectively. At this stage, the total power output of the segment and the overall cabin has not yet been calculated.

Segment	TF ID	EX ID	12,5	16	20	25	31,5	40	50	63	80	100
1.1	1-1-1	ETOM1	0,429003	0,259693	0,207472	0,158475	0,137076	0,346705	0,934244	2,614931	4,026801	6,80707
1.2	1-2-1	ETOM1	0,429003	0,259693	0,207472	0,158475	0,137076	0,346705	0,934244	2,614931	4,026801	6,80707
1.3	1-3-1	ETOM1	0,429003	0,259693	0,207472	0,158475	0,137076	0,346705	0,934244	2,614931	4,026801	6,80707
Confi.	A	ETOM1	0,429003	0,259693	0,207472	0,158475	0,137076	0,346705	0,934244	2,614931	4,026801	6,80707
Parallel	P1	ETOM1	0,429003	0,259693	0,207472	0,158475	0,137076	0,346705	0,934244	2,614931	4,026801	6,80707

Figure 42: Extract of the sheet for calculation of output power for each transmission path

6.4 Calculated output power

The calculated output power is particularly interesting for the user as it shows the main outcomes. For each segment, this is determined by multiplying the total equivalent TF of the segment by the excitation. Figure 43 shows the approach for calculating the total TF of a segment: TFs in series are multiplied, while parallel TFs are added [40]. In this configuration, H_1, H_2, H_3 are in series while H_4 is parallel to the others. X represents the input power in the segment and Y the radiated power output.

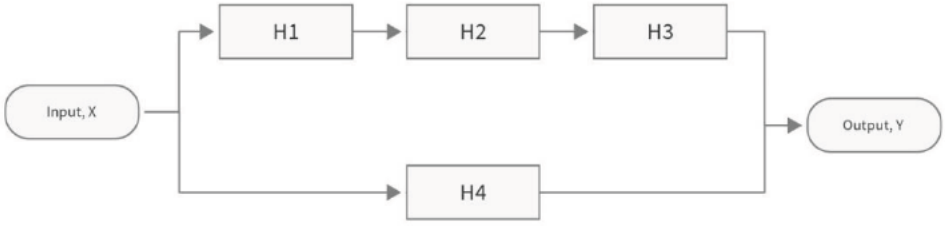

Figure 43: Approach to calculate the equivalent total TFs

The output power for each 13 segments can therefore be given as follows:

$$Y = X\left((H_1 \cdot H_2 \cdot H_3) + H_4\right) \quad 6.6$$

Finally, the total power output in the cabin is obtained by summing the individual power outputs of all 13 segments.

$$Power_{\ total,\ cabin}(\omega) = \sum_{1}^{13} Power_{\ segment,\ i}(\omega) \quad 6.7$$

The results are then displayed in the last sheet for each segment as well as the total power in the cabin across the one third octave scale. This is shown in Figure 44.

Segment	12,5	16	20	25	31,5	40	50	63	80	100
1	1,48E-30	4,63E-31	7,76E-28	1,48E-30	4,63E-31	7,76E-28	2,16E-24	8,12E-21	2,57E-19	1,71E-17
2	1,22E-15	6,8E-16	2,78E-14	1,22E-15	6,8E-16	2,78E-14	1,47E-12	9,01E-11	5,07E-10	4,14E-09
3	1,48E-30	4,63E-31	7,76E-28	1,48E-30	4,63E-31	7,76E-28	2,16E-24	8,12E-21	2,57E-19	1,71E-17
4	1,48E-30	4,63E-31	7,76E-28	1,48E-30	4,63E-31	7,76E-28	2,16E-24	8,12E-21	2,57E-19	1,71E-17
5	1,48E-30	4,63E-31	7,76E-28	1,48E-30	4,63E-31	7,76E-28	2,16E-24	8,12E-21	2,57E-19	1,71E-17
6	1,48E-30	4,63E-31	7,76E-28	1,48E-30	4,63E-31	7,76E-28	2,16E-24	8,12E-21	2,57E-19	1,71E-17
7	1,48E-30	4,63E-31	7,76E-28	1,48E-30	4,63E-31	7,76E-28	2,16E-24	8,12E-21	2,57E-19	1,71E-17
8	1,48E-30	4,63E-31	7,76E-28	1,48E-30	4,63E-31	7,76E-28	2,16E-24	8,12E-21	2,57E-19	1,71E-17
9	1,48E-30	4,63E-31	7,76E-28	1,48E-30	4,63E-31	7,76E-28	2,16E-24	8,12E-21	2,57E-19	1,71E-17
10	1,48E-30	4,63E-31	7,76E-28	1,48E-30	4,63E-31	7,76E-28	2,16E-24	8,12E-21	2,57E-19	1,71E-17
11	1,48E-30	4,63E-31	7,76E-28	1,48E-30	4,63E-31	7,76E-28	2,16E-24	8,12E-21	2,57E-19	1,71E-17
12	1,48E-30	4,63E-31	7,76E-28	1,48E-30	4,63E-31	7,76E-28	2,16E-24	8,12E-21	2,57E-19	1,71E-17
13	1,48E-30	4,63E-31	7,76E-28	1,48E-30	4,63E-31	7,76E-28	2,16E-24	8,12E-21	2,57E-19	1,71E-17
Total	1,22E-15	6,8E-16	2,78E-14	1,22E-15	6,8E-16	2,78E-14	1,47E-12	9,01E-11	5,07E-10	4,14E-09

Figure 44: Calculated output power

6.5 Graphical display and user interface

The user interface of the tool has been designed to comply with ISO 9241-210, such that it is intuitive to work with and easy to interpret outcomes with clear visual guidance. The input interface consists of drop-down menus that allow users to select only predefined data from the database, thereby preventing input errors. If a user attempts to select a measurement that is not found in the database, the tool highlights the corresponding cell in red, providing immediate feedback to address potential mistakes. The tool uses a colour-coded scheme to help users distinguish between different types of cells and data. For instance:

- White cells indicate input fields: indicating the user that these cells require manual data entry.
- Pale blue cells representing predefined or processed data containing pre-programmed formulae.
- Darker pale blue cells, where the calculated results are displayed.
- Blue cells are used for titles and headers

To further enhance usability, the tool and the database includes a key to explain the colour codes and abbreviations used. Additionally, a flowchart is provided as part of the user manual to guide users through the processes of the tool. Index XII includes detailed explanations of the main formulas. This ensures that users can understand the formulas and can easily make modifications if necessary or recover deleted formulas/ data. The tool maintains a consistent layout across all sheets. Measurements are stored horizontally to

match the standard practice of stakeholders, such that the user can navigate the tool efficiently without confusion.

The tool automatically generates pie charts to provide a visual depiction of the dominant sound paths in each segment and their respective contributions expressed in percentage %. For clarity and coherence, the pie charts maintain a consistent colour scheme throughout the tool, with each panel represented by the same colour code, as shown in Figure 45. This consistency ensures intuitive interpretation, allowing the user to instantly identify panels and easily compare them across different configurations.

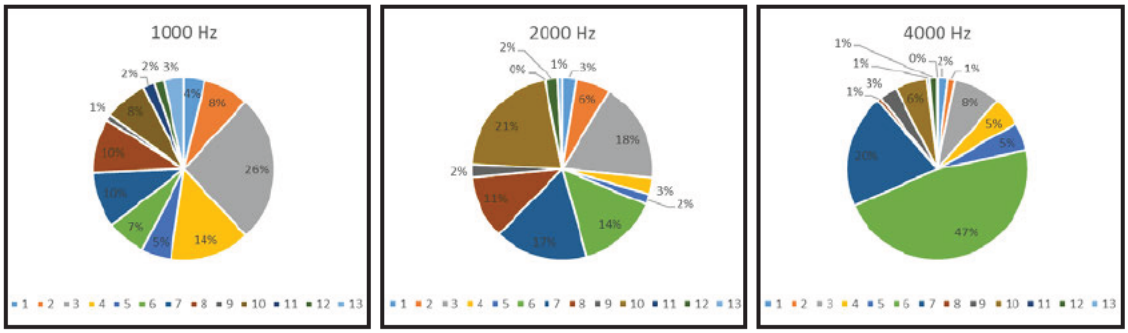

Figure 45 :Graphical illustration of the most dominant paths

In addition to the graphical charts, the tool displays the calculated power across the frequency range, allowing users to identify critical frequency bands that require attention. Additionally, the most dominant transfer paths, contributing the highest percentage to the overall noise, are highlighted in red (100%), while the least significant are marked in green (0%), as illustrated in Figure 46. Likewise, the tool is designed to prioritise intuitiveness, error prevention, and clear data visualisation, ensuring that users can efficiently analyse and interpret results with minimal risk of error.

Serial Path (1, 2, 3)	
Yes	Path is included
No	Path not included

#	Description	Colour code
1	Floor Panel Inboard	
2	Floor Panel Middle	
3	Floor Panel Outboard	
4	Dado Gap	
5	Dado Panel	
6	Lower Sidewall Panel	
7	Window (-Panel)	
8	Upper Sidewall Panel	
9	ECS Gap	
10	Closure Panel	
11	Service Area Panel	
12	Ceiling ECS Gap	
13	Ceiling	

Colour code	Description
	Title/ main heading
	Input Parameter
	Predifined process/ subtitle especially for segment number or path number
	Output
	Blocked cell/ no entry can be given
	Separator
Available	Data/ ID are available in database
Occupied	Data/ ID are NOT available/ occupied in database

Colour code	Description
0%	Least dominant noise contributor
10%	
20%	
30%	
40%	
50%	midpoint
60%	
70%	
80%	
90%	
100%	Most dominant noise contributor

Figure 46: Key and colour-code

7 Verification, testing and validation

This section is divided into three parts to ensure that the tool meets the objectives: verification, testing, and validation. First, it will be verified whether the 6 main requirements are fulfilled. This is done according to the ARP 4754 which specifically checks whether the model satisfies the pre-defined requirements [41]. Verification according to the VDI 3633 assess the accuracy of the model by comparing the assumptions made and outcomes to real world observations [42]. Complete implementation of the VDI 3633 is not realisable in this case due to the limited amount of experimental data available. Instead, the assumptions involved in the model will be discussed together with its limitations and subsequent implications in section 8.3. Secondly, the tool will be tested using dummy values to test whether all functions of the tools are working and compare results with expected outcomes. This can be achieved incompliance with the ISO-29119 by creating test cases [43]. Validation of the tool can be further divided into 2 parts: validation of the requirements and validation of the final results. According to the ARP 4754, a system can be validated by assessing whether the requirements were correctly defined when comparing outcomes [41]. Verification and validation of the requirements are subjective, requiring expert opinion and large number of iterative loops for validation. While the validation of the requirement list will be omitted, the tool will be validated using on-ground cabin measurements from the experiment conducted by Ziegner. Since the available cabin measurements were recorded in SPL [dB], The calculated power from the tool will be converted to the equivalent unit for easy comparison.

7.1 Verification of the requirements

The verification of the requirement list can be carried out using a checklist.

Table 4: Checklist for requirements

Requirement #	Description	Meet	Does not meet
1	Predict noise power in cabin		
2	Include a range of configurations		
3	Easy and intuitive		
4	Determine the noise power for each segment		
5	Databank independent of tool		
6	Graphical representation of the power output		

A verification of the main requirements revealed that four out of the six requirements were fully met. However, it is challenging to make a definitive statement on whether the tool includes a broad range of configurations and whether it is easy and intuitive to use. Although the tool is capable of handling 3 serial paths and one parallel path, and capable of storing a range of different configurations, a genuine “meet requirement” is obtained if the database consists of more real measurements in its database. The more extensive the database, the more accurate the results and the broader the range of configurations it can accommodate. On the other hand, no objective scale was found to measure how easy or intuitive the tool is to use. The user interface was designed in accordance with ISO 9241-210, to enhance user-friendliness in software. For example, the tool and the database include a key, with dominant paths graphically represented and a colour code indicating each segment. Missing data are automatically detected and highlighted in red to alert the

user that the corresponding ID is not found. Additionally, data are recorded in rows instead of columns, aligning with industry and stakeholder practices for recording measurements across the third-octave scale horizontally. To conclude, the tool consists of features to enhance user-friendliness and productivity. However, the extent to which these features are effective can only be verified after thorough testing and feedback from stakeholders.

7.2 Testing of tool

After verifying the requirements, the tool was tested through several iterative loops by varying the parameters in the input section. First, the pre-processing conversion tool was tested using dummy values (round numbers such as 1), and the results were compared to the expected values. Secondly, the tool generated unique IDs for each set of measurements. Using a separate Excel sheet, it was confirmed that the generated IDs were indeed unique. Once validated, these measurements were stored in the database. By defining the input parameters, it was confirmed that the tool retrieved the correct values and calculated the expected outcomes accurately. Then the sensitivity of the tool to recognise small changes was carried out. After the tests, the decimal factor of the calculation was increased to 4 significant figures to account for small changes in power. Initially, excitation data and TFs were stored in separate databases for better organisation. However, after several tests, it was observed that frequently switching between databases was impractical. To address this, the structure was modified to store both excitations and TFs in the same database. This change also benefits stakeholders, as measurements from campaigns can now be directly stored in the database after conversion.

7.3 Validation with on-ground measurements

Finally, the tool will be validated by comparing the outcomes it produces with real on-ground cabin measurements. The input parameters for the tool are obtained from the measurement campaign M002 (with intensity box) [5]. However, since these measurements were recorded in decibels [dB], they must be converted to W. This is achieved using the pre-processing tool as shown in Figure 32 and Figure 33. Using the converted power in the cabin and the power in the excitation room, the TF will also be determine using the TF pre-processing tool. Figure 47 shows the approach in processing the available measurement data until it is stored in the database.

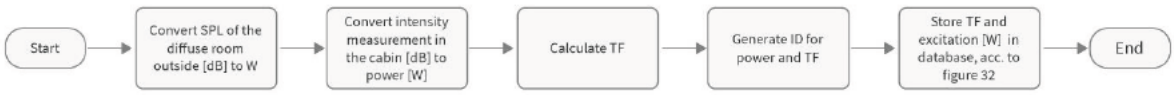

Figure 47: Approach to transform Ziegner's measurements using the tool

Since the TF is derived from known output and input, the tool can be validated by checking if it reproduces the original output power when multiplied by the TF. Although this seems evident, the purpose of this step serves as a validation of the formulae and functioning of the tool. A second validation involves, converting the calculated power output by tool into sound pressure level [dB].

To convert the recorded SPL [dB], in the diffuse field of the outside chamber, into Watts [W], equation 2.3 can be re-formulated. The pressure at each third-octave level can be calculated as follows:

$$p = 2 * 10^{-5} \cdot 10^{\frac{L_{p,i}}{20}} \quad Pa \tag{7.1}$$

As the pressures recorded were approximately the same across the fuselage for each frequency band, it is legitimate to assume that the sound field is a quasi-uniform one. The incident sound power on the skin of the fuselage panel can be calculated using equation 4.1.

$$W_{Excitation,i} = I_i \cdot A_i = \frac{p^2{}_{rms}}{pc} \cdot A_i \; [W] \tag{7.2}$$

Afterwards, the output power in the cabin is determined. The measured intensity is converted to power by re-formulating equation 2.2:

$$W_{Cabin,i} = 10^{-12} \cdot 10^{\frac{L_{W,i}}{10}} \cdot A_i \; [W] \tag{7.3}$$

From equation 4.3, the TF can therefore be expressed as:

$$H_i = \frac{W_{Excitation,i}}{W_{Cabin,i}} \tag{7.4}$$

The relationship between the SPL at the receiver and the incoming sound power level of the source is given using the equation 4.2:

$$L_{P,cabin} = L_{W,excitation,i} - 10 \cdot \log_{10} \frac{\bar{A}_{eq}}{S_0} + 6 - K_0 \;\; dB \tag{4.2}$$

Therefore, the calculated excitation power from equation 7.2 is converted to power level [dB] by using equation 2.2. Next, the total equivalent absorption surface area of the specimen, $\bar{A}_{total}$ is determined using equation 2.12 and the recorded reverberation time T in the cabin:

$$\bar{A}_{total} = 0.163 \cdot \frac{V}{T} \; m^2 \tag{7.5}$$

Since the measurement of T was not carried out in the whole section of the segment, $\bar{A}_{total}$should be corrected and scaled:

$$\bar{A}_{total,\; scaled} = \bar{A}_{total} \cdot V_{scaled} \tag{7.6}$$

As the DIN ISO 5129 (*Acoustics - Measurement of sound pressure levels in the interior of aircraft during flight*) does not specifically specify any value of c for the sound propagation and ρ for density, when measuring SPL in aircraft cabins, the value for the air density is based on the Internation Standard Atmosphere (ISA) and the DIN ISO 2533 [18]. At ground level this is approximately 1,225 $\frac{kg}{m^3}$. The characteristic impedance, $Z = \rho \cdot c$, of air is approximately $Z_0 = 400 \; \frac{N \cdot s}{m^2}$. at room temperature [8]. Hence, the correction factor K_0 is calculated using equation:

$$K_0 = 10 \; \log\left(\frac{Z_{measured}}{\rho \cdot c}\right) = -0{,}22 \; dB \tag{7.7}$$

8 Discussion

This chapter aims to provide a reflection on the whole modelling of the tool and interpretating the outcomes from section 7.3 (in section 8.1). Section 8.2 compares the approach adopted in this work with Ziegner's model. In section 8.3, the assumptions on which the model is based on and their subsequent limitations will be discussed, followed by possible sources of errors in section 8.4. Finally, section 8.5 provides some improvements and recommendations to further enhance the tool in future.

8.1 Interpretation of the results

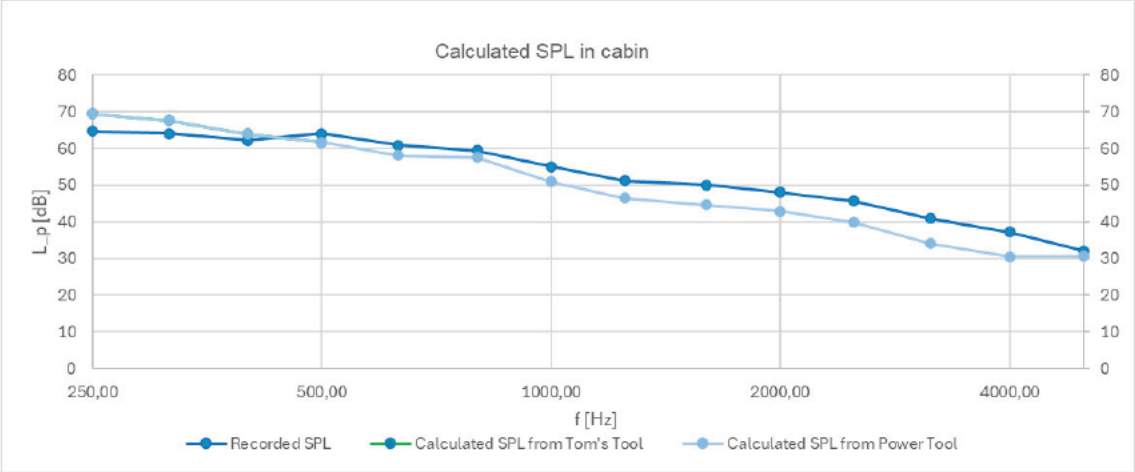

Figure 48: Comparison of calculated and measured SPL in the cabin

Based on the results from section 7.3, Figure 48 compares the measured and predicted SPLs between 250 Hz to 5000 Hz to Ziegner's results (overlapped), including the ranges of frequencies where the human ears are more sensible, which is between 2000 Hz and 5000 Hz [25]. The calculated SPL closely matched to the results from Ziegner's model, as they both used the same cabin intensity measurements (further explained in section 8.1.1). The overall trend of the graph also corresponds to the expected cabin SPL behaviour: SPL decreases with increasing frequency. This occurs because shorter wavelengths are more effectively absorbed and dissipated as transmission losses (primarily heat) through the cabin panels. Moreover, the contribution of structure-borne noise decreases at higher frequencies, while airborne noise becomes more dominant.

At 4000 Hz, the deviation of -9 dB between the measured and predicted SPL was highest. In acoustics, a 10 dB change is often perceived as the sound being twice as loud or half as quiet [8]. In the low frequency range, the SPL is overestimated. At 250 Hz, the positive deviation (+6 dB) compared to the measured SPL, could have occurred due to near-field effects or non-diffuse sound fields, calibration errors, or incorrect absorption assumptions led to overestimated intensity measurements (close to the panels) and TFs (will be further discussed in section 8.4). In the mid-frequency range, between 400 Hz and 800 Hz, the calculated SPL closely align with the measured SPL. This accuracy can be attributed to several factors, mainly the fact that the mass law is reasonably valid in this frequency range. Additionally, it can de deduced that the airborne and structure-borne noise contributions are well balanced, such that, the derived TFs fairly represent the overall sound transmission and flow of energy between the input excitation and the response.

Above 1000 Hz, the overall cabin SPL continues to decrease with frequency. However, the deviation between the calculated SPL and the recorded SPL, increases with frequency, reaching a maximum difference of -9 dB compared to the recorded SPL. This range marks a transition in the characteristics of sound transmission, where both sound mechanisms contribute to the overall SPL. The acoustic behaviour of the cabin becomes more complex, and the multi-layer panels do not behave as a single mass anymore. Predicting sound power solely with one linear TF is less reliable as they may not fully represent the complex sound transmission paths between layers. The sudden alignment at 5000 Hz could be an outlier caused by measurement inaccuracies or corrections.

8.1.1 Interpretation of the results compared to Tom Ziegner's results

After having described the trend of the produced outcome from the power model, this section aims to compare the approach of the power model to Ziegner's model. Figure 49 shows the calculated SPL derived from cabin power calculated by the Power Tool (left) and the calculated SPL from Ziegner's model (right). Both graphs show the same SPL.

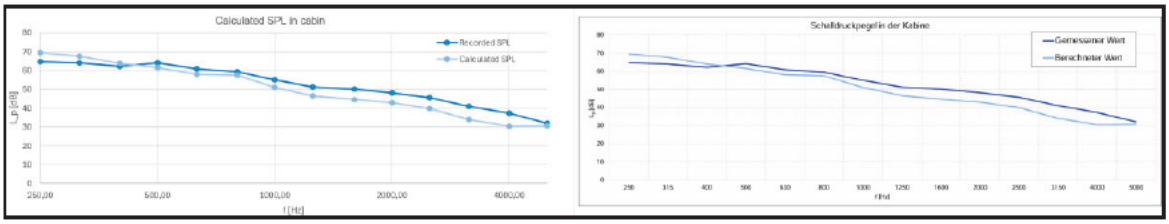

Figure 49: Comparison of TF model and Ziegner's model, left: TF approach, right: Ziegner's model from [5]

While both models rely on the fact that power is a scalar quantity [8] and the individual contribution of each panel can be linearly added to predict the cabin interior noise level (SPL), one difference is that, their method of determining the radiated sound power from each panel differ. In Ziegner's model, sound power coming from each panel is determined by converting the logarithmic intensity [dB] measurements close to the respective panel to the linear $\frac{W}{m^2}$ unit. The individual power contribution of each panel is multiplied by their respective area to subsequently obtain power in W. On the other hand, the power prediction model calculates the power contribution of each panel using TFs. Under identical external excitation conditions, the resulting power transmitted by each panel should theoretically be the same in both models, given that, TFs are frequency dependent. If the input excitation acting on the fuselage is known, the panel response can be predicted. Using the same chamber excitation as Ziegner, the model could be validated as follows:

(i) The TF model reproduced the same total power as Ziegner's (see attached excel tool and validation documentation in excel document: 3_validation_of_Tool)
(ii) The individual noise contribution and the dominants paths across each frequency band were the same in both approaches (refer to Figure 50)
(iii) Finally, the calculated SPLs were the same in both cases across the frequency range (refer to Figure 49)

This validates the approach of using TFs to predict the cabin noise level. Unlike intensity, sound power does not have a directional component, making it reasonable to omit phase related interactions or interference [8]. Hence, the contributions from multiple transmission paths can be determined through simple addition of parallel transfer paths from each panel (1-13). Figure 50 compares the results of the most dominant sound transmission paths [in %] from both approaches, demonstrating that both results are consistent. However, a direct comparison required an adjustment in the frequency scale, as the results from Ziegner were on the octave band scale, while the power tool generated outputs on a one-

third octave band scale. For the validation and comparison, the one-third octave band results across the three consecutive bands were reconstructed to the corresponding octave bands. For instance, the 1000 Hz octave band, the equivalent sound power was calculated as follows:

$$W_{octave,1000\ Hz} = W_{\frac{1}{3}octave,800\ Hz} + W_{\frac{1}{3}octave,1000\ Hz} + W_{\frac{1}{3}octave,1250\ Hz} \quad 8.1$$

Similarly, this was repeated for the frequency ranges 2000 Hz and 4000 Hz, (including 1000 Hz). Figure 50 shows the results of the most dominant paths contribution from Ziegner (above) and TF approach (below) in %.

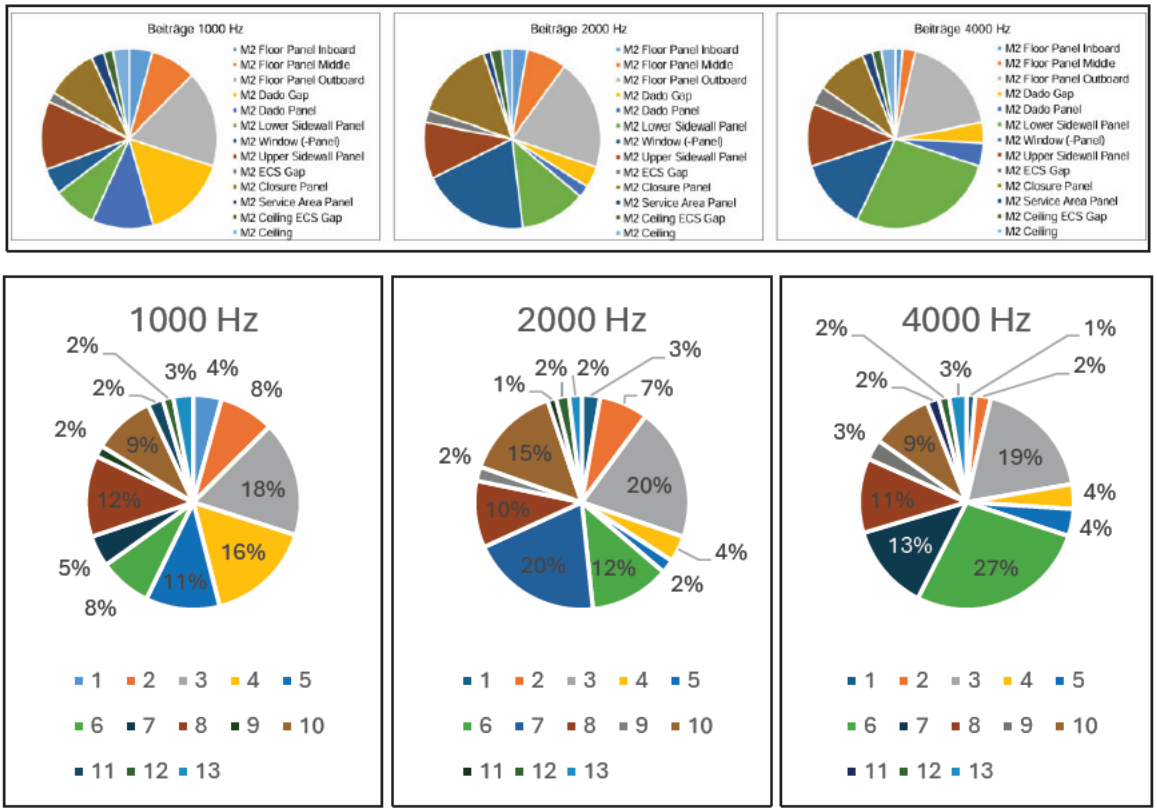

Figure 50: Most dominant paths contribution from Ziegner (above) [5] and TF approach (below) in %

At 1000 Hz, the floor panel outboard, the dado gap, and upper sidewall panel are the most dominant noise paths, contributing 18%, 14%, 12% respectively, to the total cabin sound power. The contribution of the floor panel and the upper sidewall can possibly be attributed to their position on the side of the speaker. At low frequencies, long wavelength vibration acting directly outside could be the reason for their respective noise contribution. A common noise control measure is adding mass layers to reduce sound transmission through these panel. Furthermore, possibly the 14% airborne noise leakage through the dado gap amplified the vibration of the floor panel. Since the dado area often includes joints and openings that are challenging to seal, it becomes a critical path for noise transmission. At 2000 Hz, the floor panel outboard (20%), the windows (20%) and closure panel (10%) are the most dominant noise paths. Particularly striking at 4000 Hz, is the 27% noise contribution of the lower sidewall, which demands further investigation to reach a concrete statement. Additionally, the window area remained a dominant noise source, contributing 13%. Replacing standard sunshades with acoustic sunshades or improving sealing techniques could increase the acoustic performance of window panels [44].

8.2 Comparison of the models

As established, both models are based on the principle that sound power is additive to identify the most dominant noise sources. Although the power tool and Ziegner's model share the same ultimate goal of predicting cabin interior noise levels, their methodologies of noise reduction differ in significant ways.

In Ziegner's model the mass law is employed to estimate the impact on noise mitigation by increasing the surface mass density. While this is a straightforward approach, it is only effective for single-layer panels or in frequency ranges where the relationship between mass and STL is valid. The impact of adding a new layer is calculated through an iterative loop, starting with the identification of the most dominant noise path in the cabin, and then proposing a specific mitigation measure. The user can select the mass layer (e.g. carpet, VIP mat, or mass sheet) from the database with its corresponding surface density values. Using the mass law, the expected change in STL (ΔdB) is calculated for the new layer. This corresponds to the difference in surface mass density before and after, such that ΔdB value is subtracted from the measured intensity levels of the panel. After adjusting the noise contribution of the modified panel, the model compares the new overall cabin SPL with a target value. If the target SPL is not yet reached, the loop continues by identifying the next dominant noise path and proposing another noise mitigation measure. This process is repeated until either the target SPL is achieved, or no further realistic mitigation measures can be made. On the other hand, the TF model can assess the impact of a new layer by just selecting its corresponding TF (TF-ID) in the input interface of the tool. The tool then retrieves the relevant data (e.g. expected operational exterior excitation) and automatically calculates the sound power output of the panel and the overall sound power in the cabin. This approach reduces the need for trial-and-error adjustments and is less time consuming. Additionally, it avoids cumulative errors that can propagate through multiple iterations in a loop, ensuring a more reliable and consistent prediction of noise reduction measures.

Secondly, Ziegner's model relies heavily on direct measurements of sound intensity near the panels. Here, the cabin power is derived, by measuring sound intensity near each panel in dB and subsequently converting these values into watts [W]. If noise transmission occurs simultaneously through a parallel path, for instance, parallel noise leakage through air gaps, their impact can be significant, which Ziegner's model is unable to consider. The power model, on the other hand, is capable of accounting for both parallel and serial transmission paths using TFs. Although the current model is limited to airborne sound transmission, the assumption that structure-borne contributions are captured by the TFs is reasonable, provided the measurements are conducted close to the vibrating panels and more than one TFs are used. In any case, the predicted sound power is likely to be more accurate compared to Ziegner's model.

Another key difference between the models is that the power model can quickly adjust to new inputs without requiring new measurement campaigns. Once the TFs are determined, the impact of varying external excitation can be easily analysed, as the frequency-dependant TFs will remain stable, provided the cabin layout and panel configurations are unchanged. In contrast, Ziegner's model requires new measurements each time the external excitation is changed. However, one advantage of Ziegner's model is that it can predict noise levels without information on the excitation, as it directly relates STL to panel configurations. Conversely, the power model requires both external excitation data and TFs to predict sound. Additionally, the power model is able to work with different types of acoustic input data. As the TFs are on a power-to-power basis, the tool includes a pre-processing sub-tool that converts SPL, intensity, or pressure measurements into W. This feature makes the model highly adaptable, as it can handle various data formats and quickly predict cabin noise levels based on different excitation conditions, making it more versatile and adaptable.

Yet, the TFs approach comes with some trade-offs. Possibly the main limitation of the model is its inability to differentiate between airborne and structure-borne sound transmission. Instead, the model assumes that the structure-borne contributions are indirectly included through the airborne sound radiation close to the vibrating surfaces. While this simplification reduces complexity, the accuracy of the tool decreases, particularly at lower frequencies, where structural vibrations are dominant. Unlike ABN which is often attenuated by insulation materials and sealing techniques, SBN can travel through rigid structural connections, making it harder to manage. This can possibly explain why the predicted noise from Figure 48 was overestimated at low frequencies (200 Hz and 500 Hz), assuming that, the recorded cabin SPL from the measurement campaign was accurate. The TF was derived from high-intensity measurements taken close to the panel, but as airborne sound travelled to the receiver, it was absorbed, resulting in a -6 dB difference. If the structure-borne component is dominant, airborne intensity measurements may not fully capture the transmitted energy through structural paths, leading to inaccurate predictions, if the power prediction involved only one TF.

Table 5 summarises the main aspects of between Ziegner's model and the power model.

Table 5: Summary of main differences between Ziegner's model and the power model

Aspect	Ziegner's model	Power model
Method of determining panel power	Direct intensity measurements in dB near each panel	W calculated using TF relating external excitation to internal response
Input Parameter	Measured sound intensity levels (dB), $\Delta dB, kg$	Chamber excitation & cabin output to calculate TF
Sound Power Calculation	Converts intensity (dB) to $\frac{W}{m^2}$ and multiplies by panel area to calculate W Individual power of panel are summed after converting from dB to linear units (W)	Uses TFs to predict the W transmitted through each panel Panel powers are directly summed after calculating through TFs
Main approach	Delta, Mass law	TF, FRF
Dominant Path Identification	Identifies dominant paths based on measured intensity levels ->W-> % across panels	Identifies dominant paths based on the W ->% contribution predicted by TFs for each panel
Pros	Straightforward for identifying dominant ABN. Relatively simple experimental setup when measuring internal noise. Only requires cabin measurement.	Able to consider multiple. path transmission. Simple if TF available. Works well reciprocally. Allows for future predictions without requiring additional cabin measurements. Easily analyse impact of new layers. Fast/ no iterative loops.
Cons	Relies on mass law. Delta approach-> time consuming. Sensitive to measurement inaccuracies and noise interference. Can only capture ABN. Requires manual post-processing to convert dB to W before summing contributions. Iterative loop can be time-consuming and may introduce cumulative errors from measurement corrections.	Requires further development to incorporate separate TFs for ABN & SBN. Depends on accurate TF measurements and external excitation knowledge. Requires separate TFs for each transmission path. Inaccurate in only 1 TF.

8.3 Assumptions, simplifications and further limitation of the model

While the developed tool is able to provide valuable insights when predicting sound power in VIP cabins, it should be acknowledged that the modelling is based on a few acoustical and physical assumptions, which hold greater validity in certain frequency ranges than in others. This impacts the accuracy of the tool and hence the calculated power output. Additionally, the limited experimental data available were another constraint which involved even more assumptions to obtain calculated results. However, these simplifications were paramount, so that, the tool aligns with the requirement of the task.

Generally, deriving TFs from ground-based measurements can be extrapolated to flight conditions provided the appropriate input excitations are selected in the tool. However, several factors can introduce errors during real flight scenarios. Even if the impedance, stiffness, and damping characteristics of the fuselage will be relatively stable over frequency, depending on the geographic territory of the aircraft operation, significant temperature drop can cause the properties of porous or elastomeric materials to fluctuate. If this happens, even the frequency-dependent TFs may not accurately predict noise as cold temperature induces strains in the panels, influencing the transmission paths (see section 3.2). If the input parameters selected in the tool do not account for these variations, there is a risk that the TFs will not accurately predict the resulting sound power. Additionally, one assumption made in the model and calculations is that the pressure is the same across the excitation room and close to the fuselage panels. At cruising altitude, the excitation of the panels is far from being uniform. Different sources of noise such as engines or TBL generate frequency-dependent excitations on the fuselage, causing its components, e.g. wings, to vibrate. These directional excitations propagate through the fuselage and cause localised vibrations on specific panels. Consequently, some panels experience higher excitation levels. It is worth highlighting that the tool is able to assign specific excitation input power to each panel, allowing future investigations of external and secondary noise sources to be integrated into the noise analysis.

Furthermore, the tool is an empirical model which relies on experimental data to derive power-to-power TFs. Although, the tool can consider up to four series and one parallel transmission paths, this feature is only beneficial if the respective measurements are available and feasible. Obtaining such measurements is particularly challenging within OEM partitions due to the accessibility constraints. For power-to-power magnitude-based TFs, omitting the phase information, including delays caused by different path lengths, is acceptable as the phase interactions between sound waves typically average out over time. This assumption simplifies the model and is particularly valid for broadband noise, such as TBL excitation and in diffuse sound fields. However, the pure addition of the sound power neglects potential interference effects, which can be significant for narrowband or tonal noise (e.g. noise from engine blades or gearbox components) and at higher frequencies, where shorter wavelengths result in more frequent phase interactions.

Beyond that, some limitations arise from the tool itself. In acoustics, different measurement scales are employed depending on the instruments used and the objectives of the measurement campaign. Due to time, cost, and practical constraints, measurements are typically limited to specific frequency ranges. One key limitation of the tool is its inability to process data not recorded on the third-octave band scale. On the other hand, even if the data are recorded on this scale, interpolation between missing frequency bands within the one-third-octave scale is not possible, due to the quadratic averaging process (discussed in section 2.8). In such a case, data must be manually entered based on user experience. While interpolation between FFT data points can be applied to linear datasets with sufficient resolution (e.g., every 10 Hz), incorporating this functionality into the tool would

increase its complexity and require clear specifications on the expected input format. To keep the tool straightforward and user-friendly, this pre-processing step has been omitted, relying instead on an external FFT-to-octave conversion tool. Nonetheless, integrating such functionality in future iterations will certainly improve the versatility of the tool. Additionally, the tool does not explicitly model error propagation, to consider measurement errors. An additional improvement feature would be to warn users about any potential health hazards during the prediction (e.g. noise level above 85 $dB(A)$). However, as the tool is limited to predicting sound power in W, from $dB(Z)$ intensity measurements, integrating such warnings was not feasible during the development.

Finally, some limitations arose through the validation and verification process. First, the tool could only be validated using Ziegner's measurement. While this could validate the model, further testings using different sets of measurements are required for a more comprehensive validation. An even more interesting aspect would be to broaden the validation process and determine the efficiency of decomposing a transmission path into sub-paths in series. Likewise, it should be investigated to what extent, the assumption that airborne TFs can be linearly multiplied hold and how much of the contribution of SBN are captured by airborne intensity measurements, particularly at lower frequencies where SBN dominates.

Beyond that, the requirement-list and the tool could not be fully tested according to the defined norms. For instance, verification according to DIN 3633 was not achievable due to the lack of experimental data. This guideline also implies verification of assumptions, which is challenging for a simplified model. Additionally, it remains unclear whether the tool complies with the user-friendliness criteria outlined in ISO 9241-210, as this necessitates extensive testing in practice to ensure compliance. Finally, it can be argued that recording data vertically would be more practical, as it allows easier application of formulas by dragging cells in Excel. If vertical data entry is required, users can the "transpose feature" in Excel to convert horizontal data to vertical format. Concluding, it should be highlighted that the current model is based on only one section of the cabin. The acoustic field within this section depends on the location of the receiver in relation to the source of noise and layout/ configuration of the cabin. For instance, the acoustic properties of the cockpit, passenger area, and aft sections would vary due to variations in geometry, materials, and local excitation. Hence, extrapolating results from a single section to the entire cabin is not suitable, as the derived TFs are only valid for the specific fuselage section.

8.4 Consideration of errors

This section highlights the main sources of error which could have arisen during the sound prediction and or in the future. These errors primarily occur as a result of the limitations and assumptions made in the modelling. As previously discussed, the accuracy of an empirical model depends on the accuracy of the raw data inserted into the tool. Measurement uncertainties mainly arise from random and systematic errors. While random errors cannot be fully avoided, they usually tend to cancel out from averaging and filtering. On the other hand, systematic errors are often caused by wrong calibration of the measuring instruments used [45]. While the purpose of the intensity box was to shield the measurements from external transmission paths and background noise, it could also be a potentially be a source of systematic error by shielding background noise. Furthermore, the "Basotect" foam can possibly absorb short wavelengths such that the intensity measurements are underestimated, and the derived TFs will subsequently underpredict sound power, especially at high frequencies. Additionally, converting intensity and

pressure to power may also introduce potential errors, rounding inaccuracies and use of correction factors. Other measurement error could have arisen as a result of the phase difference using the p-p probes to measure intensity. At low frequencies, the sound field close to the panels could possibly be not diffuse enough, with huge fluctuations in pressure. If the sound field close to the panels is a near field, these fluctuating pressure differences can result in an overestimation of the measured intensity, due to the huge pressure gradient between the two microphones. Additionally, misaligning the probe relative to the incoming sound wave can introduce phase errors.

Another potential errors may have arisen during the conversion of SPL into power. The tool assumes identical radiating and incident surface areas inside and outside the cabin when converting SPL measurement to power. Although, this is a reasonable approach, and also the fundamental assumption in window transmission loss experiments, it overlooks differences in geometry. Unlike flat window panels the geometry and surface area of the outer skin of the fuselage may not necessarily be identical to the interior panel in the cabin, especially if rigid partitions are firmly attached to the skin of the fuselage.

8.5 Improvement and recommendation

Despite its limitations and potential sources of error, the developed tool effectively identifies dominant noise paths and reproduced the same overall power as Ziegner's model. Since the accuracy of the predicted sound power levels depends on the quality and accuracy of the input data rather than the tool itself, this aspect will not be addressed in this discussion. Nevertheless, several improvements can be made to enhance the precision of the model.

One major development would be to incorporate SBN components into the model. In a vibro-acoustic system, the total sound transmission of the system can be described, analogous to the first law of thermodynamics, as the flow of energy with the system. In a system where energy is conserved, the total energy of the system is given as the sum of the structure borne and airborne components (see equation 2.7). For instance, in a panel, the airborne $TF_{Airborne}$ ($\frac{W_{out,Air}}{W_{in}}$) determines how much sound pressure is excited in the air gap while the structure borne $TF_{Structure}$ ($\frac{W_{out,Structure}}{W_{in}}$) measures how much the sound energy radiates from the structural vibrations. When ABN interacts with SBN, the mechanical response of the panels and acoustic response of the cavity occur simultaneously and both depend on each other [3].This is because the structural vibrations and the airborne sound field are both coupled. Hence a coupling factor C is required to describe how energy is transferred between them.

$$TF_{Total} = TF_{Air} + TF_{Structure} + C \qquad 8.2$$

The coupling factor, C, depends on the material properties (stiffness, damping, density) and boundary conditions of the panels (how is it mounted). Like the TF, C varies with frequencies and characterises how much energy transfers between the panel vibration and the neighbouring air volume. Some practical methods to determine C is through experimental measurements, analytical models or empirical data from similar structures [46] [47]. Additionally, the tool could include Rayleigh Integral to estimate how much of the structural vibration energy is converted into ABN radiation using the vibration velocity and radiation efficiency of the panel. This method is a simplified yet effective way to consider the radiation efficiency of surfaces and ultimately include the structure borne contributions. As discussed, directly measuring SBN paths can be challenging. In such cases, a more feasible approach would be applying simplified assumptions and models such as the

mass-spring-damper model together with natural frequencies, damping characteristics and material properties to approximate the contributions of unmeasured transfer paths. Another approach is to estimate the velocity using averaged values from similar panels or use empirical correction factors derived from existing data. Likewise, the tool remains practical and does not rely on “guessed” values from experience, when data are incomplete.

A practical way to implement this within the existing 13-panel approach is to split each path into its airborne and structure-borne contribution. Figure 51 shows a concept of the input interface, demonstrating how the existing Power tool can incorporate SBN and the coupling factor (to note that this is only a concept and not part of the tool).

Number	Description	Serial Path 1 ABN	Serial Path 1 SBN	Serial Path 1 CF	Serial Path 2 ABN	Serial Path 2 SBN	Serial Path 2 CF	Configuration	Excitation	Excitation
P1	Floor Panel Inboard	11-A1	11-S1	C-1	12-A1	12-S1	C-11	-	E1	ETOM1
P2	Floor Panel Middle	21-A1	21-S1	C-2	21-A1	21-S1	C-12	-	E2	ETOM2
P3	Floor Panel Outboard	31-A1	31-S1	C-3	31-A1	31-S1	C-13	-	E3	ETOM3
P4	Dado Gap	41-A1	41-S1	C-4	41-A1	41-S1	C-14	-	E4	ETOM4
P5	Dado Panel	51-A1	51-S1	C-5	51-A1	51-S1	C-15	-	E5	ETOM5
P6	Lower Sidewall Panel	61-A1	61-S1	C-6	61-A1	61-S1	C-16	-	E6	ETOM6
P7	Window (-Panel)	71-A1	71-S1	C-7	71-A1	71-S1	C-17	-	E7	ETOM7
P8	Upper Sidewall Panel	81-A1	81-S1	C-8	81-A1	81-S1	C-18	-	E8	ETOM8
P9	ECS Gap	91-A1	91-S1	C-9	91-A1	91-S1	C-19	-	E9	ETOM9
P10	Closure Panel	101-A1	101-S1	C-10	101-A1	101-S1	C-1001	-	E10	ETOM10
P11	Service Area Panel	111-A1	111-S1	C-11	111-A1	111-S1	C-1101	-	E11	ETOM11
P12	Ceiling ECS Gap	121-A1	121-S1	C-12	121-A1	121-S1	C-1201	-	E12	ETOM12
P13	Ceiling	131-A1	131-S1	C-13	131-A1	131-S1	C-1301	-	E13	ETOM13

Figure 51: Concept of input interface of future Power Tool to include SBN and coupling factor

Using the same approach of the current tool, the total TF of a path involving ABN and SBN can be calculated, incorporating equation 8.2 in the tool. The coupling factor can be determined on another sheet together with its material properties, boundary conditions, and empirical correction factors.

Path #	TF ID	Description	12,5	16	20	25	31,5	40	50	63	80
1.1-ABN	11-A1	ABN	0,1	0,2	0,3	0,4	0,5	0,6	0,7	0,8	0,9
1.2-SBN	11-S1	SBN	0,2	0,18	0,16	0,14	0,12	0,1	0,08	0,06	0,04
1.C	C-1	C	0,1	0,08	0,06	0,04	0,02	0	-0,02	-0,04	-0,06
Total			0,4	0,46	0,52	0,58	0,64	0,7	0,76	0,82	0,88

Figure 52: Concept of TF calculator future Power Tool to include SBN and coupling factor

Another further improvement of the tool is to include the phase component in TFs as discussed in section 2.9 to improve predictions. However, it should be investigated whether the errors caused by time delays are significant and whether this improvement is worthwhile and achievable without adding much complexity. Additionally, the accuracy of used correction factors in this work should be further investigated. For instance, correction factors during data processing could also help to adjust TFs, especially if the coupling

factors for SBN are included in the database in future. However, the challenge is determining the correction factor itself, as this depends on measurement instruments. One way of implementing this, is using the Gaussian error propagation law to include the percentage error in the TFs in the tool. For a ratio function, $f = \frac{x}{y}$, the uncertainty σ_f can be determined as follows: [48]

$$\frac{\sigma_f}{f} = \sqrt{\left(\frac{\sigma_x}{x}\right)^2 + \left(\frac{\sigma_y}{y}\right)^2}$$

8.3

If the TFs are calculated from pressure and since power is proportional to the square of pressure, $W \alpha p^2$, the uncertainty $\sigma_{H,i}$ of the TF, H_i can be determined as follows:

$$\frac{\sigma_{H,i}}{H_i} = \sqrt{\left(\frac{2 \cdot \sigma_{p,\ Excitation}}{p_{excitation}}\right)^2 + \left(\frac{2 \cdot \sigma_{p,\ cabin}}{p_{cabin}}\right)^2}$$

8.4

Where $\sigma_{p,\ Excitation}$ and $\sigma_{p,\ cabin}$ are the uncertainty in the measurement of the excitation and cabin pressure respectively, $p_{excitation}$ and p_{cabin} are the recorded pressure, H_i is the calculated TFs. Hence, the uncertainty of each parameter depends on the instrument and method used for measurement.

Beyond the already discussed improvement, a valuable add-on for cabin manufacturers would be, to include a feature to calculate cost per noise reduction ($€/dB$), fuel efficiency, and operative cost. This can provide manufacturers a depiction of the break-even and benchmark each measure.

9 Conclusion

The developed tool is part of the ENTIRETY project, a collaboration between the Lufthansa Technik AG, ZAL and HAW Hamburg, aimed at improving acoustic comfort, without increasing the weight of the VIP cabin. This work focuses on developing a power prediction tool, that is at the same time, able of identifying and quantifying the most dominant transmission paths and analysing the impact of noise reduction strategies.

This power prediction tool is an empirical model, based on on-ground experimental data, applying a similar approach as Transfer Path Analysis (TPA) or Frequency Response Function (FRF) and describes the response of a system to external excitation, through transfer functions (TFs). This methodology is particularly suitable for enclosed acoustic boundaries systems, such as aircraft cabins, which operate in a relatively stable exterior medium at cruising altitude and consists of a relatively fixed interior layout. The development of the tool followed the VDI 2221 guidelines, where applicable, and at the same time aligning itself to a requirement list, created in collaboration with Lufthansa Technik AG. This approach ensured that the tool remained practical, efficient, and compliant with aviation regulations. Furthermore, a framework was created to ensure that the tool remained aligned within established guidelines as well as industry best-practices. After the development process, the approach and methodology could be validated using available measurement data and industry norms, such as ARP and DIN ISO guidelines.

This work marks the initial investigation into the feasibility of power-to-power TFs for VIP cabin noise prediction. While the approach could be validated, the accuracy of the noise analysis depends on the specificity of each case. If the purpose of the noise analysis is qualitative and a comparative analysis of dominant sound paths, the current approach is acceptable. Ultimately, to achieve its goal of assisting cabin manufacturers increasing acoustic comfort without increasing weight of the aircraft, the tool will require further improvements and tool optimisation. A key area for future development is the integration of structure-borne noise contributions, which are currently simplified using energetic assumptions. In addition to only predicting noise levels, the tool can provide a valuable add-on to manufacturers by implementing a feature to benchmark noise reduction measures against their mass and cost impact. This will enable a more informed decision-making during the cabin completion process, allowing manufacturers to evaluate trade-offs between acoustic performance, weight, and cost, without compromising fuel efficiency or sustainability goals. In a highly competitive and cost-sensitive industry, such functionality is essential for balancing passenger comfort, operating costs, and efficiency. Beyond its immediate practical utility, the tool can hence contribute to broader industry goals by supporting sustainability and reduce carbon footprints. To reiterate, the purpose of the tool is not to replace traditional SEA or FEA models, but rather to bridge the gap between practicability, cost-effectiveness, and precision, particularly for small- to medium-sized cabin manufacturers or the VIP jet market, where the number of completions is relatively low. By calculating sound power through a loop of just 10 steps (refer to Annex X), the tool prioritises qualitative noise path analysis within a short runtime, adhering to the principle of:

"as simple as possible, and as accurate as needed"

In conclusion, the tool shows promising potential to evolve into a practical, productive and reliable resource for cabin manufacturers, delivering efficient noise reduction solutions, while balancing efficiency and comfort, likewise, supporting the future of sustainable VIP air travel.

VI. References

[1] Statista. "Business jets: market size 2020-2028 | Statista." Accessed: Jun. 1, 2025. [Online]. Available: https://www.statista.com/statistics/1280516/business-jet-market-size-worldwide/

[2] M. J. Crocker, *Engineering Acoustics: Noise and Vibration Control* (Wiley Series in Acoustics Noise and Vibration Ser). Newark: John Wiley & Sons Incorporated, 2021. [Online]. Available: https://onlinelibrary.wiley.com/doi/book/10.1002/9781118693902

[3] I. Dimino, *Active control of aircraft cabin noise* (Computational and experimental methods in structures Vol. 7). London: Imperial College Press, 2015.

[4] V. Mellert, I. Baumann, N. Freese, and R. Weber, "Impact of sound and vibration on health, travel comfort and performance of flight attendants and pilots," *Aerospace Science and Technology*, vol. 12, no. 1, pp. 18–25, 2008. doi: 10.1016/j.ast.2007.10.009. [Online]. Available: https://www.sciencedirect.com/science/article/pii/s1270963807001174

[5] Tom Ziegner, "Quantifizierung und Minimierung von Schallleistungsbeiträgen in der VIP-Flugzeugkabine und Prognose des Kabinenpegels anhand eines Schallleistungsmodells," Master Thesis, HAW Hamburg, Hamburg, 2023.

[6] Bennett Bögle, "Anforderungen und Funktionen für ein Schallleistungsmodell von Flugzeugkabinen mit Konzeptentwicklung," Projekt im Master, HAW Hamburg, 2024.

[7] M. J. T. Smith, *Aircraft Noise* (Cambridge aerospace series 3). Cambridge: Cambridge University Press, 1989.

[8] G. R. Sinambari and S. Sentpali, *Ingenieurakustik: Physikalische Grundlagen und Anwendungsbeispiele,* 5th ed. Wiesbaden: Springer Vieweg, 2014.

[9] Jakob Putner, *Operational transfer path analysis predicting contributions to the vehicle interior noise for different excitations from the same sound source*, 2012. [Online]. Available: https://mediatum.ub.tum.de/doc/1137875/document.pdf

[10] Andrey Hense, Mahdi Ahi, Said El Kadmiri Pedraza, Fabien Chauvicourt, Sjoerd, "Active reduction of noise transmitted into and from enclosures through encapsulated structures: Review on Cabin Noise Simulation Framework," IN-NOVA MSCA Doctoral Network, May. 2024.

[11] D. A. Bies, *Engineering noise control: Theory and practice,* 4th ed. London: Spon Press, 2009.

[12] W. V. Bhat and J. F. Wilby, "Interior noise radiated by an airplane fuselage subjected to turbulent boundary layer excitation and evaluation of noise reduction treatments," *Journal of Sound and Vibration*, vol. 18, no. 4, pp. 449–464, 1971. doi: 10.1016/0022-460X(71)90097-6. [Online]. Available: https://www.sciencedirect.com/science/article/pii/0022460X71900976

[13] J. F. Wilby, "Interior Noise of General Aviation Aircraft," in *SAE Technical Paper Series*, 400 Commonwealth Drive, Warrendale, PA, United States, vol. 91, 1982, doi: 10.4271/820961.

[14] Wan-Ho Cho and Ji-Ho Chang, *Investigation of effect on the acoustic transfer function in a vehicle cabin according to change of configuration*, 2019. [Online]. Available: https://publications.rwth-aachen.de/record/770208/files/770208.pdf

[15] Siemens Digital Industries Software. "An Introduction to Transfer Path Analysis." Accessed: May 1, 2025. [Online]. Available: https://community.sw.siemens.com/s/article/an-introduction-to-transfer-path-analysis

[16] T. H. A. Boratto, C. M. Saporetti, S. C. A. Basilio, A. A. Cury, and L. Goliatt, "Data-driven cymbal bronze alloy identification via evolutionary machine learning with automatic feature selection," *J Intell Manuf*, vol. 35, no. 1, pp. 257–273, 2024, doi: 10.1007/s10845-022-02047-3.

[17] Romain Boulandet, *Active reduction of sound transmission in aircraft cabins: a smarter use of vibration exciters*, 2014. [Online]. Available: https://www.acoustics.asn.au/conference_proceedings/internoise2014/papers/p552.pdf

[18] *Standard Atmosphere*, 2533, International Organisation for Standardisation, 1975.

[19] G. R. Sinambari, *Design acoustics: Primary and secondary noise mitigation*. Wiesbaden, Heidelberg: Springer, 2023. [Online]. Available: http://www.springer.com/

[20] J. Begin, "Transfer Function Measurements with APx500 Audio Analyzers," [Online]. Available: https://www.admess.de/tl_files/admess-2013/pdf/Audio%20Precision/TN138%20-%20Transfer%20Function%20Measurements%20with%20APx500%20Audio%20Analyzers.pdf

[21] Siemens Digital Industries Software. "What is the Fourier Transform?" Accessed: Mar. 1, 2025. [Online]. Available: https://community.sw.siemens.com/s/article/what-is-the-fourier-transform

[22] Prof. Dr.-Ing Benedikt Plaumann, *Akustik: Grundlagen – Signalanalyse im Frequenz- und Zeitbereich*, WiSe 2024.

[23] "Transfer Path Analysis: Qualifying and quantifying vibro-acoustic transfer paths," Siemens Digital Industries Software.

[24] Prof. Dr.-Ing Benedikt Plaumann, *Akustik: Schallübertragung*, Wisem 2024.

[25] Harvey H. Hubbard, *Aeroacoustics of Flight Vehicles: Theory and Practice: Volume 2: Noise Control*. Hampton, VA, United States: NASA Langley Research Center, 1992.

[26] Anderson Proença, "Aeroacoustics of isolated and installed jets under static and in-flight conditions," University of Southampton, 2018. [Online]. Available: https://www.researchgate.net/publication/329672486_Aeroacoustics_of_isolated_and_installed_jets_under_static_and_in-flight_conditions

[27] Florida Flyers, "Indicated Airspeed vs True Airspeed," *Florida Flyers Flight Academy Flight School*, 27 Jan., 2024. Accessed: Nov. 23, 2024. [Online]. Available: https://www.flightschoolusa.com/indicated-airspeed-vs-true-airspeed-what-1/?srsltid=AfmBOopANr3mZptVHXKH3p3Pmnt2JUiliYLen3uwysAq-MLLRwGAW3yy#introduction-to-airspeed

[28] ATR. "ATR HighLine - ATR." Accessed: Dec. 1, 2025. [Online]. Available: https://www.atr-aircraft.com/innovation/cabin/highline/

[29] Safran. "Economy class seat Z400." Accessed: Dec. 1, 2025. [Online]. Available: https://www.safran-group.com/products-services/economy-class-seat-z400

[30] *Determination of sound power levels and sound energy levels of noise sources using sound pressure: Precision methods for reverberation test rooms*, 3741, International Organisation for Standardisation, 2010.

[31] Prof. Dr.-Ing Benedikt Plaumann, *Akustik Skript: Akustische Mess- und Versuchstechnik*. HAW Hamburg, WiSem 2024.

[32] *Entwicklung technischer Produkte und Systeme - Modell der Produktentwicklung*, 2221, Verein Deutscher Ingenieure e.V.

[33] N. K. Mandal, *Semi Empirical Modeling of Engineering Systems Nirmal Kumar Mandal,* 1st ed. Saarbrücken: LAP LAMBERT Academic Publishing, 2017.

[34] J. Gordon Leishman, *Acoustics of Flight Vehicles* (Introduction to Aerospace Flight Vehicles). Embry-Riddle Aeronautical University, 2023. [Online]. Available: https://eaglepubs.erau.edu/introductiontoaerospaceflightvehicles/chapter/noise-of-flight-vehicles/

[35] *Acoustics - Measurement of sound pressure levels in the interior of aircraft during flight*, 5129, International Organisation for Standardisation.

[36] ICAO, "Annex 16 - Environmental Protection - Volume I - Aircraft Noise," Jul. 2017.

[37] E. Hering, *Software-Engineering*. Wiesbaden: Springer Vieweg. in Springer Fachmedien Wiesbaden GmbH, 1984. [Online]. Available: https://ebookcentral.proquest.com/lib/kxp/detail.action?docID=6711265

[38] J. Zhang, P. Li, Z. Zhao, and H. Wang, "Research and Application of Function Requirements Validation Process for Civil Aircrafts Based on ARP 4754A," in *2024 3rd International Symposium on Aerospace Engineering and Systems (ISAES)*, 2024, pp. 274–277, doi: 10.1109/isaes61964.2024.10751556.

[39] *Ergonomie der Mensch-System-Interaktion*, 9241-220, DIN Deutsches Institut für Normung e.V.

[40] J. O. Smith, *Introduction to digital filters: With audio applications,* 2nd ed. USA: W3K Publishing, 2008.

[41] *Guidelines for Development of Civil Aircraft and Systems*, 4754A, SAE Aerospace.

[42] *Simulation von Logistik-, Materialfluss- und Produktionssystemen*, 3633, Verein Deutscher Ingenieure e.V.

[43] *Software and systems engineering - Software testing*, 29119, International Organisation for Standardisation, 2022.

[44] Mojtaba Sadeghian, Mofid Gorji Bandpy, "Technologies for Aircraft Noise Reduction: A Review,"

[45] L. Kirkup and R. B. Frenkel, *An Introduction to Uncertainty in Measurement: Using the GUM (Guide to the Expression of Uncertainty in Measurement)*. Cambridge, New York, Melbourne, Madrid, Cape Town, Singapore, São Paulo: Cambridge University Press, 2010.

[46] K. Sato and N. Lalor, "Obtaining internal and coupling loss factors by a transient test method," *The Journal of the Acoustical Society of America*, vol. 86, S1, S64-S64, 1989, doi: 10.1121/1.2027593.

[47] R. Ming, "The measurement of coupling loss factors using the structural intensity technique," *The Journal of the Acoustical Society of America*, vol. 103, no. 1, pp. 401–407, 1998, doi: 10.1121/1.421096.

[48] M. Grabe, *Generalized Gaussian Error Calculus*. Berlin, Heidelberg: Springer Berlin Heidelberg, 2010.

VII. Requirement list

Table 6 shows the requirement list from 5.1, on which the tool was based on.

Table 6: Requirement list

#	# in Bögle list	Category	Description
F1		Requirement	The tool should be able to predict noise power inside the cabin.
F2	F2	Requirement	The tool should be able to identify the most dominant sound power paths.
F3		Requirement	The tool should include a range of excitations representing the sources of noise TBL, engine noise, aerodynamics etc.
F4	A6	Requirement	The power output should be displayed graphically over the frequency band.
F5	F5	Requirement	The data stored in the databank should be able be altered, modified, corrected or replaced
F5		Requirement	The databank for the parameters used in the calculations must be independent of the tool and stored separately.
F6		Requirement	The model should be able to differentiate between noises in series and noises in parallel
F7		Requirement	The tool should be operated using MS Excel.

VIII. Parameter list

Table 7 is the list of parameters from section 5.2.

Table 7: Parameter list

#	# in Bögle list.	Category	Description
P1	P1	Parameter	The tools should be able to include a large range of excitations coming from outside, for example: engine noise, TBL, aerodynamics.
P2	P2	Parameter	The input parameters should be limited to a reasonable scale.
P3	P17	Parameter	The model should be valid for different frequency bands.
P4	P14	Parameter	The aircraft cabin section is divided into panels and area.
P5	P15	Parameter	The panels and area are further divided into their respective sub-panels.
P6	P6	Parameter	The cabin panels consist of different layers.
P7		Parameter	The parameters in the model must be able to be altered to predict the noise power in the cabin.
P8	P12	Parameter	The database consists of the power-loss-factor (TF) and noise power (excitations) over frequencies.
P9		Parameter	Depending on the parameters and the unit of the input, the model should also be able to convert unit.
P10		Parameter	The model should be able to differentiate between serial sound paths and parallel paths.
P11		Parameter	The model should include all path possibilities for sound to penetrate the cabin.

IX. Application of Tool using case M002

This section serves as a user-manual on how to use the tool based a concrete case: measurements M002 conducted by Zieger in work [5]. The steps follow the flowchart from Figure 31. The recorded SPL measurement for the excitation chamber and intensity measurements for each segment of the cabin were provided. Figure 53 shows the recorded SPL from the experiment M002, with the intensity box. (see Figure 53)

f_Hz	SPL_dB
12,5	54,16
16	49,8
20	47,85
25	45,51
31,5	44,25
40	52,31
50	60,92
63	69,86
80	73,61
100	78,17
125	81,86
160	82,74
200	91,97
250	93,07
315	95,51
400	95,8
500	95,21
630	96,28
800	98,46
1000	99,81
1250	98,76
1600	98,77
2000	99,52
2500	99,26
3150	97,46
4000	97,03
5000	94,88
6300	89,61
8000	87,82
10000	82,04
12500	69,78
16000	55,98
20000	37,78

Figure 53: Measured SPL [dB] in the excitation chamber from experiment M002 (results provided)

Figure 54 shows the recorded sound intensity [dB] across the 13 panels from the experiment M002 (with intensity box). After the measurements are obtained, it is checked if they are in the standardised one-third scale. If the measurements are in FFT, they should be converted using the existing tool provided from the LHT. Since, this is the case, step 2 is to check if the measurements are consistent in units (power in W).

	Panels #												
f_Hz	1	2	3	4	5	6	7	8	9	10	11	12	13
25	59,41	64,32	61,16	46,11	49,27	54,06	53,13	42,68	50,43	50,23	55,08	53,72	58,2
31,5	58,91	60,05	55,09	50,23	52,21	52,84	53,4	53,02	49,78	53,4	49,97	45,42	54,19
40	58,15	59,86	42,84	46,97	45,02	57,86	51,83	46,86	49,84	54,26	54,23	48,03	53,9
50	50,65	53,03	50,73	50,13	48,36	56,43	51,03	49,45	55,18	55,71	47,17	55,25	57,95
63	34,61	44,95	48,54	55,35	51,16	62,17	62,04	59,68	58,21	57,32	56,1	54,75	56,1
80	47,42	49,4	49,44	52,3	45,44	59,5	60,89	54,92	57,58	54,98	54,19	51,67	51,87
100	40,63	39,47	44,55	55,02	51,8	54,15	51,15	57,45	58,29	59	49,99	54,54	55,93
125	40,72	48,45	51,77	60,47	55,03	53,35	49,97	57,13	62,12	59,4	54,96	58,12	55,94
160	48,51	51,14	52,65	55,48	49,79	51,85	57,12	53,91	51,71	52,27	52,57	59,53	57,02
200	55,6	60,61	58,94	63,13	60,29	64,53	64,94	60,95	58,12	55,33	55,41	64,28	62,97
250	58,74	61,76	61,3	68,88	66,26	64,44	63,2	61,09	61,94	59,92	62,11	65,01	63,02
315	58,86	61,88	62,4	70,45	65,98	62,87	62,42	61,88	63,31	62,59	60,78	64,07	62,94
400	52,76	55,67	57,56	66,35	61,01	60,51	58,19	60,09	61,43	60,89	58,7	60,9	60,6
500	49,91	52,14	56,84	64,54	58,44	54,95	55,55	55,94	60,76	56,1	52,92	59,18	57,93
630	49,88	50,91	55,12	63,45	54,62	52,62	51,42	53	61,69	53,56	48,29	55,65	50,31
800	46,64	49,45	52,7	62,03	52,5	49,28	49,5	51,35	55,43	51,16	45,33	52,16	44,75
1000	39,81	43,19	48,79	55,09	42,33	42,35	48,22	43,81	46,74	43,93	38,3	46,66	39,61
1250	37,09	39,68	42,45	50,44	37,47	38,31	43,4	39,13	44,72	40,87	32,19	44,9	35,86
1600	33,1	37,56	41,13	43,98	32,99	38,01	46,09	37,82	41,44	39,03	31,99	40,69	32,03
2000	29,08	33,12	38,3	39,33	28,93	36,61	41,68	35,55	41,53	39,44	17,58	38,98	24,24
2500	25	28,02	37,79	37,85	23,46	33,7	36,43	31,48	41,7	36	24,21	35,88	24,91
3150	17,42	20,38	31,54	32,79	23,82	29,88	31,52	28,02	35,98	28,58	17,82	29,9	20,52
4000	15,71	14,04	22,68	29,54	20,99	29,5	30,25	11,34	30,4	21,48	10,74	24,34	4,91
5000	15,16	19,36	25,47	24,47	20,77	27,85	28,66	25,66	18,25	23,7	21,69	24,89	21,07
6300	15,9	15,13	18,11	9,36	22,71	27,83	28,3	22,46	19,8	22,88	23,05	22,85	19,29
8000	9,58	7,43	6,12	19,27	21,93	28,56	31,04	10,24	16,02	10,5	8,47	9,68	9,55
10000	-19,22	-0,64	15,08	13,15	18,99	28,13	30,56	5,72	9,16	9,54	15,45	7,39	-2,57
Area	0,53	0,53	0,47	0,06	0,42	0,55	0,2	0,55	0,03	0,42	0,41	0,05	0,53

Figure 54: Measured sound intensity [dB] in cabin from experiment M002 (results provided)

In step 2, each set of measurements [$in\ dB$] will be converted using the pre-processing power convertor, found in the database. Figure 55 is an extract of the pre-processing tool until 400 Hz.

#1: First, the intensity measurements manually are entered in the white field

Intensity [dB]		Intensity [dB]									
Panel #		12,5	16	20	25	31,5	40	50	63	80	100
1					5,94100E+01	5,89100E+01	5,81500E+01	5,06500E+01	3,46100E+01	4,74200E+01	4,06300E+01
2					6,43200E+01	6,00500E+01	5,98600E+01	5,30300E+01	4,49500E+01	4,94000E+01	3,94700E+01
3					6,11600E+01	5,50900E+01	4,28400E+01	5,07300E+01	4,85400E+01	4,94400E+01	4,45500E+01
4					4,61100E+01	5,02300E+01	4,69700E+01	5,01300E+01	5,53500E+01	5,23000E+01	5,50200E+01
5					4,92700E+01	5,22100E+01	4,50200E+01	4,83600E+01	5,11600E+01	4,54400E+01	5,18000E+01
6					5,40600E+01	5,28400E+01	5,78600E+01	5,64300E+01	6,21700E+01	5,95000E+01	5,41500E+01
7					5,31300E+01	5,34000E+01	5,18300E+01	5,10300E+01	6,20400E+01	6,08900E+01	5,11500E+01
8					4,26800E+01	5,30200E+01	4,68600E+01	4,94500E+01	5,96800E+01	5,49200E+01	5,74500E+01
9					5,04300E+01	4,97800E+01	4,98400E+01	5,51800E+01	5,82100E+01	5,75800E+01	5,82900E+01
10					5,02300E+01	5,34000E+01	5,42600E+01	5,57100E+01	5,73200E+01	5,49800E+01	5,90000E+01
11					5,50800E+01	4,99700E+01	5,42300E+01	4,71700E+01	5,61000E+01	5,41900E+01	4,99900E+01
12					5,37200E+01	4,54200E+01	4,80300E+01	5,52500E+01	5,47500E+01	5,16700E+01	5,45400E+01
13					5,82000E+01	5,41900E+01	5,39000E+01	5,79500E+01	5,61000E+01	5,18700E+01	5,59300E+01
Intensity [W/m2]		Intensity [W/m2]						Intensity [W/m2]			
Panel #		12,5	16	20	25	31,5	40	50	63	80	100
1					8,72971E-07	7,78037E-07	6,53131E-07	1,16145E-07	2,89068E-09	5,52077E-08	1,15611E-08
2					2,70396E-06	1,01158E-06	9,68278E-07	2,00909E-07	3,12608E-08	8,70964E-08	8,85116E-09
3					1,30617E-06	3,22849E-07	1,92309E-08	1,18304E-07	7,14496E-08	8,79023E-08	2,85102E-08
4					4,08319E-08	1,05439E-07	4,97737E-08	1,03039E-07	3,42768E-07	1,69824E-07	3,17687E-07
5					8,45279E-08	1,66341E-07	3,17687E-08	6,85488E-08	1,30617E-07	3,49945E-08	1,51356E-07
6					2,54683E-07	1,92309E-07	6,10942E-07	4,39542E-07	1,64816E-06	8,91251E-07	2,60016E-07
7					2,05589E-07	2,18776E-07	1,52405E-07	1,26765E-07	1,59956E-06	1,22744E-06	1,30317E-07
8					1,85353E-08	2,00447E-07	4,85289E-08	8,81049E-08	9,28966E-07	3,10456E-07	5,55904E-07
9					1,10408E-07	9,50605E-08	9,63829E-08	3,29610E-07	6,62217E-07	5,72796E-07	6,74528E-07
10					1,05439E-07	2,18776E-07	2,66686E-07	3,72392E-07	5,39511E-07	3,14775E-07	7,94328E-07
11					3,22107E-07	9,93116E-08	2,64850E-07	5,21195E-08	4,07380E-07	2,62422E-07	9,97700E-08
12					2,35505E-07	3,48337E-08	6,35331E-08	3,34965E-07	2,98538E-07	1,46893E-07	2,84446E-07
13					6,60602E-07	1,63422E-07	2,45431E-07	6,22735E-07	4,07280E-07	1,53815E-07	3,01792E-07
Intensity [W/m2]		Power [W]						Power [W]			
Panel #		12,5	16	20	25	31,5	40	50	63	80	100
1	0,53				4,6267E-07	4,1236E-07	3,4616E-07	6,1557E-08	1,5321E-09	2,926E-08	6,1274E-09
2	0,53				1,4331E-06	5,3614E-07	5,1319E-07	1,0648E-07	1,6568E-08	4,6161E-08	4,6911E-09
3	0,47				6,139E-07	1,5174E-07	9,0385E-09	5,5603E-08	3,3581E-08	4,1314E-08	1,34E-08
4	0,06				2,4499E-09	6,3263E-09	2,9864E-09	6,1823E-09	2,0566E-08	1,0189E-08	1,9061E-08
5	0,42				3,5502E-08	6,9863E-08	1,3343E-08	2,8791E-08	5,4859E-08	1,4698E-08	6,357E-08
6	0,55				1,4008E-07	1,0577E-07	3,3602E-07	2,4175E-07	9,0649E-07	4,9019E-07	1,4301E-07
7	0,2				4,1118E-08	4,3755E-08	3,0481E-08	2,5353E-08	3,1991E-07	2,4549E-07	2,6063E-08
8	0,55				1,0194E-08	1,1025E-07	2,6691E-08	4,8458E-08	5,1093E-07	1,7075E-07	3,0575E-07
9	0,03				3,3122E-09	2,8518E-09	2,8915E-09	9,8883E-09	1,9866E-08	1,7184E-08	2,0236E-08
10	0,42				4,4284E-08	9,1886E-08	1,1201E-07	1,564E-07	2,2659E-07	1,3221E-07	3,3362E-07
11	0,41				1,3206E-07	4,0718E-08	1,0859E-07	2,1369E-08	1,6703E-07	1,0759E-07	4,0906E-08
12	0,05				1,1775E-08	1,7417E-09	3,1767E-09	1,6748E-08	1,4927E-08	7,3446E-09	1,4222E-08
13	0,53				3,5017E-07	1,3908E-07	1,301E-07	3,3058E-07	2,1591E-07	8,1522E-08	2,0762E-07

Figure 55: Conversion sound intensity [dB] to power using the pre-processing tool

#2: Secondly, the user gives the surface area for each panel manually

#3: The tool automatically converts the measurement into W using the area

This decision step also involves verifying whether the SPL in W. Following, the SPL [dB] will be converted into W using the pre-processing tool for SPL conversion. (see Figure 56)

#4 the SPL measurements manually are entered in the white field

SPL [dB] to W		SPL [dB] to W						SPL [dB] to W			
Experiment parameters		12,5	16	20	25	31,5	40	50	63	80	100
Density [kg/ m^3]	1,225										
Speed of sound [m/s]	343										
SPL [dB]		SPL [dB]						SPL [dB]			
Panel #		12,5	16	20	25	31,5	40	50	63	80	100
1	INPUT SPL (RIGHT)	54,16	49,8	47,85	45,51	44,25	52,31	60,92	69,86	73,61	78,17
2		54,16	49,8	47,85	45,51	44,25	52,31	60,92	69,86	73,61	78,17
3		54,16	49,8	47,85	45,51	44,25	52,31	60,92	69,86	73,61	78,17
4		54,16	49,8	47,85	45,51	44,25	52,31	60,92	69,86	73,61	78,17
5		54,16	49,8	47,85	45,51	44,25	52,31	60,92	69,86	73,61	78,17
6		54,16	49,8	47,85	45,51	44,25	52,31	60,92	69,86	73,61	78,17
7		54,16	49,8	47,85	45,51	44,25	52,31	60,92	69,86	73,61	78,17
8		54,16	49,8	47,85	45,51	44,25	52,31	60,92	69,86	73,61	78,17
9		54,16	49,8	47,85	45,51	44,25	52,31	60,92	69,86	73,61	78,17
10		54,16	49,8	47,85	45,51	44,25	52,31	60,92	69,86	73,61	78,17
11		54,16	49,8	47,85	45,51	44,25	52,31	60,92	69,86	73,61	78,17
12		54,16	49,8	47,85	45,51	44,25	52,31	60,92	69,86	73,61	78,17
13		54,16	49,8	47,85	45,51	44,25	52,31	60,92	69,86	73,61	78,17
Power [W]		Power [W]						Power [W]			
Panel #	Area	12,5	16	20	25	31,5	40	50	63	80	100
1	0,53	1,3149E-07	4,8184E-08	3,0754E-08	1,7943E-08	1,3425E-08	8,5883E-08	6,236E-07	4,8855E-06	1,1585E-05	3,3106E-05
2	0,53	1,3149E-07	4,8184E-08	3,0754E-08	1,7943E-08	1,3425E-08	8,5883E-08	6,236E-07	4,8855E-06	1,1585E-05	3,3106E-05
3	0,47	1,1661E-07	4,2729E-08	2,7273E-08	1,5912E-08	1,1905E-08	7,616E-08	5,53E-07	4,3324E-06	1,0274E-05	2,9358E-05
4	0,06	1,4886E-08	5,4548E-09	3,4816E-09	2,0313E-09	1,5198E-09	9,7226E-09	7,0596E-08	5,5307E-07	1,3115E-06	3,7478E-06
5	0,42	1,042E-07	3,8184E-08	2,4371E-08	1,4219E-08	1,0638E-08	6,8058E-08	4,9417E-07	3,8715E-06	9,1808E-06	2,6235E-05
6	0,55	1,3646E-07	5,0003E-08	3,1915E-08	1,8621E-08	1,3931E-08	8,9124E-08	6,4713E-07	5,0698E-06	1,2022E-05	3,4355E-05
7	0,2	4,962E-08	1,8183E-08	1,1605E-08	6,7711E-09	5,0659E-09	3,2409E-08	2,3532E-07	1,8436E-06	4,3718E-06	1,2493E-05
8	0,55	1,3646E-07	5,0003E-08	3,1915E-08	1,8621E-08	1,3931E-08	8,9124E-08	6,4713E-07	5,0698E-06	1,2022E-05	3,4355E-05
9	0,03	7,4431E-09	2,7274E-09	1,7408E-09	1,0157E-09	7,5989E-10	4,8613E-09	3,5298E-08	2,7654E-07	6,5577E-07	1,8739E-06
10	0,42	1,042E-07	3,8184E-08	2,4371E-08	1,4219E-08	1,0638E-08	6,8058E-08	4,9417E-07	3,8715E-06	9,1808E-06	2,6235E-05
11	0,41	1,0172E-07	3,7275E-08	2,3791E-08	1,3881E-08	1,0385E-08	6,6438E-08	4,8241E-07	3,7793E-06	8,9622E-06	2,561E-05
12	0,05	1,2405E-08	4,5457E-09	2,9013E-09	1,6928E-09	1,2665E-09	8,1021E-09	5,883E-08	4,6089E-07	1,0929E-06	3,1232E-06
13	0,53	1,3149E-07	4,8184E-08	3,0754E-08	1,7943E-08	1,3425E-08	8,5883E-08	6,236E-07	4,8855E-06	1,1585E-05	3,3106E-05

Figure 56: Conversion sound intensity [dB] to power using the pre-processing tool

#4: Secondly, the user gives the surface area for each panel manually

#5: The tool automatically converts the measurement into W

After, having converted both measurements in W, the TF can be calculated using the TF calculator on sheet 2 of the database. (Refer Figure 57)

TF		TF			TF							
Panel #	12,5	16	20	25	31,5	40	50	63	80	100		
1				25,785183	30,7163931	4,0306048	0,09871206	0,0003136	0,00252563	0,00018508	8,07	
2				79,8675234	39,9365199	5,97544451	0,17075374	0,00339133	0,00398447	0,0001417	0,00	
3				38,5807102	12,7458915	0,118678	0,10054725	0,00775122	0,00402133	0,00045643	0,00	
4				1,20606362	4,16265308	0,30716393	0,087573	0,03718521	0,00776909	0,00508593	0,00	
5				2,49672217	6,5670484	0,19605152	0,05825996	0,01417001	0,00160092	0,00242309	0,00	
6				7,52263893	7,59224506	3,7702506	0,37356847	0,17880111	0,04077277	0,00416265	0,00	
7				767	8,63714514	0,94052473	0,10773832	0,17352826	0,05615264	0,00208627	0,00	
8				247	7,91352935	0,29948165	0,07488076	0,10077904	0,01420268	0,00889959	0,00	
9				581	3,75292787	0,59479898	0,28013683	0,07184064	0,02620416	0,01079867	0,01	
10				007	8,63714514	1,64577408	0,31649745	0,05852888	0,01440026	0,01271658	0,0	
11				9,51415489	3,92075963	1,63444465	0,04429658	0,0441947	0,01200522	0,00159724	0,00	
12				6,95617049	1,37521379	0,39207596	0,28468869	0,03238696	0,00672001	0,00455376	0,00	
13				19,5150747	10,3602496	1,51485204	0,53011515	0,0441947	0,00703672	0,00627148	0,00	
Pressure in [Pa]		Pressure in [Pa]										

#6: Calculate TF on sheet 2

Power_Converter | TF_Converter | ID_Generator | Database | Key

Figure 57: Calculation of TF

In step #7 the user generates the respective IDs of the measurements using the ID generator or manually given as shown below in Figure 58.

Check ID	Segment	Sub-path	Configuration	Generated ID	Proposed ID	Status		Transfer ID	Segment	Serial path number	Description	Date
Proposed ID #1	1	1	TOM	1-1-TOM1		Available						
Proposed ID #2					1TOM	Available						
Proposed ID #3					2TOM	Occupied		2Tom	1	2	TEST #1	4.8.2024
Proposed ID #E	1			E11	ETOM	Available						

Figure 58: ID generation

Finally, in step #8, the user saves the data in the database together with any additional information, completing the pre-processing loop, as shown in Figure 59.

ID #	Segment	Serial path numbe	Description	Date	Weight	Cost	Area [m^2]	Reverbera tion time [s]	1/3 scale [Hz]	12,50	16,00	20,00	25,00	31,50	40,00	50,00
ETOM1	1	1	itation aus Tom Messu	4.4.2023	/	/	/	/		4,290029	2,59693	2,074723	1,584748	1,370756	3,467051	9,342438
ETOM2	2	1	itation aus Tom Messu	4.4.2023	/	/	/	/		4,290029	2,59693	2,074723	1,584748	1,370756	3,467051	9,342438
ETOM3	3	1	itation aus Tom Messu	4.4.2023	/	/	/	/		4,290029	2,59693	2,074723	1,584748	1,370756	3,467051	9,342438
ETOM4	4	1	itation aus Tom Messu	4.4.2023	/	/	/	/		4,290029	2,59693	2,074723	1,584748	1,370756	3,467051	9,342438
ETOM5	5	1	itation aus Tom Messu	4.4.2023	/	/	/	/		4,290029	2,59693	2,074723	1,584748	1,370756	3,467051	9,342438
ETOM6	6	1	itation aus Tom Messu	4.4.2023	/	/	/	/		4,290029	2,59693	2,074723	1,584748	1,370756	3,467051	9,342438
ETOM7	7	1	itation aus Tom Messu	4.4.2023	/	/	/	/		4,290029	2,59693	2,074723	1,584748	1,370756	3,467051	9,342438
ETOM8	8	1	itation aus Tom Messu	4.4.2023	/	/	/	/		4,290029	2,59693	2,074723	1,584748	1,370756	3,467051	9,342438
ETOM9	9	1	itation aus Tom Messu	4.4.2023	/	/	/	/		4,290029	2,59693	2,074723	1,584748	1,370756	3,467051	9,342438
ETOM10	10	1	itation aus Tom Messu	4.4.2023	/	/	/	/		4,290029	2,59693	2,074723	1,584748	1,370756	3,467051	9,342438

Figure 59: Saving of data in database

The next loop involves processing the data. The corresponding ID of the panel for which the user wishes to perform the noise analysis is given in the input field of the main tool. (step #9) (refer to Figure 60)

Number	Description	Serial Path 1	Serial Path 2	Serial Path 3	Parallel	Configuration	Excitation		Serial Path 1	Serial Path 2	Serial Path 3	Parallel	Configuration	Excitation
P1	Floor Panel Inboard	11TOM					ETOM1		OK	NOT OK	NOT OK	NOT OK	NOT OK	OK
P2	Floor Panel Middle	21TOM					ETOM2		OK	NOT OK	NOT OK	NOT OK	NOT OK	OK
P3	Floor Panel Outboard	31TOM					ETOM3		OK	NOT OK	NOT OK	NOT OK	NOT OK	OK
P4	Dado Gap	41TOM					ETOM4		OK	NOT OK	NOT OK	NOT OK	NOT OK	OK
P5	Dado Panel	51TOM					ETOM5		OK	NOT OK	NOT OK	NOT OK	NOT OK	OK
P6	Lower Sidewall Panel	61TOM					ETOM6		OK	NOT OK	NOT OK	NOT OK	NOT OK	OK
P7	Window (-Panel)	71TOM					ETOM7		OK	NOT OK	NOT OK	NOT OK	NOT OK	OK
P8	Upper Sidewall Panel	81TOM					ETOM8		OK	NOT OK	NOT OK	NOT OK	NOT OK	OK
P9	ECS Gap	91TOM					ETOM9		OK	NOT OK	NOT OK	NOT OK	NOT OK	OK
P10	Closure Panel	101TOM					ETOM10		OK	NOT OK	NOT OK	NOT OK	NOT OK	OK
P11	Service Area Panel	111TOM					ETOM11		OK	NOT OK	NOT OK	NOT OK	NOT OK	OK
P12	Ceiling ECS Gap	121TOM					ETOM12		OK	NOT OK	NOT OK	NOT OK	NOT OK	OK
P13	Ceiling	131TOM					ETOM13		OK	NOT OK	NOT OK	NOT OK	NOT OK	OK
											CHECK ONLY			

Figure 60: Input definition

Finally, in step #10, the tool automatically calculates the output power for the defined panels, as shown in Figure 61.

Segment	250	315	400	500	630	800	1000	1250	1600	2000	2500	3150	4000	5000
1	3,97E-07	4,08E-07	1E-07	5,19E-08	5,16E-08	2,44E-08	5,07E-09	2,71E-09	1,08E-09	4,29E-10	1,68E-10	2,93E-11	1,97E-11	1,74E-11
2	7,95E-07	8,17E-07	1,96E-07	8,68E-08	6,54E-08	4,67E-08	1,1E-08	4,92E-09	3,02E-09	1,09E-09	3,36E-10	5,78E-11	1,34E-11	4,57E-11
3	6,34E-07	8,17E-07	2,68E-07	2,27E-07	1,53E-07	8,75E-08	3,56E-08	8,26E-09	6,1E-09	3,18E-09	2,83E-09	6,7E-10	8,71E-11	1,66E-10
4	4,64E-07	6,66E-07	2,59E-07	1,71E-07	1,33E-07	9,58E-08	1,94E-08	6,64E-09	1,5E-09	5,14E-10	3,66E-10	1,14E-10	5,4E-11	1,68E-11
5	1,78E-06	1,66E-06	5,3E-07	2,93E-07	1,22E-07	7,47E-08	7,18E-09	2,35E-09	8,36E-10	3,28E-10	9,32E-11	1,01E-10	5,28E-11	5,01E-11
6	1,53E-06	1,07E-06	6,19E-07	1,72E-07	1,01E-07	4,66E-08	9,45E-09	3,73E-09	3,48E-09	2,52E-09	1,29E-09	5,35E-10	4,9E-10	3,35E-10
7	4,18E-07	3,49E-07	1,32E-07	7,18E-08	2,77E-08	1,78E-08	1,33E-08	4,38E-09	8,13E-09	2,94E-09	8,79E-10	2,84E-10	2,12E-10	1,47E-10
8	7,07E-07	8,48E-07	5,62E-07	2,16E-07	1,1E-07	7,51E-08	1,32E-08	4,5E-09	3,33E-09	1,97E-09	7,73E-10	3,49E-10	7,49E-12	2,02E-10
9	4,69E-08	6,43E-08	4,17E-08	3,57E-08	4,43E-08	1,05E-08	1,42E-09	8,89E-10	4,18E-10	4,27E-10	4,44E-10	1,19E-10	3,29E-11	2,01E-12
10	4,12E-07	7,63E-07	5,16E-07	1,71E-07	9,53E-08	5,49E-08	1,04E-08	5,13E-09	3,36E-09	3,69E-09	1,67E-09	3,03E-10	5,91E-11	9,85E-11
11	6,66E-07	4,91E-07	3,04E-07	8,03E-08	2,77E-08	1,4E-08	2,77E-09	6,79E-10	6,48E-10	2,35E-11	1,08E-10	2,48E-11	4,86E-12	6,05E-11
12	1,58E-07	1,28E-07	6,15E-08	4,14E-08	1,84E-08	8,22E-09	2,32E-09	1,55E-09	5,86E-10	3,95E-10	1,94E-10	4,89E-11	1,36E-11	1,54E-11
13														
Total	8E-06	8,08E-06	3,59E-06	1,62E-06	9,48E-07	5,56E-07	1,31E-07	4,57E-08	3,25E-08	1,75E-08	9,15E-09	2,64E-09	1,05E-09	1,16E-09

Figure 61: Calculated power output

X. Tool definition for validation

In the database, the excitation from the measurement campaign M002 are stored with the following ID as shown in Figure 62. The IDs have the prefix Exxx. For example, excitation ID for panel 1 is named ETOM1.

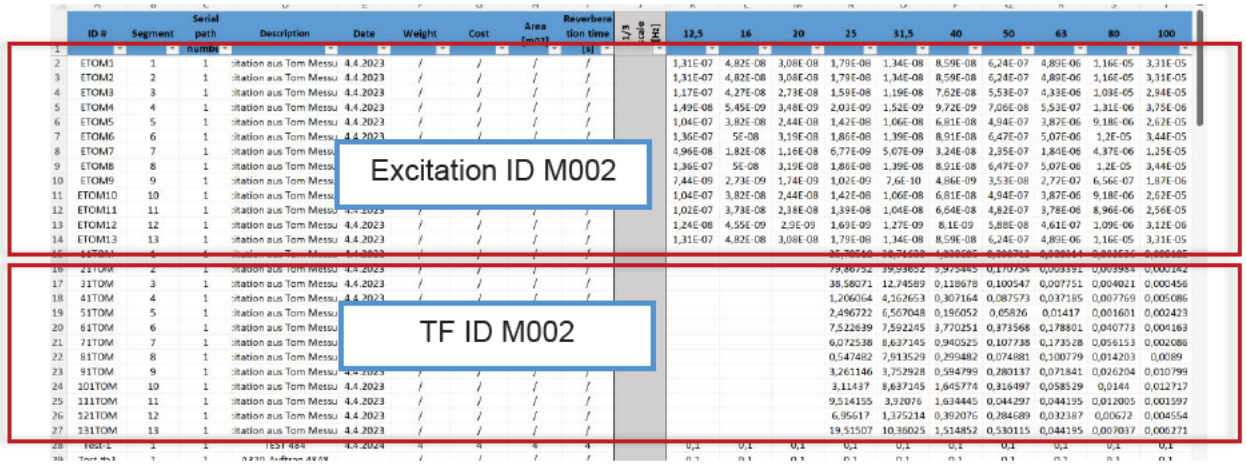

Figure 62: Excitation and TF IDs for Ziegner M002 measurements

Similarly, the TFs are stored from row 15 to row 27 in the database. As they are single path TF, the second index are x1x. For instance, in case of panel 1 (Floor panel inboard), the TF ID is 11TOM.

Figure 63 shows, how the user can define his input parameters if he wishes to reproduce Ziegner's calculated sound power/ M002.

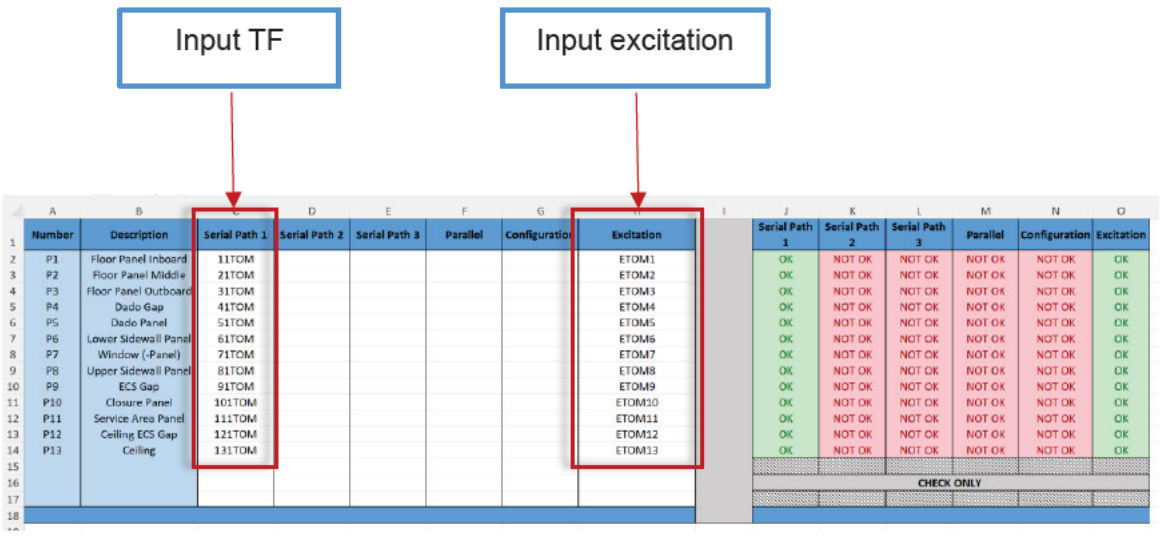

Figure 63: Input parameter to reproduce Ziegner's results.

Finally, the SPL was calculated in a completely different excel sheet, called 3_Validation_Tool, together with all measurement from the M002 campaign, including the reverberation time. Figure 64 shows an extract of the calculation.

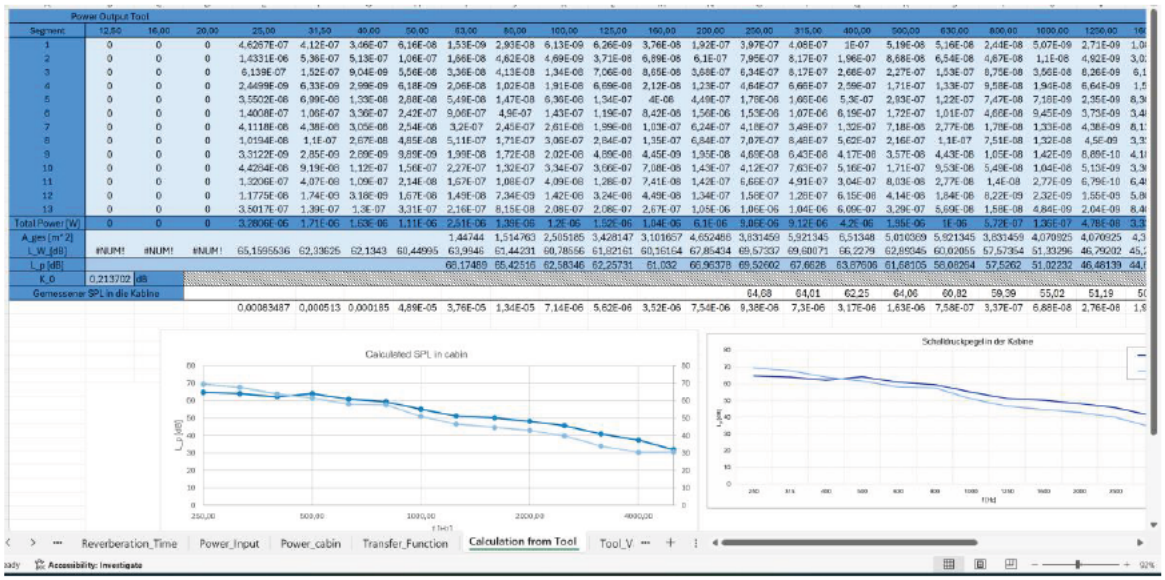

Figure 64: Validation of tool I

In another sheet in the excel file 3_Tool_Validation, the most dominant sound transmission paths were calculated to check whether, the outcome matched with Ziegner results. This was done separately in another sheet as the pie charts from the tool is based on the third octave scale, while the results from Ziegner were on the octave band scale. the validation and comparison, the one-third octave band results were were linearly summed in W across three consecutive bands to reconstruct the corresponding octave bands. The calculation can be found in the sheet Tool_Validation as shown in Figure 65.

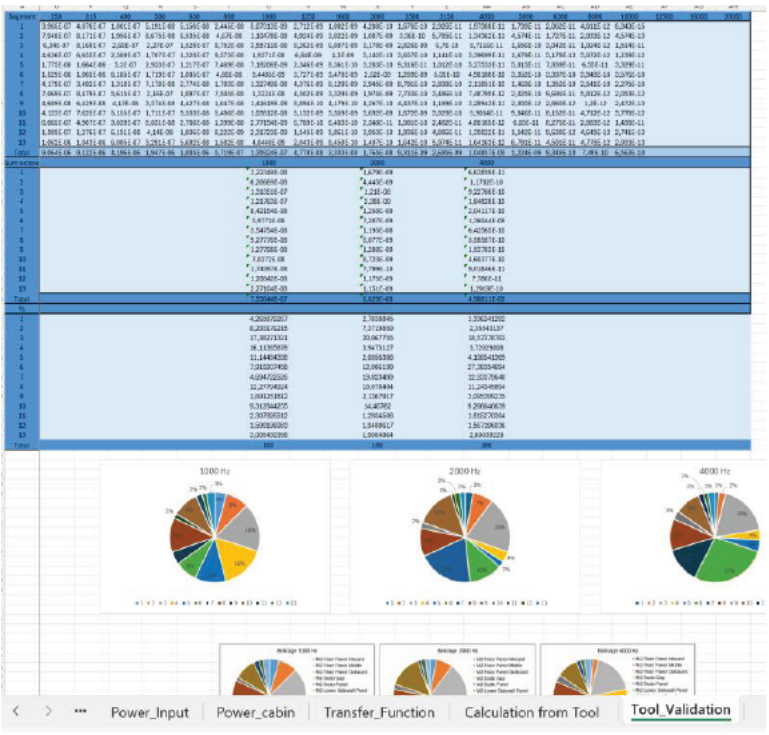

Figure 65: Validation of tool II

XI. Key

Figure 66 shows the key of the pre-processing tool, and Figure 67 illustrates the key of the main tool, each also showing the main stages involved and colour scheme. The keys in both cases are found in the last sheet of the tool and the database and help user have a clear understanding and depiction of their meaning.

Colour code	Description
	Title/ main heading
	Input Parameter
	Predifined process/ subtitle especially for segment number or path number
	Output
	Blocked cell/ no entry can be given
	Separator
Available	Data/ ID are available in database
Occupied	Data/ ID are NOT available/ occupied in database

Pre-processing stages involved:

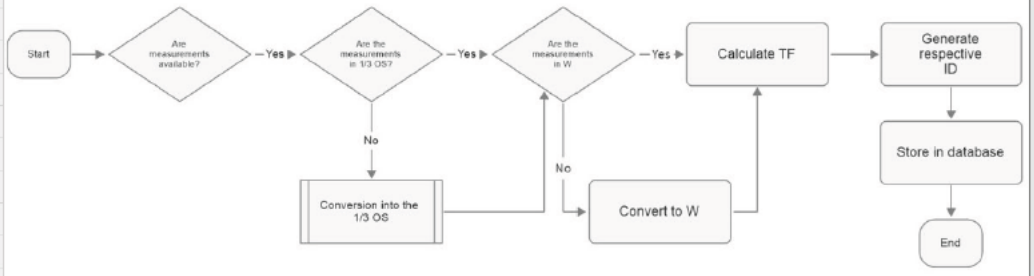

Figure 66: Key (legend) for Database

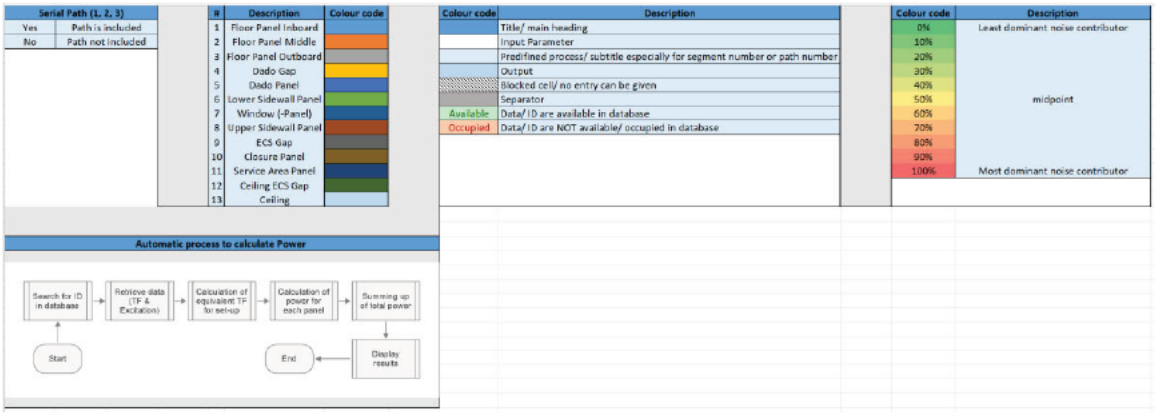

Figure 67: Key (legend) Tool

XII. Main formula in Excel

Table 8 is a list of the main excel formulae for the database, including the programming logic involved in the computation of TFs and generation of IDs.

Table 8: Main Excel formulae for database

#	Database formula
1	=IF(C7="";"";((C7)^2/(B3*B4))*B23)
	Converts measured pressure in cell C7 to power, IF condition ensures if no value of pressure is given, the answer in the cell is empty and not 0 or #nv, B3 and B4 contain density and speed of sound respectively
2	=IF(C44="";"";(0,00002*10^(C44/20))^2/(B40*B41)*$B60)
	Converts SPL from cell C44 [dB] to W, IF condition ensures if no value of SPL is given, the answer in the cell is empty and not 0 or #nv, B40 and B41 contain density and speed of sound respectively, B60 is area
3	=IF(C77="";"";(0,000000000001)*10^(C77/10))
	Converts intensity [dB] from cell C77 to W/m2
4	=IF(C92="";"";C92*$B107)
	Converts intensity W/m2 to W
	TF Calculator
4	=IF(OR(B3="";B19="");"";B19/B3)
	Converts power output/ input to TF
	ID Generator
5	=B2 &"-"& C2 &"-"& D2 & TEXT(COUNTIF(Database!A:A; B2 &"-"& C2 &"-"& D2 & "*") + 1; "0")
	This formula creates a unique identifier based on values from columns B, C, and D, followed by a sequential number that increments based on how many similar entries already exist in column A of the Database sheet.
6	=IF(COUNTIF(Database!$A:$A; F2) > 0; "Occupied"; "Available")
	Checks if ID (F2 here) is already available in database
7	=IFERROR(INDEX(Database!$A:$AQ; MATCH($F2; Database!$A:$A; 0); COLUMN(Database!A1)); "")
	Search for a value from cell F2 in the "Database" sheet, retrieves the corresponding data from the same row, and returns it. If there's an error (e.g., if the value in F2 is not found), it returns an empty string ("") instead of an error message.
8	=IFERROR(INDEX(Database!$A:$AQ; MATCH($F2; Database!$A:$A; 0); COLUMN(Database!C1)); "")
	Retrieves a value from the Database sheet based on the value in F2. The MATCH function finds the row number where the value in F2 appears in Database!A:A, the INDEX function returns the value from that row and the column determined by COLUMN(Database!C1), and IFERROR ensures that an empty cell is returned if no match is found.

Main Formulae for Power Tool, cont.

Table 9 is a list of the main excel formulae used in the Power Tool, in order to search, match and retrieve the TFs and IDs from the database to the tool.

Table 9: Main Excel formulae for Power Tool

#	Main formula for Power Tool
1	=IFERROR(IF(INDEX('C:\Desktop\Power_Tool_ENTIRETY\[2_Database_ENTIRETY.xlsx]Database'!$A:$A; MATCH(C2; 'C:\Desktop\Power_Tool_ENTIRETY\[2_Database_ENTIRETY.xlsx]Database'!$A:$A; 0); COLUMN('C:\Desktop\Power_Tool_ENTIRETY\[2_Database_ENTIRETY.xlsx]Database'!A:A))<>""; "OK"; "NOT OK"); "NOT OK")
	Retrieves a value from an external file located at C:\Desktop\Power_Tool_ENTIRETY, specifically from the Database sheet in the 2_Database_ENTIRETY.xlsx file, and compares it to C2. The MATCH function identifies the row number where the value in C2 is found, and the INDEX function retrieves the corresponding value from the same row and column. If the retrieved value is not empty, the formula returns "OK"; otherwise, it returns "NOT OK". The IFERROR function ensures that if no match is found or an error occurs, "NOT OK" is returned.
2	=IFERROR(INDEX('C:\Desktop\Power_Tool_ENTIRETY\[2_Database_ENTIRETY.xlsx]Database'!$A:$AQ; MATCH($B2; 'C:\Desktop\Power_Tool_ENTIRETY\[2_Database_ENTIRETY.xlsx]Database'!$A:$A; 0); COLUMN('C:\Desktop\Power_Tool_ENTIRETY\[2_Database_ENTIRETY.xlsx]Database'!K:K)); "")
	Retrieves a value from the Database sheet in the external file 2_Database_ENTIRETY.xlsx located at C:\Desktop\Power_Tool_ENTIRETY, based on a match with the value in B2. The MATCH function finds the row number where the value in B2 appears in column A of the external sheet. The INDEX function then retrieves the value from that row in column K, as determined by COLUMN(K:K). If no match is found or an error occurs, the IFERROR function returns an empty cell instead of an error.
3	=Input!C2
	Give content from C2
4	=IFERROR(INDEX('C:\Desktop\Power_Tool_ENTIRETY\[2_Database_ENTIRETY.xlsx]Database'!$A:$AQ; MATCH($B2; 'C:\Desktop\Power_Tool_ENTIRETY\[2_Database_ENTIRETY.xlsx]Database'!$A:$A; 0); COLUMN('C:\Desktop\Power_Tool_ENTIRETY\[2_Database_ENTIRETY.xlsx]Database'!K:K)); "")
	Looks up the value in B2 in column A of the external 2_Database_ENTIRETY.xlsx file, specifically in the Database sheet. The MATCH function identifies the row where the value from B2 is found. The INDEX function then retrieves the value from that row and from column K in the external file. If no match is found, the IFERROR function returns an empty cell instead of an error.
	Excitation
4	=IF(OR(TFs!Q32=""; Excitation!Q$7=""); ""; TFs!Q32*Excitation!Q$7)
	Calculates power involving 1 path Checks if either TFs!Q32 or Excitation!Q$7 is empty. If either cell is empty, it returns an empty cell. Otherwise, it multiplies the values in TFs!Q32 and Excitation!Q$7.
	TF
5	=IF(COUNTIF(D2:D6;">0")=0; ""; PRODUCT(IF(D2<>""; D2; 1); IF(D3<>""; D3; 1); IF(D4<>""; D4; 1); IF(D5<>""; D5; 1)) + IF(D6<>""; D6; 0))
	Calculate TF Checks if any values in D2:D6 are greater than 0. If none are, it returns an empty cell. If there are values, it multiplies the non-empty values in D2:D5, treating empty cells as 1, and adds the value in D6 if it is not empty.